Titre: Title:	Étude biomécanique du traitement de la scoliose idiopathique par orthèse: effets des paramètres de conception des corsets sur les corrections géométriques et sur les contraintes internes du rachis.
Auteur: Author:	Julien Clin
Date:	2010
Type:	Mémoire ou thèse / Dissertation or Thesis
Référence: Citation:	Clin, J. (2010). Étude biomécanique du traitement de la scoliose idiopathique par orthèse: effets des paramètres de conception des corsets sur les corrections géométriques et sur les contraintes internes du rachis. [Thèse de doctorat, École Polytechnique de Montréal]. PolyPublie. https://publications.polymtl.ca/280/

URL de PolyPublie: PolyPublie URL:	https://publications.polymtl.ca/280/
Directeurs de recherche: Advisors:	Carl-Éric Aubin, Hubert Labelle, & Stefan Parent
Programme: Program:	Génie biomédical

UNIVERSITÉ DE MONTRÉAL

ÉTUDE BIOMÉCANIQUE DU TRAITEMENT DE LA SCOLIOSE IDIOPATHIQUE PAR ORTHÈSE: EFFETS DES PARAMÈTRES DE CONCEPTION DES CORSETS SUR LES CORRECTIONS GÉOMÉTRIQUES ET SUR LES CONTRAINTES INTERNES DU RACHIS

JULIEN CLIN
INSTITUT DE GÉNIE BIOMÉDICAL
ÉCOLE POLYTECHNIQUE DE MONTRÉAL

THÈSE PRÉSENTÉE EN VUE DE L'OBTENTION
DU DIPLÔME DE PHILOSOPHIAE DOCTOR
(GÉNIE BIOMÉDICAL)
AVRIL 2010

UNIVERSITÉ DE MONTRÉAL

ÉCOLE POLYTECHNIQUE DE MONTRÉAL

Cette thèse intitulée:

ÉTUDE BIOMÉCANIQUE DU TRAITEMENT DE LA SCOLIOSE IDIOPATHIQUE PAR ORTHÈSE: EFFETS DES PARAMÈTRES DE CONCEPTION DES CORSETS SUR LES CORRECTIONS GÉOMÉTRIQUES ET SUR LES CONTRAINTES INTERNES DU RACHIS.

Présentée par : CLIN Julien

en vue de l'obtention du diplôme de : Philosophiae Doctor

a été dûment accepté par le jury d'examen constitué de :

Mme PÉRIÉ-CURNIER Delphine, D.Sc., présidente

M. AUBIN Carl-Éric, Ph.D., membre et directeur de recherche

M. LABELLE Hubert, M.D., membre et codirecteur de recherche

M. PARENT Stefan, Ph.D., M.D., membre et codirecteur de recherche

M. PETIT Yvan, Ph.D., membre

M. MONGRAIN Rosaire, Ph.D., membre

REMERCIEMENTS

Je voudrais remercier mes directeurs de recherche, le Dr Carl-Éric Aubin, le Dr Hubert Labelle et le Dr Stefan Parent pour m'avoir permis de travailler sur ce projet et pour m'avoir encadré. J'ai apprécié l'autonomie qu'ils m'ont accordée, leur sens critique et leur rigueur.

J'aimerais également remercier mes collègues du Laboratoire Informatique de Scoliose 3D (LIS3D), notamment Younes Madjouline, les frères Driscoll, Nadine Lalonde, Archana Sangole, Christian Bellefleur, pour les conseils qu'ils m'ont donnés et leur sens du travail d'équipe.

Je remercie les gens avec qui je vis.

Ce travail de recherche a été financé par l'Institut de recherche en santé du Canada (IRSC), le Conseil de recherches en sciences naturelles et en génie du Canada (CRSNG), et le Programme des chaires de recherche du Canada.

RÉSUMÉ

La scoliose est une déformation tridimensionnelle évolutive de la colonne vertébrale et de la cage thoracique. Pour des déformations modérées, le principal traitement utilisé est le traitement par corset. Son objectif est, à court-terme, de réduire les déformations scoliotiques et, à long-terme, d'en empêcher la progression. Toutefois le traitement par corset tel qu'il est effectué actuellement n'est pas optimal. La conception des corsets repose encore principalement sur des principes empiriques et l'expérience variée des orthésistes. Aucune étude, clinique ou numérique, n'a étudié directement l'effet des paramètres de conception d'un corset sur son efficacité. De nombreuses controverses existent encore de ce fait sur les paramètres de conception optimaux. De même, aucune étude, expérimentale ou numérique, n'a tenté de prouver que le traitement par corset permet de modifier favorablement les contraintes agissant sur les plaques de croissance d'un sujet scoliotique, démontrant ainsi de façon théorique l'efficacité du traitement à empêcher la progression des déformations.

L'objectif général de ce projet est donc d'étudier l'effet du design des corsets sur la correction immédiate des déformations scoliotiques et sur les contraintes agissant sur les plaques de croissance. L'hypothèse que nous souhaitons vérifier est que le traitement par corset peut annuler l'asymétrie des contraintes de compression s'exerçant sur les plaques de croissance à l'apex des courbures scoliotiques mais que cet effet est dépendant des paramètres de conception du corset, ce qui nécessite un ajustement optimal.

Cette étude a été divisée en cinq parties. Une méthode a tout d'abord été développée pour représenter les forces de gravité sur un modèle d'éléments finis (MEF) du tronc d'un patient scoliotique tout en respectant sa géométrie 3D. Un processus d'optimisation a permis de déterminer les forces à soustraire au MEF, dont la géométrie a été construite à partir d'une reconstruction 3D par radiographies biplanaires du patient, afin d'obtenir suite à l'application de la gravité un modèle correspondant à la géométrie réelle du patient. La différence entre la position 3D des vertèbres issue des radiographies et la position simulée des vertèbres du modèle EF après application de la gravité s'est avéré être inférieure à 3 mm. Les contraintes de compression et les moments d'inflexion latérale agissant sur les plateaux vertébraux ont été calculés. Il a été constaté que dans le plan frontal la concavité

des courbures scoliotiques était soumise à des contraintes de compression moyennes supérieures de 0.1 à 0.4 MPa à celles de la convexité.

Dans une deuxième partie, une méthode de simulation du traitement par corset intégrant la représentation des forces de gravité précédemment décrite a été développée. Afin de démontrer la faisabilité de l'approche, des corsets suivant les mêmes principes que le corset de Boston ont été conçus pour cinq patients scoliotiques et leurs installations simulées. Les corrections géométriques immédiates et les pressions à l'interface corset-tronc ont été calculées. L'effet du corset sur l'asymétrie des contraintes de compression agissant sur les plateaux vertébraux dans le plan frontal a été analysé. L'influence de la tension de courroie, de la flexibilité de la colonne vertébrale et de la présence des forces de gravité dans le modèle a été évaluée. Les résultats ont montré que la présence des forces de gravité était essentielle pour simuler de façon appropriée le traitement par corset. Une grande part de l'action biomécanique du corset est d'empêcher les courbures scoliotiques de ployer sous l'effet de la gravité. La correction des angles de Cobb dépendait de la tension de courroie et de la flexibilité spinale. La distribution et l'amplitude des pressions exercées par le corset virtuel étaient similaires à celles exercées par le corset réel des patients. Après installation du corset, l'asymétrie des pressions agissant sur les corps vertébraux dans le plan frontal était réduite de 96% en moyenne à l'apex thoracique et de 85% à l'apex lombaire.

Dans une troisième partie, le modèle a été adapté pour simuler le corset de Charleston, qui se porte la nuit et impose en position couchée une inflexion latérale au patient dans la direction de sa courbure scoliotique principale. Pour deux patients, des corsets virtuels ont été conçus et leur installation simulée. Leur efficacité a été étudiée en calculant les corrections géométriques immédiates et l'évolution des contraintes internes à la colonne vertébrale. La réduction de l'angle de Cobb de la courbure principale était comprise entre 58 et 97%, ce qui est en conformité avec les données disponibles dans la littérature. Des contraintes de compression allant jusqu'à 1 MPa ont été générées dans la convexité de la courbure principale et des contraintes de tension maximales d'1 MPa ont été générées dans sa concavité. Cependant, une augmentation de la compression dans la concavité de la courbure secondaire et de la tension dans sa convexité a été observée. Cette étude a confirmé le principe de fonctionnement du corset de Charleston tel qu'il était énoncé par ses concepteurs, soit d'inverser l'asymétrie des pressions s'exerçant sur les plateaux

vertébraux de la courbure principale dans le plan frontal. Il empire toutefois cette asymétrie pour la courbure secondaire.

Dans une quatrième partie, pour 3 patients présentant différents types de courbures scoliotiques, des corsets sur-mesure suivant les principes du corset de Boston ont été modélisés et leurs installations simulées. Pour chaque patient, deux flexibilités différentes de la colonne vertébrale ont été testées. L'influence de 15 paramètres de conception des corsets sur les corrections 3D immédiates a été évaluée grâce à un plan d'expériences permettant de calculer les effets principaux et d'interaction des différents facteurs. Un total de 12288 corsets ont ainsi été testés. Les résultats ont montré une grande variabilité de l'efficacité des corsets. Les facteurs les plus influents se sont avérés être la position de l'ouverture du corset (antérieure ou postérieure), la tension des courroies, la position de l'extension trochantérique, le profil sagittal du corset et la forme de la coque rigide dans le plan frontal. La position de l'ouverture du corset a modifié les mécanismes de correction du corset. La position de l'extension trochantérique a influencé l'efficacité des coussinets lombaires et thoraciques en modifiant leur bras de levier. Le profil de lordose du corset avait un impact sur la forme de la colonne vertébrale dans le plan sagittal mais pas dans le plan frontal.

Dans une cinquième partie, pour les 3 patients de l'étude précédente, 1024 différents corsets ont été testés et, pour chaque corset, la correction immédiate des angles de Cobb coronaux et le moment d'inflexion latérale agissant sur les vertèbres apicales ont été calculés et leur corrélation a été étudiée. Pour chaque patient, deux flexibilités différentes de la colonne vertébrale ont été testées. Les résultats ont montré que la correction immédiate des courbures coronales et le moment d'inflexion latérale au niveau des vertèbres apicales étaient fortement corrélés (R^2 = 0.88 en moyenne). Le niveau de correction immédiate nécessaire pour annuler le moment d'inflexion latérale variait entre 19 et 61% et valait en moyenne 48% pour le modèle de colonne flexible et 27% pour le modèle de colonne rigide. Cette étude a ensuite été étendu à 30 patients afin de renforcer ses conclusions et sa portée. La corrélation entre la correction immédiate des courbures coronales et le moment d'inflexion latérale au niveau des vertèbres apicales a été confirmée (R^2 = 0.86 en moyenne). Le niveau de correction immédiate nécessaire pour annuler l'asymétrie du chargement en compression sur les vertèbres apicales dans le plan frontal

variait entre 10 et 99% et valait en moyenne 49% pour le modèle de colonne flexible et 35% pour le modèle de colonne rigide. Dans le cadre du principe de modulation de croissance de Hueter-Volkmann, la corrélation entre la correction immédiate des courbures scoliotiques et la correction du moment d'inflexion latéral peut être interprétée comme une corrélation entre la correction immédiate et l'efficacité du traitement par corset à long-terme. Cela confirme l'importance de la correction immédiate d'un point de vue biomécanique. La règle empirique fréquemment utilisé par les orthésistes est de plus confirmée pour les courbures flexibles: une correction immédiate minimum de 50% est nécessaire pour stopper la progression des déformations scoliotiques. Cependant, pour les courbures rigides, la progression des déformations scoliotiques pourrait être potentiellement stoppée avec une correction immédate moindre (35%).

En conclusion, ce projet doctoral a permis de développer un modèle original et innovant. Les études réalisées grâce à ce modèle ont apporté une base théorique supplémentaire au traitement par corset permettant de mieux comprendre sa biomécanique. La contimuation de ce projet, qui devra encore intégrer diverses améliorations, pourra alors permettre éventuellement la conception de corsets plus performants et une amélioration du traitement pour les patients.

ABSTRACT

Scoliosis is defined as a three-dimensional deformity of the spine and rib cage. For moderate deformities, bracing is the most common treatment. Its aim is to reduce the scoliotic deformities in a short-term perspective and to prevent their progression in a long-term perspective. The brace treatment is however not optimal as it is practiced today. The braces design is mostly based on empirical principles and on the experience of the orthotists. The effects of the design parameters of a brace on its efficiency have never been studied, experimentally nor numerically. As a consequence, the optimal brace design parameters are still controversial. No study demonstrated that the brace treatment modifies favorably the stresses in the vertebral growth plates of a scoliotic patient, in order to prove thus that the brace treatment is theoretically efficient in preventing the scoliotic deformities from progressing.

The objective of this project was consequently to study the effect of the brace design on the immediate correction of the scoliotic deformities and on the spinal stresses. The hypothesis is that the brace treatment is able to nullify the asymmetry of the compressive stresses exerted on the growth plates at the apex of the scoliotic curves but this effect depends on the design parameters of the brace and an optimal adjustment is thus required.

This study was divided into 5 parts. A simulation process was firstly developed to represent the gravity forces in a finite element model (FEM) of the trunk of a scoliotic patient. An optimization process computed the forces to be substracted from the FEM, based on the 3D reconstruction of biplanar x-rays of the patient, in order to obtain after the inclusion of the gravity forces a model corresponding to the actual geometry of the patient. The difference in the vertebral positions from the geometry acquired from radiographs and the computed geometry of the model including the gravity forces was inferior to 3 mm. The forces and compressive stresses in the scoliotic spine were then computed. An asymmetrical load in the coronal plane, particularly at the apices of the scoliotic curves, was present. Difference of mean compressive stresses between concavity and convexity of the scoliotic curves ranged between 0.1 and 0.4 MPa.

In a second part, a method to simulate brace treatment including the representation of gravity forces previously described was developed. To show the feasibility of the approach, custom-fit braces following the Boston brace system principles were designed for five scoliotic patients and their installations were simulated. Immediate geometrical corrections and pressures generated by the brace were computed. The brace's effect on the asymmetrical compressive loading of the vertebral endplates in the coronal plane was analyzed. The influence of the strap tension, of the spine stiffness and of the presence of the gravity forces was evaluated. Results showed that the presence of the gravity forces is essential to adequately simulate brace treatment. A major part of the brace biomechanical action is to prevent the scoliotic spine from bending under the gravity forces. Correction of coronal curves Cobb angles depended on the tensions of the straps and on the spine stiffness. The distribution and amplitude of pressures computed for the virtual brace were similar to those measured with the real brace of the patients. After the brace installation, the asymmetrical compressive loading on the vertebral endplates was reduced by 96% on average at the thoracic apex and by 85% at the lumbar apex.

The brace model was in a third part adapted to simulate the Charleston brace, which is worn over the night and imposes a supine side-bending to the patient in the direction of its major scoliotic curve. Braces were designed for two scoliotic patients and their installation was simulated. The efficiency of the simulated Charleston braces was studied by computing the geometrical corrections and the effect on the internal stresses of the spine. The reduction of the major scoliotic curve varied between 58% and 97% and was in the range of published clinical data. Internal compressive stresses of up to 1 MPa were generated on the convex side of the major scoliotic curve and tensile stresses up to 1 MPa on its concavity. However, increased compressive stresses were exerted on the concavity of the secondary curves and added tensile stresses in their convexity. The study confirmed the working principle of the brace assumed by its designers, which consists in inverting the asymmetrical compressive loading at the level of the major scoliotic curve. It also highlighted a shorthcoming of the supine side-bending principle which is to worsen the asymmetrical compressive loading in the compensatory curves.

In the fourth part, for three patients presenting different types of scoliotic curves, custom-fit braces following the Boston brace system principles were modeled and their installations

simulated. Two sets of mechanical properties of the spine (stiff and flexible) were tested. The influences of 15 design factors on the 3D correction generated by the brace were evaluated following a design of experiments simulation protocol allowing computing the main and two-way interaction effects of the design factors. A total of 12,288 different braces were tested. Results showed a great variability of the braces effectiveness. The most influential design factors were the position of the brace opening (posterior vs anterior), the strap tension, the trochanter extension side, the lordosis design and the rigid shell shape. The position of the brace opening modified the correction mechanism. The trochanter extension position influenced the efficiency of the thoracic and lumbar pads by modifying their lever arm. Increasing the strap tension improved corrections of coronal curves. The lordosis design had an influence in the sagittal plane but not in the coronal plane.

In the fifth part, for the same three patients of the precedent study, 1024 different virtual braces were tested and, for each brace, immediate in-brace correction of the coronal Cobb angles and the bending moment acting on the apical vertebrae were computed and their correlation was studied. Two sets of mechanical properties of the spine (stiff and flexible) were tested. Immediate correction of coronal curves and corresponding impact on the apical vertebrae bending moments were linearly correlated (mean $R^2 = 0.88$). The amount of immediate correction necessary to nullify the bending moment ranged between 19% and 61% with average 48% (flexible spine model) and 27% (stiff spine model). This study was then extended to a total of 30 patients in order to reinforce its conclusions. The correlation between immediate correction of coronal curves and corresponding impact on the apical vertebrae bending moments was confirmed (mean $R^2 = 0.86$). 10% to 99% of immediate correction was necessary to nullify the asymmetrical loads, with an average of 49% (flexible spine model) and 35% (stiff spine model). In the framework of the Hueter-Volkmann principle, the correlation between coronal immediate in-brace correction and corresponding apical bending moment can be interpreted as a correlation between immediate in-brace correction and long-term treatment outcome. It confirms biomechanically the importance of the immediate in-brace correction. Moreover, for the flexible spines, the rule-of-the thumb frequently adopted by orthotists was confirmed. A 50% immediate correction was found to be necessary for long-term brace effectiveness.

However, for stiff spines, it was possible to prevent curve progression with less immediate correction (35%).

In conclusion, this Ph.D. project allowed the development of an original and innovative model. The studies that were done using this model have brought an additional theoretical basis to the brace treatment, enabling thus a better understanding of its biomechanics. The prolongation of this project, that should still integrate some improvements, will hopefully lead to the design of more performant braces and to a better treatment for the patients.

TABLE DES MATIÈRES

LISTE DES TABLEAUX

LISTE DES FIGURES

LISTE DES SIGLES ET ABRÉVIATIONS

3D	Tridimensionnel
CT	Costo-transverse
CV	Costo-vertébral
CVCT	Costo-vertébral et costo-transverse
DLT	Direct Linear Transformation
L1 à L5	Première à la cinquième vertèbre lombaire
MEF	Modèle éléments finis
mm	Millimètre
mm^2	Millimètre carré
MPa	Méga Pascal
N	Newton
T1 à T12	Première à la douzième vertèbre thoracique
TLSO	Thoraco-Lombo-Sacral Orthèse
S1	Première vertèbre sacrale

INTRODUCTION

La scoliose idiopathique est une déformation tridimensionnelle évolutive de la colonne vertébrale, de la cage thoracique et du bassin. Pour des déformations modérées, le principal traitement utilisé est le traitement par corset. Son objectif est d'appliquer des forces sur le tronc d'un patient afin de réduire au maximum ses déformations scoliotiques et d'empêcher leur progression.

Toutefois, les principes biomécaniques du traitement restent mal compris. La conception des corsets repose encore principalement sur des principes empiriques. De ce fait, de nombreuses incertitudes existent encore sur les paramètres de conception optimaux. De plus, l'effet biomécanique du traitement par corset sur les processus à l'œuvre dans la progression des déformations scoliotiques reste un sujet d'étude insuffisamment exploré.

Par conséquent, ce projet doctoral a visé à étudier l'effet de différents paramètres de conception des corsets sur la correction immédiate des déformations scoliotiques et sur les contraintes rachidiennes impliquées dans les processus d'évolution des déformations scoliotiques.

Cette thèse se divise en huit chapitres. La figure 0.1 à la page suivante décrit son organisation. Suite à une revue de la littérature pertinente, la problématique et les objectifs du projet seront définis. Ces objectifs seront réalisés à l'aide de 5 articles présentés dans les chapitres 3 à 7. La thèse se termine par une discussion générale du projet et une conclusion.

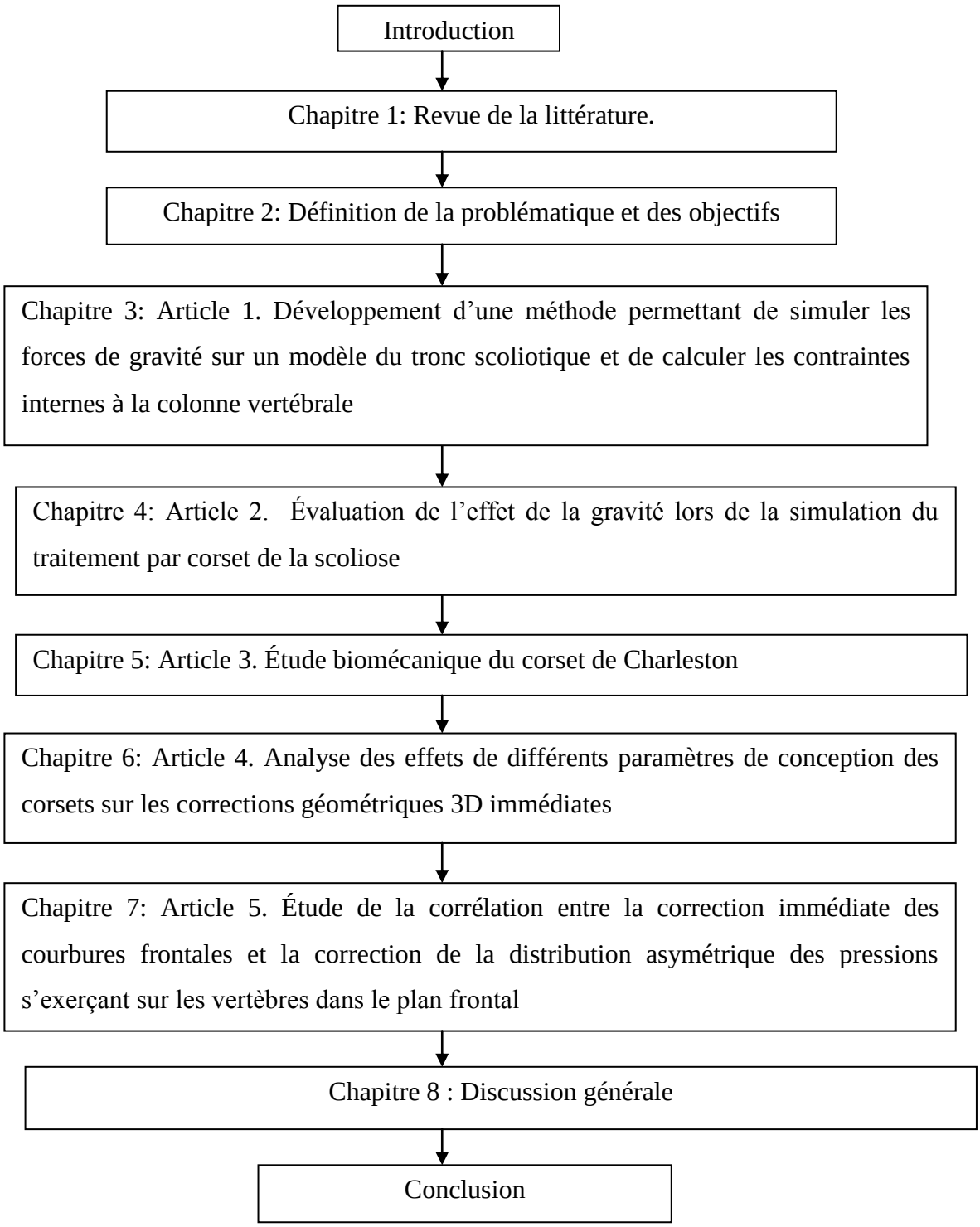

Figure 0.1: Organisation de la thèse

CHAPITRE 1. REVUE DES CONNAISSANCES

1.1 Anatomie du tronc humain

Le rachis est composé de cinq parties (figure 1.1):

- Le rachis cervical qui comprend 7 vertèbres cervicales (C1 à C7).
- Le rachis thoracique qui comprend généralement 12 vertèbres thoraciques (T1 à T12).
- Le rachis lombaire qui comprend généralement 5 vertèbres lombaires (L1 à L5).
- Le sacrum qui comprend 5 vertèbres sacrées soudées entre elles (S1 à S5).
- Le coccyx qui comprend 4 à 5 vertèbres soudées entre elles.

La colonne vertébrale saine est rectiligne dans le plan frontal mais présente 4 courbures distinctes dans le plan sagittal : une lordose cervicale, une cyphose thoracique, une lordose lombaire et une cyphose sacrée.

Les vertèbres comportent deux parties distinctes (figure 1.2). La partie antérieure est constituée par un bloc osseux et massif, le corps vertébral. Dans la partie postérieure, on trouve l'arche neurale qui est composée de deux pédicules et de deux lames formant le canal vertébral, qui a pour fonction de protéger la moelle épinière. Au niveau postérieur de l'arche neurale se détache l'apophyse épineuse. Les vertèbres thoraciques possèdent au niveau antérieur des pédicules 4 facettes dites facettes costo-vertébrales (CV) et, au niveau des apophyses transverses, 2 facettes articulaires dites costo-transverses (CT). Ces facettes servent à établir la liaison avec les côtes.

Au niveau antérieur, l'articulation entre les corps vertébraux se réalise par l'intermédiaire des disques intervertébraux et des ligaments longitudinaux antérieurs et postérieurs. Au niveau postérieur, on trouve le ligament jaune qui relie les lames vertébrales, les ligaments intertransverses qui relient les apophyses transverses, les ligaments surépineux et interépineux qui relient les apophyses épineuses et le ligament capsulaire qui contribue à la

liaison des facettes zygapophysaires inférieures et supérieures de deux vertèbres consécutives.

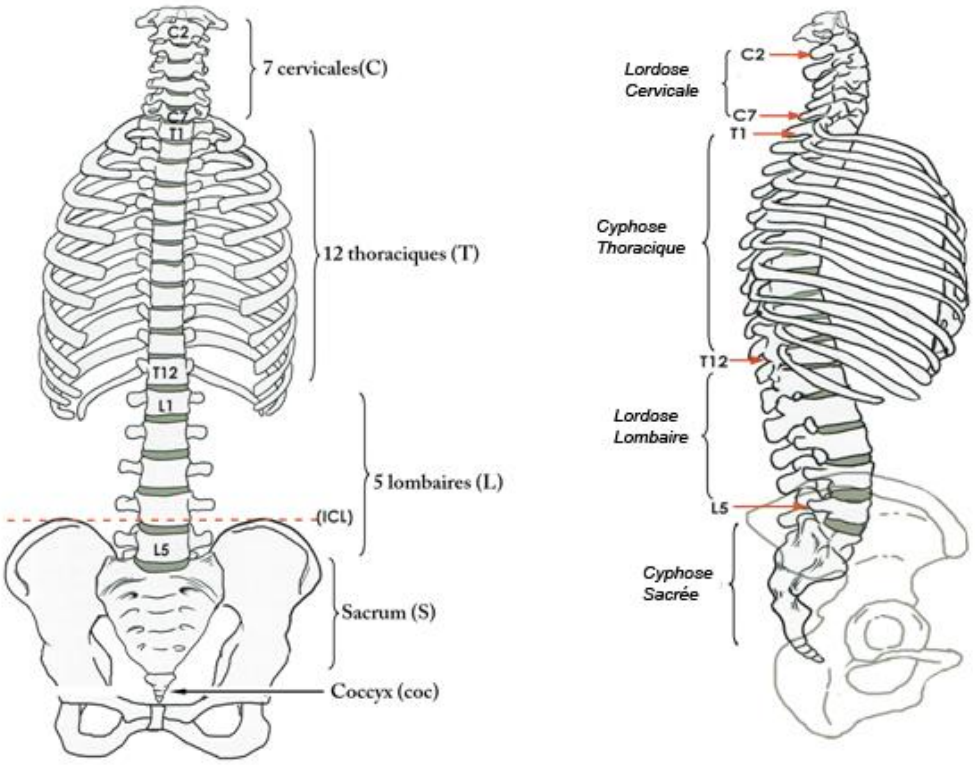

Figure 1.1: Le rachis (Radiographic Measurement Manual, autorisé par Medtronic)

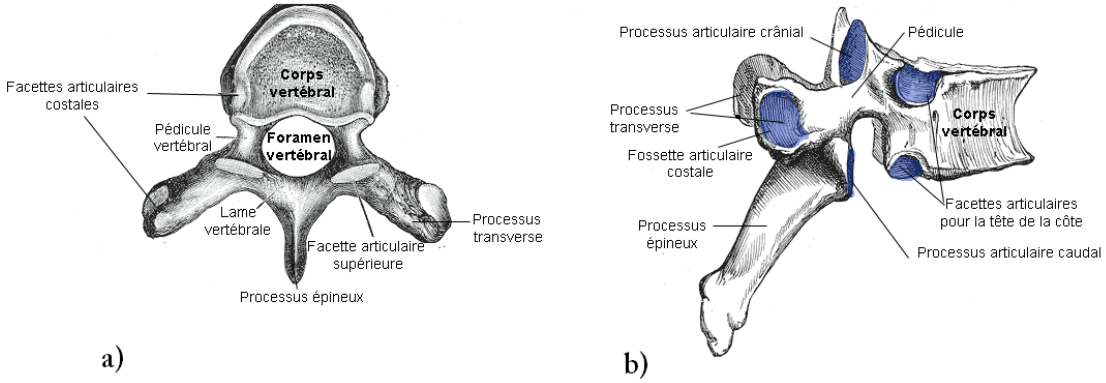

Figure 1.2: Structure d'une vertèbre: a) vue de dessus b) vue latérale (adapté de White, 1990)

À la structure du rachis vient se coupler la cage thoracique. On y distingue trois grands sous-ensembles : les côtes, les cartilages costaux et le sternum. On dénombre 12 côtes : 7 vraies côtes (côtes 1 à 7) qui sont reliées au sternum directement par les cartilages costaux, 3 fausses côtes (côtes 8 à 10) dont les cartilages costaux fusionnent avant de se lier au sternum et 2 côtes flottantes (côtes 11 et 12) dont les extrémités sont libres.

À son extrémité inférieure, la colonne vertébrale établit une liaison avec le bassin, par l'intermédiaire du sacrum. Le bassin se divise en trois parties. Les 2 os de la hanche (ou os coxal) qui sont reliés entre eux par la symphyse pubienne au niveau antérieur et par le sacrum au niveau postérieur. Les os coxaux sont délimités à leur extrémité supérieure par les crêtes iliaques.

1.2 La scoliose idiopathique adolescente

La scoliose se définit comme une déformation pathologique tridimensionnelle de la colonne vertébrale, de la cage thoracique et du bassin. Cette maladie apparaît généralement durant l'adolescence (période de croissance) et touche principalement les filles (90 % des cas) (Rogala, 1978; Roach, 1999). Dans la grande majorité des cas, la scoliose est idiopathique (sa cause est inconnue). Elle touche environ 5 personnes sur 1000 et 10 % des malades nécessiteront un traitement (Rogala, 1978; Roach, 1999).

Les composantes de la déformation scoliotique sont multiples : on a tout d'abord une déviation latérale du rachis dans le plan frontal entraînant l'apparition de courbures pathologiques (figure 1.3). L'apparition de courbures dans le plan frontal peut de plus entraîner un déplacement latéral de la vertèbre T1 par rapport à sa position normale (située à la verticale de S1) (figure 1.3). La scoliose peut ainsi se traduire par un déséquilibre global du rachis. La mesure de la déviation latérale de T1 est appelée 'déjettement '.

Figure 1.3: Courbures frontales et déjettement

À ces modifications des courbures du rachis se superpose une rotation dans le plan transverse (rotation axiale) des vertèbres scoliotiques. Le corps vertébral des vertèbres scoliotiques s'oriente vers la convexité de la courbure scoliotique (figure 1.4: B). Le sens de la rotation axiale des vertèbres scoliotiques est pathologique, puisque que pour un sujet sain en inflexion latérale on observe également une rotation axiale des vertèbres, mais alors le corps vertébral s'oriente vers la concavité de la courbure du rachis (figure 1.4: A).

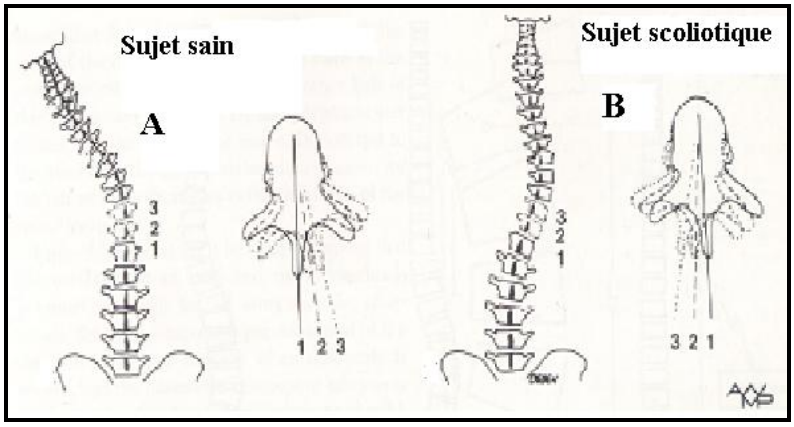

Figure 1.4: Rotation axiale d´une vertèbre scoliotique (White, 1990)

Les sujets scoliotiques présentent également une déformation des côtes : c'est la 'gibbosité' (figure 1.5). Les côtes subissent un déplacement postérieur du côté convexe de la courbure scoliotique, et un déplacement antérieur du côté concave. Elles se rapprochent les unes des

autres et sont plus horizontales du côté concave de la courbure tandis qu'elles s'éloignent les unes des autres et sont plus inclinées du côté convexe.

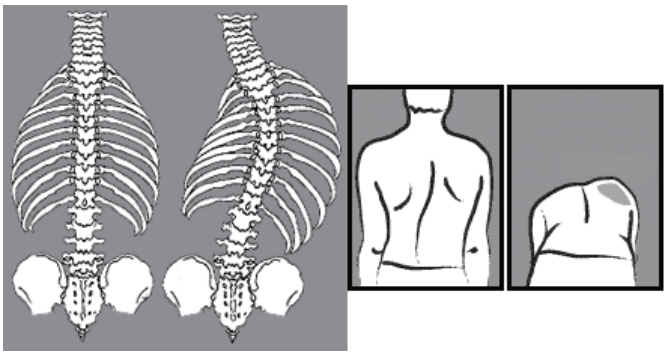

Figure 1.5: La gibbosité (White, 1990)

Toutefois, les déformations scoliotiques ne sont pas seulement globales, la structure même des vertèbres scoliotiques est modifiée. Ainsi les plateaux supérieurs et inférieurs ne sont pas parallèles. La vertèbre prend donc la forme d'un coin (cunéiformisation, figure 1.6). Un certain nombre de déformations sont également observées dans le plan transverse. On a une déviation de l'apophyse épineuse et des apophyses transverses. La largeur du pédicule du côté concave de la courbure diminue (Parent, 2004).

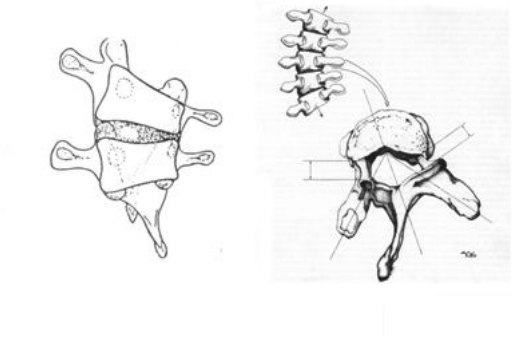

Figure 1.6: Déformations locales des vertèbres (White, 1990)

La scoliose est une maladie évolutive. Les déformations scoliotiques peuvent progresser dans le temps, particulièrement lors de la poussée de croissance pubertaire. La théorie du cercle vicieux explique cette progression d'un point de vue biomécanique (Roaf, 1960; Stokes, 2007; Villemure, 2004). Les déformations scoliotiques entraînent l'apparition de pressions asymétriques sur les plaques de croissance vertébrales, ce qui, selon le principe

de Hueter-Volkmann (une augmentation de compression ralentit la croissance, une augmentation de tension accélère la croissance), génère une croissance asymétrique des vertèbres et une aggravation des déformations scoliotiques.

1.3 Traitement de la scoliose par corset orthopédique

1.3.1 Principes généraux

On distingue communément deux types de traitement pour la scoliose : le traitement par corset orthopédique et le traitement chirurgical. Le traitement par corset s'applique aux patients dont les déformations restent modérées (angle de Cobb compris entre 20 et 40 degrés), tandis que le traitement chirurgical s'applique aux cas plus graves (angle de Cobb supérieur à 40 degrés) (Emans, 1986).

L'objectif des corsets orthopédiques est de stopper la progression des déformations scoliotiques, et si possible de réduire l'amplitude de ces déformations. Pour ce faire, leur principe d'action est d'appliquer une combinaison de forces au niveau de la surface externe du tronc, ces efforts se transmettant ensuite au rachis par l´intermédiaire de la peau, de la couche musculaire sous-jacente, de l'abdomen et de la cage thoracique. Les efforts ainsi exercés par le corset doivent alors permettre une réduction maximale des déformations scoliotiques (dans l'idéal, de toutes les déformations et pas seulement des courbures pathologiques du rachis).

La correction des déformations scoliotiques par application de forces externes sur le tronc est appelée processus de correction «passive». Les corsets engendreraient toutefois un autre processus de correction : la correction «active». Le patient, dans son corset, tendrait à fuir les zones de pression qui lui sont imposées, mettant ainsi à contribution son système musculaire. Il opèrerait ainsi un redressement actif de sa colonne vertébrale. La contribution relative de ces deux processus de correction, passif et actif, reste cependant peu connue. Wynarsky (1987) n'a pas trouvé de différence significative entre les activités musculaires de patients sans corset et avec corset. Odermatt (2003), avec un plus grand nombre d'électrodes réparties sur les régions thoracique, lombaire et abdominale, a cependant trouvé une augmentation significative de l'activité musculaire lorsque les patients portent le corset, notamment au niveau lombaire.

1.3.2 Exemples de différents corsets

Dans cette section seront décrits les différents types de corsets utilisés actuellement pour le traitement de la scoliose idiopathique. Nous profiterons de cette description pour expliciter leurs principes d'action fondamentaux et souligner les différences existant au niveau de leur conception.

Les corsets existent depuis très longtemps. Des corsets en acier étaient déjà fabriqués au moyen-âge. Mais le premier corset de l'ère moderne est le corset de Milwaukee (figure 1.7).

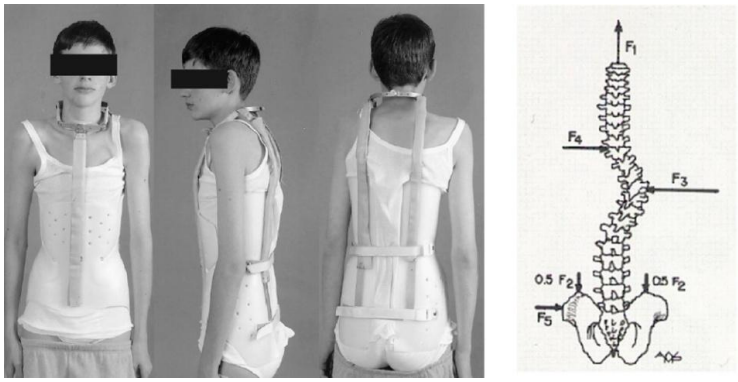

Figure 1.7: Le corset de Milwaukee (Lonstein, 1994; White, 1990)

Ce corset est un corset CTLSO (cervico-thoraco-lumbar-sacral-orthosis). Il comporte en effet un appui pelvien pour se stabiliser sur le bassin (élément commun à tous les corsets) et une superstructure composée de deux tiges métalliques postérieures et d'une tige métallique antérieure qui relient l'appui pelvien à un appui cervical. La présence de cet appui cervical permet d'exercer une force de traction sur la colonne (figure 1.7, forces F1 et F2). Sur cette superstructure sont ensuite accrochés des coussinets afin d'exercer un système de trois points de force (figure 1.7, forces F3, F4, F5). Ce système de trois points de force (une force correctrice au niveau de l'apex de la courbure, deux forces stabilisatrices aux limites supérieures et inférieures de la courbure) est le principe fondamental de correction utilisé par les corsets.

Le corset de Milwaukee est aujourd'hui conçu de façon à exercer une correction à la fois active et passive de la colonne vertébrale. Lonstein (2003) affirme qu'il est le seul corset nord-américain à être efficace pour la correction des courbures thoraciques hautes. Toutefois, le problème majeur du corset de Milwaukee réside dans son aspect cosmétique

qui peut entraîner un mauvais suivi du traitement par le patient ou même un refus de ce traitement (Lonstein, 2003).

Pour palier à ce problème ont été créés les corsets TLSO (thoraco-lumbar-sacral-orthosis). Ils ne possèdent pas d'appui cervical comme le corset de Milwaukee. Leur limite supérieure est l'aiselle. Parmi ces corsets, l'un des plus utilisés en Amérique du Nord est le corset de Boston (figure 1.8). Son concept de base est une gamme de modules standards, symétriques, de tailles prédéfinies, adaptés au type de courbure scoliotique à corriger. L'ouverture est postérieure. La présence de deux ou trois courroies postérieures (une au niveau pelvien et une ou deux aux niveaux thoracolombaire et thoracique) permet de refermer le corset sur le patient. A partir de la gamme proposée, l'orthésiste choisit alors le corset le plus approprié à son patient puis détermine, à l'aide des radiographies notamment, les lieux d'application des forces correctrices et stabilisatrices afin d'ajouter des coussinets à l'intérieur du corset. Des fenêtres sont découpées à l'opposé des coussinets pour favoriser le processus de correction actif. La figure 1.8 montre l'emplacement de ces coussinets correcteurs et stabilisateurs pour une scoliose lombaire gauche - thoracique droite

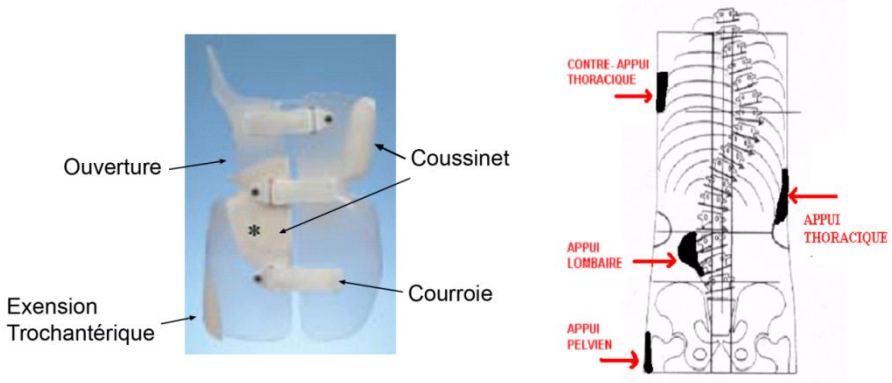

Figure 1.8: Le corset de Boston (Emans, 2003)

Les autres corsets TLSO se basent globalement sur des principes similaires. On peut toutefois relever quelques différences. Ainsi le corset de Chêneau, très populaire en Europe, n'est pas conçu à partir d'un module symétrique (figure 1.9A). Sa coque est asymétrique par rapport au plan sagittal. De plus, son ouverture et ses courroies sont placées antérieurement.

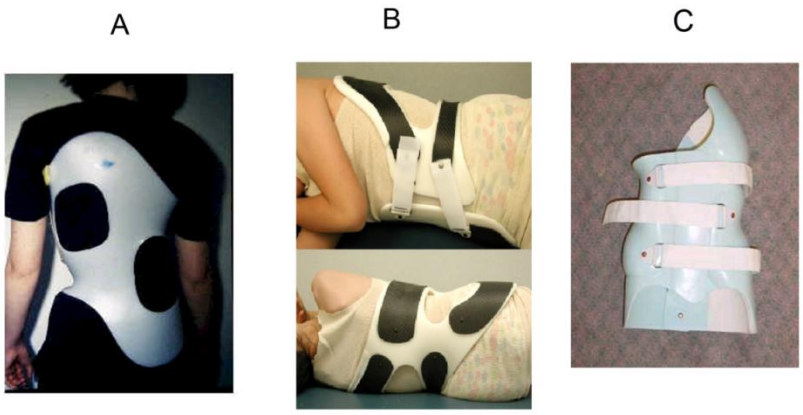

Figure 1.9: A) Corset de Chêneau; B) Corset Providence; C) Corset de Charleston

Les corsets de type Boston ou Chêneau se portent généralement à plein temps (23 heures par jour). Afin de réduire les contraintes liées à un tel régime et d'améliorer le suivi du traitement (D'Amato, 2001; Hooper, 2003; Price, 1997) des corsets destinés à être portés exclusivement la nuit ont été conçus, tel le corset de Providence (figure 1.9B) ou le corset de Charleston (figure 1.9C). Ce dernier se base sur un principe de correction des courbures scoliotiques différent de celui utilisé par les corsets précédemment décrits. En plus d'appliquer un système de trois points de forces, il impose au patient une inflexion latérale. Les raisons pour lesquelles l'inflexion latérale du patient pourrait favoriser le contrôle des courbures scoliotiques ne sont pas clairement comprises. Une des hypothèses avancées est que cette posture permettrait de réduire les contraintes pathologiques s'exerçant sur les vertèbres d'un rachis scoliotique (Hooper, 2003).

Les corsets décrits précédemment sont monocoques. Leur structure se base sur une coque rigide et continue. Mais il existe également des corsets dits souples, tel le corset SpineCor ou le corset TriaC (figure 1.10). Ces corsets sont généralement constitués de bandes élastiques et favorisent le principe de correction active des courbures. Leur avantage principal est d'être plus discrets à porter, plus esthétiques. Un meilleur suivi du traitement par le patient est donc espéré.

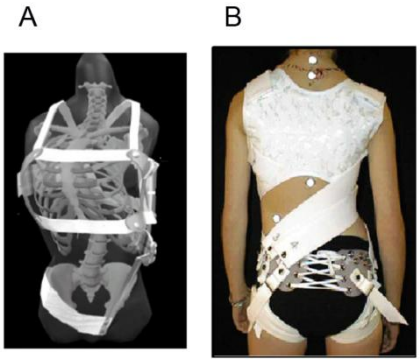

Figure 1.10: A Corset TriaC; B Corset SpineCor

1.3.3 Conception des corsets

Divers recommandations et analyses concernant la conception des corsets peuvent être recensées dans la littérature. Ainsi les concepteurs du corset de Boston (Emans, 2003) précisent à son propos :

- la symétrie du module de base doit permettre une correction «naturelle» des déformations asymétriques scoliotiques.
- le corset cherche à créer une hypolordose de la colonne lombaire, par flexion pelvienne et lombaire, afin de favoriser la correction des courbures lombaires frontales.
- les coussinets lombaires et thoraciques ne doivent pas être placés au dessus des apex lombaires et thoraciques mais au niveau et en dessous de ces apex.
- le coussinet lombaire doit être placé de façon à exercer une pression sur les muscles paraspinaux de la colonne lombaire, soit postérieurement.
- pour corriger la rotation axiale et la gibbosité, des coussinets doivent être placés postéro-latéralement et antéro-latéralement afin d'exercer des moments de dérotation.

Toutefois, certains de ces principes sont remis en cause dans la litérature. Ainsi Carlson (2003) a utilisé un modèle expérimental simple de patient scoliotique et a alors constaté qu'appliquer une force correctrice sur une côte supérieure à la côte apicale apportait une meilleure correction qu'une force correctrice située en dessous de l'apex. Le principe de flexion lombaire a été critiqué du fait de son effet négatif sur les courbures sagittales

(réduction de la lordose et de la cyphose) (Labelle, 1996). Différentes versions du corset de Boston présentant des flexions lombaires de différents degrés ont alors été proposées.

Afin d'étudier la variabilité des principes de conception de corsets, Rigo (2006) a demandé à 21 orthésistes de répondre à un questionnaire offrant différentes possibilités pour concevoir un corset pour un patient présentant une scoliose thoracique droite. Les avis se sont avérés divisés sur la position verticale optimale de la force correctrice principale au niveau thoracique (figure 1.11). Au niveau du plan transverse, la majorité des orthésistes recommandaient une force postéro-latérale mais différaient au niveau de la forme de coussinet appropriée pour générer cette force. La forme de la section pelvienne et la position du coussinet abdominal sont également très variées (figure1.11). Les orthésistes étaient divisés sur la nécessité d'un coussinet thoracique antérieur.

Le rôle de la tension des courroies a aussi été étudié. Une corrélation positive entre la tension de courroie et les forces exercées par le corset a été trouvée (Mac-Thiong, 2004). Mais l'existence d'une corrélation entre la tension de courroie et la réduction des courbures frontales reste controversée (Chase, 1989; Wong, 2000). Il faut toutefois souligner que les études sur ce sujet étudiaient une éventuelle corrélation au niveau global d'un groupe. Une étude de la correction où différentes tensions de courroie seraient testées sur un patient donné n'a jamais été menée. De même, l'effet de la tension de courroie sur les autres déformations scoliotiques tridimensionnelles (gibbosité, etc.) n'a jamais été évalué.

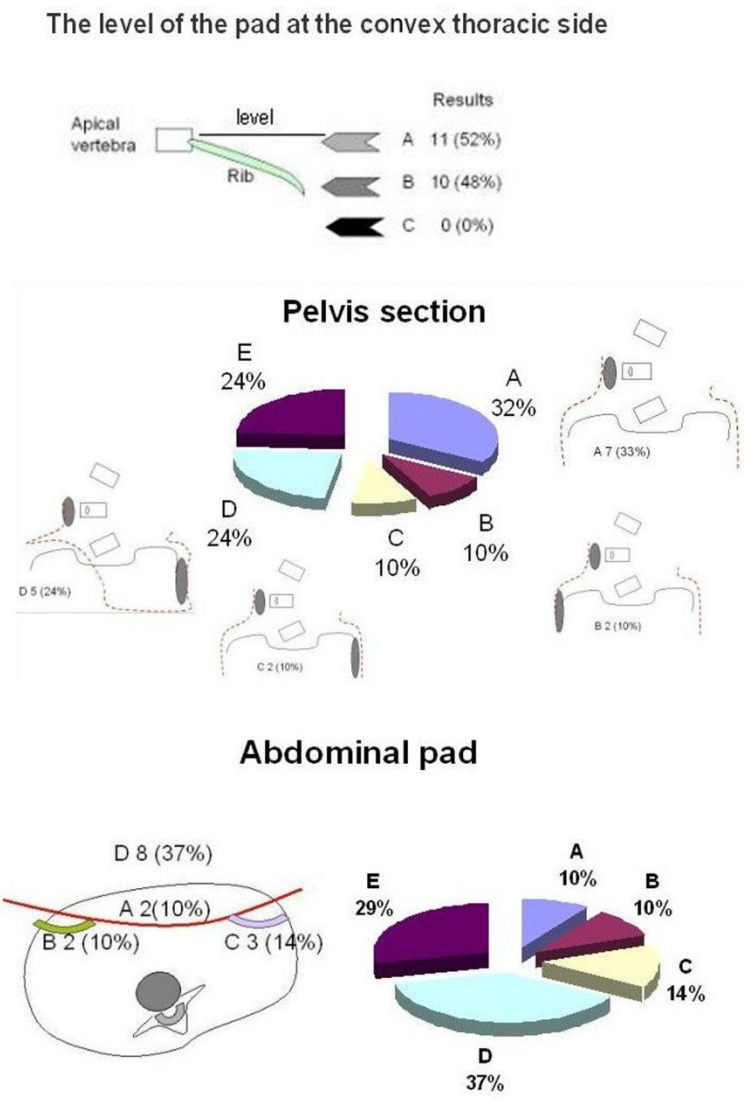

Figure 1.11: Variabilité de conception des corsets (Rigo (2006))

1.3.4 Efficacité du traitement par corset

Afin de décrire l'efficacité d'un corset, les angles de Cobb avant le port du corset et à la fin du traitement sont comparés. Si l'angle de Cobb n'a pas progressé de plus de 5 degrés durant cette période, on considère que le traitement est un succès. Suivant ce critère, il est généralement admis que le traitement par corset est plus efficace que l'observation seule (Nachemson, 1995; Rowe, 1997 ; Price, 1997, Périé, 2001; Daniellson, 2007 ; Coillard, 2007, Schiller, 2010). Toutefois, certains auteurs mettent encore en doute cette efficacité (Dickson, 1999; Goldberg, 2001; Noonan, 1996; Lonstein, 1994). Le point crucial est de

savoir si les corsets altèrent réellement l'histoire naturelle de progression des déformations scoliotiques. Ainsi Lonstein (1994) a observé 727 patients non-traités présentant des courbures dont l'angle de Cobb était compris entre 5 et 29° et a constaté que seul 23.2 % de ces courbures progressaient naturellement. Toutefois, Nachemson (1995) a comparé un groupe contrôle de 129 patients scoliotiques non-traités et de 111 patients traités par corset TLSO et a trouvé que 26 % des courbures traitées progressaient contre 66% pour les courbures non-traitées.

Limiter l'analyse de l'efficacité d'un corset à la réduction des courbures frontales peut cependant être considéré comme insuffisant, étant donné la nature tridimensionnelle des déformations scoliotiques. Labelle (1992, 1996) ont ainsi étudié l'effet immédiat tridimensionnel du corset de Boston et ont conclu qu'il réduisait effectivement les courbures dans le plan frontal mais qu'il n'avait pas d'effet significatif sur les rotations vertébrales, la gibbosité, le déjettement et qu'il réduisait la cyphose thoracique (effet négatif en cas d'hypocyphose). Korovessis (2000) et Willers (1993) ont étudié le comportement de ces paramètres tridimensionnels à long-terme et ont montré qu'à la fin du traitement, ils demeuraient au même niveau qu'avant le traitement. Ils concluent que les corsets empêchent la progression des déformations scoliotiques tridimensionnelles.

Des études ont de plus essayé de déterminer les facteurs ayant une influence significative sur l'issue à long-terme d'un traitement par corset. Il a été notamment remarqué que la correction initiale apportée par le corset se réduit progressivement au cours du traitement mais qu'une corrélation existait entre la correction initiale de l'angle de Cobb frontal et les chances de succès à long-terme du traitement (Emans, 1986; Katz, 1997; Olafsson, 1995; Upadhyay, 1995).

Il faut toutefois noter que seul l'effet des corsets sur l'évolution des déformations scoliotiques globales a été généralement étudié. À notre connaissance une seule étude (Castro, 2003) a tenté de prouver que le traitement par corset permettait de modifier l'évolution naturelle des déformations scoliotiques locale. Castro (2003) a mesuré la cunéiformisation des vertèbres apicales dans le plan frontal via le rapport : 'hauteur du corps vertébral du côté concave de la courbure / hauteur du corps vertébral du côté convexe de la courbure' avant le traitement par corset, à l'initiation du traitement par corset et à la fin du traitement pour 41 patients scoliotiques. Il a constaté que quand le traitement par corset permettait de stopper la progression des courbures frontales il permettait aussi de

stopper la progression de la cunéiformisation frontale. L'étude ne permet toutefois pas de distinguer les effets d'un réel processus de modelage/remodelage osseux et d'un simple processus de dérotation géométrique des vertèbres.

Aucune étude, expérimentale ou numérique, n'a été menée afin de prouver que le traitement par corset permet de modifier favorablement les efforts internes agissant sur les plaques de croissance. Les difficultés expérimentales reliées à une telle étude restent encore très importantes.

1.3.5 Simulations numériques du traitement par corset

Les études expérimentales sur l'effet des paramètres de conception des corsets sur l'efficacité de la correction des déformations scoliotiques restent limitées du fait qu'il est difficile d'exposer un patient plusieurs fois à des rayons X. Des modèles numériques ont donc été utilisés pour palier à ces limitations et mieux comprendre la biomécanique des corsets. La méthode généralement utilisée est de définir un modèle éléments finis (MEF) du tronc humain et d'appliquer directement sur ce modèle les forces exercées par le corset. Ainsi, Andriacchi (1976) a défini cinq modèles génériques de rachis scoliotiques et ont simulé l'effet immédiat du corset de Milwaukee sur ces rachis en appliquant les forces moyennes exercées par le corset telles que rapportées dans la littérature. Il a montré que le corset de Milwaukee était en théorie efficace pour corriger les courbures frontales.

Aubin (1996) et Périé (2003, 2004) ont simulé le traitement par corset de Boston de façon personnalisée. Pour ce faire, les géométries tridimensionnelles du rachis et de la cage thoracique d'un patient sans son corset et avec son corset ont été reconstruites. Lors de l'acquisition avec corset, une matrice de pression placée entre le tronc du patient et son corset a permis de mesurer les forces exercées sur le patient et de connaître leur localisation. L'effet immédiat du corset a alors été simulé en appliquant sur le modèle éléments finis du tronc humain les forces calculées précédemment. La déformée obtenue a été comparée à la géométrie du patient avec corset afin de valider la simulation. La différence moyenne entre la position des vertèbres du patient dans son corset réel et après simulation de ce corset était de 6 mm dans le plan frontal et de 8.8 mm dans le plan sagittal.

Utilisant la méthode d'application directe de forces sur un modèle éléments finis du tronc, des études d'optimisation du traitement par corset ont été menées. Wynarsky (1991) ont

recherché quelle est la localisation et l'amplitude optimale des forces passives exercées par un corset pour un patient présentant une scoliose thoracique droite. Ils ont ensuite recherché, indépendamment des forces passives, quels sont les muscles optimaux permettant de corriger activement cette scoliose. La fonction objectif était une fonction pondérée incluant la position sagittale et frontale des vertèbres ainsi que leurs rotations axiales et frontales. Au niveau des forces, les résultats obtenus sont globalement en accord avec les principes d'action des corsets classiques : force thoracique sur la convexité de la courbure au niveau de l'apex (T7, T8, T9, T10), contre-appui au niveau thoracique gauche (T5, T6) et contre-appui au niveau lombaire gauche (L2, L4). La correction de l'angle de Cobb de la courbure thoracique droite obtenue avec ces forces optimales était de 50%. De même, l'action optimale des muscles (sans présence de forces) ont permis d'obtenir une correction de 57 %.

L'optimisation de Wynarsky s'est effectuée sur un modèle non-personnalisé représentant un seul type de scoliose. De plus, dans le plan sagittal, le processus d'optimisation cherchait seulement à maintenir les courbures de la colonne initiale. Afin de dépasser ces limitations, Gignac (2000) ont utilisé un modèle éléments finis personnalisé du rachis et de la cage thoracique de 20 patients atteints de scolioses thoracique droite – lombaire gauche. Ils ont recherché la localisation et l'amplitude optimale des forces correctrices d'un corset pour chacun de ces patients. La fonction objectif est une fonction pondérée incluant la position sagittale et frontale des vertèbres ainsi que la gibbosité. Une colonne sagittale 'optimale' a été définie à partir d'une banque de données de patients sains. Les forces optimales trouvées se situent sur la convexité des courbures. Même avec les forces optimales, la correction moyenne des courbures s'est avérée faible, de même que la correction des rotations vertébrales, de l'angle du plan de déformation maximale et de la gibbosité.

L'étude de Gignac fait suite à une étude préliminaire d'Aubin (1997) sur le couplage biomécanique entre la colonne vertébrale et la cage thoracique. Pour une courbure thoracique droite, les effets d'une force latérale sur la convexité du thorax, d'une force antérieure sur la gibbosité et d'une force antéro-latérale ont été comparés. La force antérieure permet de réduire la gibbosité et la rotation axiale mais aggrave la déviation latérale des vertèbres et réduit la cyphose thoracique. La force latérale réduit la déviation latérale des vertèbres, ne modifie pas les courbures sagittales, mais aggrave la gibbosité et

la rotation axiale. La force antéro-latérale combine l'effet des deux forces précédentes. Aubin souligne tout particulièrement l'effet hypocyphosant de la force antérieure du coussinet thoracique.

Une autre étude utilisant une approche différente a été menée par Patwardhan (1986). Il a considéré que le rachis scoliotique pouvait être assimilé à une poutre en flambage (poutre en situation d'instabilité), a appliqué des forces correspondant au traitement par corset et a évalué l'effet de ces forces sur la stabilité du rachis. Il a trouvé que le traitement par corset augmentait la stabilité du rachis scoliotique, que les forces correctrices devaient se situer en dessous de l'apex des courbures et que plus la courbure était grande, plus il était difficile d'améliorer sa stabilité.

Simuler l'installation d'un corset en appliquant des forces directement sur un modèle du tronc possède des limites. Les forces appliquées ne sont pas nécessairement en équilibre (somme nulle) contrairement à celles appliquées par un corset réel. Les forces de réaction au niveau des conditions limites sont alors nécessaires pour équilibrer le modèle. Divers paramètres, comme la tension de courroies, la forme des coussinets, la géométrie de la coque rigide, ne peuvent pas être étudiées. Une nouvelle approche, consistant à créer explicitement un modèle éléments finis du corset afin de simuler son action correctrice de façon directe et non plus par simple application de forces, a donc été introduite. Lacroix (2003) et Périé (2004) ont ainsi modélisé le corset de Boston. Pour un patient donné, la géométrie personnalisée du corset est obtenue à partir de la reconstruction 3D de la matrice de pression que porte le patient lors des radiographies avec corset. Pour modéliser l'interface corset-patient, des éléments de contact ont été créés sur la surface interne du corset et sur les tissus mous du modèle du tronc. La simulation se déroule alors en deux étapes : on ouvre le corset en lui imposant des déplacements afin qu'il englobe complètement le patient puis on impose les déplacements inverses pour simuler la fermeture du corset sur le patient. On obtient au final la géométrie du patient après correction. On peut alors comparer cette géométrie à la géométrie réelle du patient avec corset pour valider la simulation.

Clin (2005, 2007) a raffiné cette méthode en introduisant un modèle paramétrique de corset incluant ses différentes composantes (coque externe rigide, coussinets, ouvertures). Le processus de simulation a été amélioré en refermant le corset à l'aide des forces exercées

par les courroies et non plus par des déplacements. Le phénomène de stabilisation du corset sur le patient a ainsi pu être modélisé.

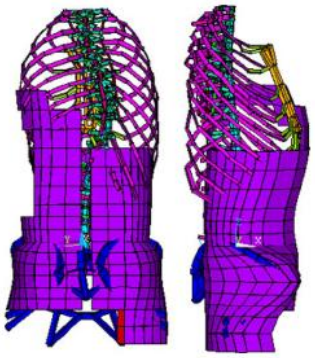

Figure 1.12: Modèle de Clin (2005)

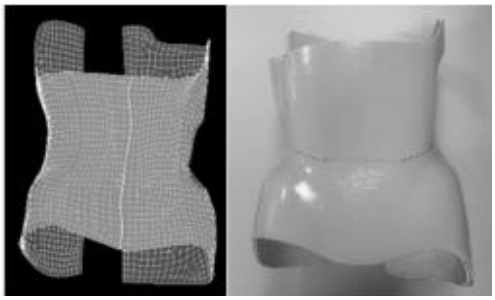

Figure 1.13: Modèle de Liao (2007)

Liao (2007) a également modélisé explicitement le corset de Boston d'un patient. Les pressions exercées par le corset sur le patient ont été mesurées grâce à une matrice de pression. Un algorithme d'optimisation topologique a alors permis de modifier la coque rigide du corset virtuel modélisé en enlevant certaines parties superflues (qui n'exercent pas de pressions sur le patient). Un corset réel a alors été fabriqué à partir de ce corset virtuel optimisé. Son effet a été comparé au corset initial. Tout en étant 12% plus léger, le corset optimisé générait les mêmes corrections que le corset initial. Toutefois, si l'étude de Liao utilise un modèle de corset, aucune simulation de l'installation du corset sur le patient n'est effectuée, contrairement à Périé (2004) et Clin (2007).

Aucune des méthodes de simulation du traitement par corset développées jusqu'à présent n'a tenté d'évaluer l'effet du corset sur les efforts internes à la colonne vertébrale, et en

particulier l'effet sur la distribution des contraintes de compression agissant sur les plaques de croissance vertébrale. Différentes études (Carrier, 2003, 2004) ont déjà abordé cette problématique mais elles portaient sur d'autres traitements que le traitement par corset.

CHAPITRE 2. PROBLÉMATIQUE ET OBJECTIFS

La revue de la littérature permet de dégager un certain nombre de problématiques reliées au traitement par corset :

1) Le traitement par corset tel qu'il est effectué actuellement n'est pas optimal. La correction des déformations se fait principalement dans le plan frontal au détriment des autres plans de l'espace.

2) La conception des corsets repose encore principalement sur des principes empiriques et sur l'expérience des orthésistes. Aucune étude, clinique ou numérique, n'a étudié directement l'effet des paramètres de conception d'un corset sur son efficacité. De nombreuses incertitudes existent encore de ce fait sur les paramètres de conception optimaux.

3) Aucune étude, expérimentale ou numérique, n'a tenté de démontrer que le traitement par corset permet de modifier favorablement les contraintes agissant sur les plaques de croissance d'un sujet scoliotique, démontrant ainsi l'efficacité théorique du traitement à empêcher la progression des déformations.

L'objectif général de ce projet est d'étudier l'effet du design des corsets sur la correction immédiate des déformations scoliotiques **et** sur les contraintes agissant sur les plaques de croissance (interprétation de l'effet à long-terme).

L'hypothèse principale de recherche que nous souhaitons vérifier est que le traitement par corset peut annuler l'asymétrie des contraintes de compression s'exerçant sur les plaques de croissance à l'apex des courbures scoliotiques mais que cet effet est dépendant des paramètres de conception du corset, ce qui nécessite un ajustement optimal.

Quatre objectifs spécifiques sont proposés :

Objectif 1 : Développer une méthode permettant de représenter adéquatement la gravité sur un modèle de tronc scoliotique et calculer les contraintes agissant sur les vertèbres.

Objectif 2 : Améliorer la méthode de simulation du traitement par corset développée dans notre équipe afin de l'adapter à une étude détaillée de l'effet des paramètres de conception d'un corset sur les corrections géométriques immédiates générées par le traitement et sur les contraintes internes à la colonne vertébrale.

Objectif 3 : Simuler grâce au modèle obtenu les traitements par corset de Boston et corset de Charleston et évaluer leurs effets sur les contraintes internes à la colonne vertébrale.

Objectif 4 : Évaluer l'effet de différents paramètres de conception sur les corrections géométriques générées et sur les contraintes agissant dans le rachis.

Ces objectifs ont été réalisés à l'aide de 5 articles (voir figure 0.1). Le premier objectif a été réalisé à l'aide de l'article 1 présenté au chapitre 3. Les objectifs 2 et 3 ont été réalisés dans les chapitres 4 et 5. Dans le chapitre 4, l'article 2 présente le modèle permettant de simuler le corset de Boston. Dans le chapitre 5, l'article 3 présente le modèle permettant de simuler le corset de Charleston. Le dernier objectif est réalisé à l'aide de 2 articles présentés aux chapitres 6 et 7. L'article 4 étudie l'influence des paramètres de conception des corsets sur les corrections géométriques 3D (chapitre 6). L'article 5 analyse la corrélation entre la correction immédiate des courbures frontales et la correction de la distribution asymétrique des pressions s'exerçant sur les vertèbres dans le plan frontal (chapitre 7).

CHAPITRE 3. MODÉLISATION DES FORCES DE GRAVITÉ ET CALCUL DES EFFORTS INTERNES SUR LE RACHIS D'UN MODÈLE DU TRONC SCOLIOTIQUE

3.1 Situation du premier article

Le premier article porte sur le développement d'une méthode pour représenter la gravité sur un modèle du tronc scoliotique. Un algorithme d'optimisation est utilisé afin d'inclure les forces de gravité tout en respectant la géométrie du patient telle qu'acquise par les radiographies. Les contraintes internes au rachis scoliotique sont également calculées et interprétées. Une visualisation de ces contraintes a pu être effectuée grâce à l'intégration dans le modèle d'éléments poutres de nouvelle génération. Ces éléments poutres possèdent des nœuds internes qui permettent le calcul explicite des contraintes au sein de leur section et un affichage volumique tridimensionnel.

Cet article est intitulé :« A new method to include the gravitational forces in a finite element model of the scoliotic spine », et a été soumis pour publication à la revue Medical and Biologocal Engineering and Computing en Janvier 2010. La contribution du premier auteur à la préparation et la rédaction de l'article est évaluée à 85%.

3.2 Article #1: A new method to include the gravitational forces in a finite element model of the scoliotic spine

A new method to include the gravitational forces in a finite element model of the scoliotic spine

Julien Clin[1,2], Carl-Éric Aubin[1,2], Nadine Lalonde[1,2], Stefan Parent[2], Hubert Labelle[2]

1- Dept. of Mechanical Engineering, École Polytechnique de Montréal

P.O. Box 6079, Station Centre-ville

Montréal, Québec, H3C 3A7, Canada

2- Sainte-Justine University Hospital Center

3175 Côte-Ste-Catherine Rd.

Montréal, Québec, H3T 1C5, Canada

Address for notification, correspondence and reprints:

Carl-Eric Aubin, Ph.D., P.Eng., Full Professor

Canada Research Chair 'CAD Innovation in Orthopedic Engineering' & NSERC-Medtronic industrial Research Chair in Spine Biomechanics

Ecole Polytechnique, Department of Mechanical Engineering

P.O. Box 6079, Station "Centre-ville", Montreal (Quebec), H3C 3A7 CANADA

E-mail: carl-eric.aubin@polymtl.ca

Phone: 1 (514) 340-4711 ext 2836; FAX: 1 (514) 340-5867

3.2.1 Abstract The distribution of stresses in the scoliotic spine is still not well known despite its biomechanical importance in the pathomechanisms and treatment of scoliosis. Gravitational forces are one of the sources of these stresses. Existing finite element models (FEM), when considering gravity, applied these forces on a geometry acquired from radiographs while the patient was already subjected to gravity, which resulted in a deformed spine different from the actual one. A new method to include gravitational forces on a scoliotic trunk FEM and compute the stresses in the spine was consequently developed. The 3D geometry of three scoliotic patients was acquired using a multi-view x-ray 3D reconstruction technique and surface topography. The FEM of the patients' trunk was created using this geometry. A simulation process was developed to apply the gravitational forces at the centers of gravity of each vertebra level. First the "zero-gravity" geometry was determined by applying adequate upwards forces on the initial geometry. The stresses were reset to zero and then the gravity forces were applied to compute the geometry of the spine subjected to gravity. An optimization process was necessary to find the appropriate zero-gravity and gravity geometries. The design variables were the forces applied on the model to find the zero-gravity geometry. After optimization the difference between the vertebral positions acquired from radiographs and the vertebral positions simulated with the model was inferior to 3 mm. The forces and compressive stresses in the scoliotic spine were then computed. There was an asymmetrical load in the coronal plane, particularly at the apices of the scoliotic curves. Difference of mean compressive stresses between concavity and convexity of the scoliotic curves ranged between 0.1 and 0.2 MPa. In conclusion, a realistic way of integrating gravity in a scoliotic trunk FEM was developed and stresses due to gravity were explicitly computed. This is a valuable improvement for further biomechanical modeling studies of scoliosis.

Keywords: *Scoliosis, Finite element model, Spine, Gravity, Stresses*

3.2.2 Introduction

Adolescent idiopathic scoliosis is characterized as a three-dimensional (3D) deformity of the spine and rib cage. To study scoliosis pathomechanisms and treatments, it is important not only to assess the geometrical deformity but also to analyze the stresses in the scoliotic spine, and particularly the difference of compressive stresses between concave and convex sides of the scoliotic curves because of their mechanobiological importance [1, 2]. The stresses come mainly from three sources: gravity, muscle activity and dynamical effects (absent in the quasi-static approximation). Experimentally, it is difficult to measure them on patients. Meir et al. [3] measured the stress profile in the discs of scoliotic spines but patients were in a lateral decubitus position. The difference of compressive stresses in the disc annulus between concave and convex sides of scoliotic curves was up to 1 MPa.

Computer models have been used to analyze spinal stresses [1, 2, 4-7]. To compute the stresses in the scoliotic spine, the gravitational forces were generally included in the models and sometimes an assumption about the muscles contribution was made. Gravity forces were frequently applied on the spinal geometry acquired from radiographs in a standing position, so while gravity forces were already acting on the patient. Then the resulting geometry did not correspond anymore to the real patient's geometry.

In previous studies, gravitational forces were applied either directly on the vertebral bodies [2, 4] or on the center of gravity of each vertebral trunk slice as measured experimentally in the sagittal plane for non-scoliotic subjects [8-10]. In the coronal plane, the centers of gravity were hypothetically assumed to be positioned along the scoliotic spine curve [2, 4, 6]. The influence of this simplifying hypothesis was not evaluated.

The objectives of this paper are to describe a method improving the representation of gravity in a scoliotic spine FEM and to evaluate spinal forces and compressive stresses.

3.2.3 Methods

Trunk model

The 3D geometry of the spine, rib cage and pelvis of each patient was acquired using a multiview radiography reconstruction technique (Figure 1A) [11]. On three radiographs (lateral, postero-anterior and postero-anterior with a 20˚ tilted down incidence) anatomical landmarks were digitized and reconstructed in 3D. An atlas of detailed reconstructed vertebrae, ribs and pelvis along with a free-form interpolation technique were then used to obtain the final geometry. The accuracy of this reconstruction method is 3.3±3.8 mm [11].

In addition the external trunk surface of the patient was digitized using a surface topography technique (3-dimensional Capturor, Inspeck Inc., Montreal, Quebec, Canada) (Figure 1B) [12]. Using fiducial radiopaque markers visible on both the x-rays and the trunk surface, the internal and external geometries were then superimposed using a point-to-point least square algorithm [13] (Figure 1C). A global coordinate system Rg, with origin at the center of the first sacral vertebra S1, was associated with this geometry such that the z-axis was directed vertically upwards, x-axis was postero-anterior and the y-axis was lateral (oriented from left to right) (Figure 1C).

The method was applied to three scoliotic patients (thoracic and lumbar Cobb angles: P1 (38˚, 23˚); P2 (36˚, 16˚); P3: (20˚, 33˚)) (Figure 5).

Based on the patient-specific geometry, a non linear finite element model of each patients' torso was built using Ansys 11.0 FE package (Ansys Inc., Canonsburg, PA, USA). Main components of the model of the spine, rib cage and pelvis have been described elsewhere [14] and are here summarized (Figure 1D). The thoracic and lumbar vertebrae, intervertebral discs, ribs, sternum and cartilages were represented by 3D elastic beam elements, the zygapophyseal joints by shells and surface-to-surface contact elements and the vertebral and intercostal ligaments by tension-only spring elements. The abdominal cavity was modeled by equivalent beam elements whose nodes were interpolated from the nodes of the rib cage, vertebrae and pelvis. The external nodes of the beam model were then projected on the torso surface of the patient and hexahedral solid elements were created to model the external soft tissues. Geometrical and mechanical nonlinearities were taken into account.

Mechanical properties of all the components of the model were taken from experimental and published data [14]. A second version of the model was created with softer spine stiffness (rigidity of the intervertebral discs divided by 2) to cover a range of possible stiffnesses of the spine [15].

Finally, 17 nodes representing the centers of gravity of each trunk slice corresponding to a vertebral level were created. The center of gravity of the head and neck was associated to the center of gravity of the T1 level and the center of gravity of upper limbs was associated to the centers of gravity of T3, T4, T5 levels [16]. Non-deformable beam elements connected these nodes to their relative vertebra to transmit gravity forces to the spine. Their position in the sagittal plane was derived from the literature (Figure 2) [8-10]. In the coronal plane, their position was parameterized as follow:

$$Y_i^{cog} = \alpha \times Y_i^{vc} \quad \text{(Eq.2)}$$

Where: Y_i^{cog} = coordinate on the y-axis (coronal plane) of the center of gravity node for each vertebral level i (i = 1..17), Y_i^{vc} = coordinate on the y-axis of each vertebral center (vc), α = adjustable parameter. Three values of α were tested: α = 0.5, 1 or 1.5 (Figure 3) (α = 1: original position, α = 0.5: 50% closer to the sagittal plane, α = 1.5: 50% farther from the sagittal plane).

Simulation process

The magnitude of the gravitational forces $F^g_i = m_i.g$ (i: vertebral level, varies from 1 (T1) to 17 (L5), m_i: mass of the trunk slice corresponding to the vertebral level i, g: gravity field of 9.8 $m.s^{-2}$) applied on the centers of gravity of the trunk was issued from the literature [8-10] and was adapted to the patient's specific weight (Table 1).

Boundary conditions were applied on the model: the pelvis was fixed in space and the displacement of the first thoracic vertebra was blocked only in the transverse plane, allowing vertical translation. The simulation process was then divided into 2 steps: *(i)* Inverted gravitational forces $F^{-g}_i = m_i.(-g)$ (i = 1..17) were applied vertically upwards on the patient's geometry acquired from x-rays (Figure 2B) and the model was solved. At the end of this step the geometry was updated and stresses present in the model were reset to zero ('zero-gravity' state of the patient, Figure 2C) *(ii)* Gravitational forces $F^g_i = m_i.g$ (i = 1..17)

were applied vertically downward on the zero-gravity (Figure 2D). The resulting computed geometry (Figure 2E) did not correspond exactly to the real geometry of the patient (Figure 4, Table 2). An optimization process was therefore used to find the upward forces to apply at step 1 in order to obtain the appropriate zero-gravity geometry. The upward forces were divided into two components (Figure 2B): the vertical ascending forces $F^{-g}{}_i = A_i \times m_i \times (-g)$ (i = 1..17, A_i = adjustable parameter) and transverse forces Fty_i and Ftx_i (i = 3, 6, 9, 12, 15) applied respectively in the y and x directions (global reference system Rg) on the vertebral bodies T3, T6, T9, T12 and L3. Transverse forces were applied to only five vertebrae because, after a trial and error process, this method proved to be a good compromise between computational cost and optimization efficiency. Initially, Ai (i=1..17) was fixed to 1 and transverse forces were null.

The goal of the optimization process was to find the optimization variables A_i, Fty_i and Ftx_i that minimize the objective function Fct_{obj} :

$$Fct_{obj} = \sum_{i=1}^{17} (|X_f - X_i| + |Y_f - Y_i| + |Z_f - Z_i|) \quad \text{(Eq.3)}$$

where X_i, Y_i, Z_i are the positions in Rg of the vertebral body centers acquired from radiographs and X_f, Y_f , Z_f are the positions of the vertebral body centers in the simulated model including the gravitational forces. A gradient descent algorithm was used to solve the optimization problem. A difference smaller than 1% of the objective function between 2 iterations was used as convergence criterion. A maximum of 20 iterations was allowed.

After the appropriate zero-gravity geometry was found, compressive stresses, forces and moments acting on the vertebral endplates were computed in a local coordinate system R_{local} for each vertebra. The origin of R_{local} was located at the center of the vertebral body center. The z-axis was in the direction of the line joining the centers of the vertebral endplate centers. The x-axis was the projection of the global x-axis on the plane perpendicular to the z-axis. The y-axis was perpendicular to the x and z-axes.

3.2.4 Results

Before the optimization process, the computed objective function Fct_{obj} ranged between 106 and 340 mm for the three cases and the maximal difference between the 3D positions of the vertebral centers acquired form radiographs and computed positions after inclusion of gravity on the model was up to 24 mm (mean: 8.0 mm) (Table 2, Figure 4). After optimization, the objective function was inferior to 33 mm and the maximal difference between the real and simulated positions of the vertebral centers was inferior to 3 mm (mean: 1.3 mm) (Table 2).

After the optimization process, the vertical ascending forces $F^{-g}_i = A_i.m_i.(-g)$ were superior to the initial antigravitationnal forces $F^{-g}_i = m_i.(-g)$. The parameters A_i ranged between 1 and 1.11 (mean: 1.07). Transverse forces Fty_i and Ftx_i ranged between -15.6 and 9.3 N.

Between the geometry acquired from x-rays and the computed zero-gravity geometry obtained after optimization, the mean reduction of the thoracic and lumbar Cobb angles was respectively 33% (21% - 50%) and 36% (27% - 50%) and the mean reduction of the kyphosis and lordosis was respectively 71% (45% - 92%) and 21% (14% - 26%) (Table 3). The spine length increase was on average 27 mm for the flexible spine models (22 – 33 mm) and 18 mm (14 – 24 mm) for the stiff spine models.

After introduction of gravitational forces, the loading of the vertebrae was a superimposition of pure compressive forces (quantified by local forces Fz) and of bending, flexion and torsional moments (Table 4). Bending and flexion moments Mx and My quantify respectively the asymmetrical compressive loading of vertebrae in the coronal and sagittal planes. In the patients' spines, Mx was maximal at the level of the scoliotic curve apices (Table 4, Figures 5, 6). Variation of Mx was greater for the stiff spine models than for flexible spine models (Figure 6). The position of the gravity centers in the coronal plane had an influence on Mx: at the scoliotic curves apices, Mx decreased when parameter α increased (Figure 5). For instance, for the thoracic apex of patient P2 (stiff spine model), Mx decreased of 30% when α increased from 0.5 to 1.5. The position of the gravity centers in the coronal plane had no significant influence on the other forces and moments acting on the vertebrae.

Compressive stresses present in the stiff spine model of P2 ($\alpha = 1$) after the application of gravity are shown in Figure 7. Figure 8 gives the mean compressive stresses on the whole vertebral endplates and on their right and left sides ($\alpha = 1$, stiff spine model). In these figures, a negative stress corresponds to a compression state while a positive stress corresponds to a tension state. The mean compressive stress in the spine was about 0.2 MPa (Figure 8). The stresses were slightly higher for the stiff spine than for the flexible spine models, but the distribution was the same for the two cases. There was an asymmetry of the stress distribution relatively to the sagittal plane due to the scoliotic deformities. The compression was greater in the concavity of the thoracic and lumbar curves than in their convexity. At the levels of the apices of the scoliotic curves, the difference between the mean compressive stresses on the right and left sides of the vertebral endplates was in the range of 0.1 and 0.2 MPa. Maximal differences of compressive stresses of 1 MPa occured at these levels (Figure 7).

3.2.5 Discussion

The present study shows that applying gravity on a trunk model is not trivial. Simply applying the gravity forces vertically upward is not a satisfactory way of finding the zero-gravity geometry. An optimization process, requiring 5 iterations on average, is necessary. The maximal difference between the geometries acquired from the x-rays and the simulated geometry including gravity forces was under the precision of the 3D reconstruction technique after the optimization process. In order to verify the gradient descent algorithm used in the optimization process lead to a global optimum, different initial design points were tested and it did not significantly modify the optimum found.

The computed zero-gravity geometry is difficult to fully validate because of the unavailability of such data for scoliotic patients. The passage from the standing to supine or prone positions could be used as a first approximation of this state for the coronal curves as the vertical descending gravity forces are suppressed and applied in the sagittal plane. The reaction forces with the floor could however have an impact on the kyphosis and lordosis. The reduction of the scoliotic curves (mean: 34.5% (21% - 50%)) and lengthening of the

spine in the zero-gravity geometry (mean: 22.5 mm = 1.4 % total body height, min: 14 mm, max: 33 mm) found in this study are similar to experimental data that compared the standing to supine spine geometry [17-20].

Internal forces, moments and stresses computed in the spine (Table 4, Figures 6-8) showed that relatively important moments resulting from an asymmetrical compressive loading appear in the spine when it supports pure vertical gravity forces. This phenomenon was described in previous studies [21, 22]. In a normal spine, these moments are only present in the sagittal plane (Mx is null). In the scoliotic spine, gravitational forces induce also bending moments in the coronal planes (Table 4, Figures 6-8). The pattern of the asymmetrical compressive loading of the vertebrae in the coronal plane corresponded to what is generally assumed but was seldom quantified [1, 2, 23]. The compression was greater in the concavity of the scoliotic curves than in their convexity, especially at the scoliotic curve apices. According to the Hueter-Volkmann principle this would induce a growth modulation response aggravating the scoliotic deformities [1, 2]. The difference of the mean compressive stresses between the concave and convex sides of the scoliotic curves ranged between 0.1 and 0.2 MPa, which is similar to the results of Stokes [1] and Driscoll [5].

Several limits of the model should be taken into account. Vertebrae and discs were represented as homogeneous linear elastic beam elements. This simplification of the disc model did not allow fully representing the distinction between the nucleus and the annulus. Stresses computed were purely due to gravity. The muscles contribution was not included. It is possible, as other authors suggested [24, 25], that in a scoliotic patient, muscles tend to adopt strategies to reduce the scoliotic deformities and reduce the asymmetrical loading of the vertebrae, in the same way they tend to reduce sagittal flexion moments in the spine of healthy subjects [21, 22]. As almost no data exists about the stress distribution in a scoliotic spine, validation is quite difficult [3]. Even for the healthy spine, only hydrostatic pressure in the nucleus of a lumbar disc was measured for a subject in different positions [26, 27] (0.5 MPa in a standing position and between 0.15-0.2 MPa was issued from the weight of

the patient (gravity)). The mean compressive stress on the vertebra endplates of 0.2 MPa found here is similar to the experimental values.

3.2.6 Conclusion

The primary goal of this study was to develop a method to include the gravitational forces in the FEM of a scoliotic trunk while respecting the geometry of the patient in the standing position. This objective was achieved with a precision inferior to 3 mm, which is satisfactory considering it is the precision of the multi-view x-ray reconstruction technique. The developed method could be integrated in the computer modeling to study scoliosis biomechanics, where the gravitational forces and the spinal loading are of primary importance to the pathomechanisms or treatment of the deformity's progression.

Acknowledgements This study was funded by the Natural Sciences and Engineering Research Council of Canada.

3.2.7 References

1. Stokes, I.A., *Analysis and simulation of progressive adolescent scoliosis by biomechanical growth modulation.* Eur Spine J, 2007. 16(10): p. 1621-8.
2. Villemure, I., et al., *Biomechanical simulations of the spine deformation process in adolescent idiopathic scoliosis from different pathogenesis hypotheses.* Eur Spine J, 2004. 13(1): p. 83-90.
3. Meir, A.R., et al., *High pressures and asymmetrical stresses in the scoliotic disc in the absence of muscle loading.* Scoliosis, 2007. 2: p. 4.
4. Carrier, J., et al., *Biomechanical modelling of growth modulation following rib shortening or lengthening in adolescent idiopathic scoliosis.* Med Biol Eng Comput, 2004. 42(4): p. 541-8.
5. Driscoll, M., et al., *The role of spinal concave-convex biases in the progression of idiopathic scoliosis.* Eur Spine J, 2009. 18(2): p. 180-7.

6. Huynh, A.M., et al., *Pedicle growth asymmetry as a cause of adolescent idiopathic scoliosis: a biomechanical study.* Eur Spine J, 2007. 16(4): p. 523-9.

7. Stokes, I.A. and M. Gardner-Morse, *Muscle activation strategies and symmetry of spinal loading in the lumbar spine with scoliosis.* Spine, 2004. 29(19): p. 2103-7.

8. Liu, Y.K., J.M. Laborde, and W.C. Van Buskirk, *Inertial properties of a segmented cadaver trunk: their implications in acceleration injuries.* Aerosp Med, 1971. 42(6): p. 650-7.

9. Pearsall, D.J., J.G. Reid, and L.A. Livingston, *Segmental inertial parameters of the human trunk as determined from computed tomography.* Ann Biomed Eng, 1996. 24(2): p. 198-210.

10. Pearsall, D.J., J.G. Reid, and R. Ross, *Inertial properties of the human trunk of males determined from magnetic resonance imaging.* Ann Biomed Eng, 1994. 22(6): p. 692-706.

11. Delorme, S., et al., *Assessment of the 3-D reconstruction and high-resolution geometrical modeling of the human skeletal trunk from 2-D radiographic images.* IEEE Trans Biomed Eng, 2003. 50(8): p. 989-98.

12. Pazos, V., et al., *Reliability of trunk shape measurements based on 3-D surface reconstructions.* Eur Spine J, 2007. 16(11): p. 1882-91.

13. Fortin, D., et al., *A 3D visualization tool for the design and customization of spinal braces.* Comput Med Imaging Graph, 2007. 31(8): p. 614-24.

14. Clin, J., C.E. Aubin, and H. Labelle, *Virtual prototyping of a brace design for the correction of scoliotic deformities.* Med Biol Eng Comput, 2007. 45(5): p. 467-73.

15. Petit, Y., C.E. Aubin, and H. Labelle, *Patient-specific mechanical properties of a flexible multi-body model of the scoliotic spine.* Med Biol Eng Comput, 2004. 42(1): p. 55-60.

16. El-Rich, M. and A. Shirazi-Adl, *Effect of load position on muscle forces, internal loads and stability of the human spine in upright postures.* Comput Methods Biomech Biomed Engin, 2005. 8(6): p. 359-68.

17. Delorme, S., et al., *Pre-, intra-, and postoperative three-dimensional evaluation of adolescent idiopathic scoliosis.* J Spinal Disord, 2000. 13(2): p. 93-101.

18. Klepps, S.J., et al., *Prospective comparison of flexibility radiographs in adolescent idiopathic scoliosis.* Spine, 2001. 26(5): p. E74-9.

19. Krag, M.H., et al., *Body height change during upright and recumbent posture.* Spine, 1990. 15(3): p. 202-7.

20. Vedantam, R., et al., *Comparison of push-prone and lateral-bending radiographs for predicting postoperative coronal alignment in thoracolumbar and lumbar scoliotic curves.* Spine, 2000. 25(1): p. 76-81.

21. Patwardhan, A.G., et al., *A follower load increases the load-carrying capacity of the lumbar spine in compression.* Spine, 1999. 24(10): p. 1003-9.

22. Rohlmann, A., et al., *Applying a follower load delivers realistic results for simulating standing.* J Biomech, 2009. 42(10): p. 1520-6.

23. Roaf, R., *Vertebral growth and its mechanical control.* J Bone Joint Surg Br, 1960. 42-B: p. 40-59.

24. Gram, M.C. and Z. Hasan, *The spinal curve in standing and sitting postures in children with idiopathic scoliosis.* Spine, 1999. 24(2): p. 169-77.

25. Mannion, A.F., et al., *Paraspinal muscle fibre type alterations associated with scoliosis: an old problem revisited with new evidence.* Eur Spine J, 1998. 7(4): p. 289-93.

26. Nachemson, A.L., *Disc pressure measurements.* Spine, 1981. 6(1): p. 93-7.

27. Wilke, H.J., et al., *New in vivo measurements of pressures in the intervertebral disc in daily life.* Spine, 1999. 24(8): p. 755-62.

3.2.8 Figures and Tables

Tableau 3.1 Article 1 Table 1 Percentage of total body weight applied to the centers of gravity at the different levels

Vertebra level	Percentage of total body weight
T1	1.1% + 8% (Head)
T2	1.1%
T3	1.3% + 4% (Superior limbs)
T4	1.3% + 4% (Superior limbs)
T5	1.3% + 4% (Superior limbs)
T6	1.3%
T7	1.4%
T8	1.5%
T9	1.6%
T10	2.0%
T11	2.1%
T12	2.5%
L1	2.4%
L2	2.4%
L3	2.3%
L4	2.6%
L5	2.6%
Total	50.8%

Tableau 3.2 Article 1 Table 2 Objective function and maximal difference between the position of the vertebra centers before and after the optimization process

		Flexible Spine						Stiff Spine					
		α=0.5		α=1		α=1.5		α=0.5		α=1		α=1.5	
		Before	*After*	*Before*	*After*	*Before*	*After*	*Before*	*After*	*Before*	*After*	*Before*	*After*
	Objective Function (mm)	155	32	150	30	147	33	114	16	110	15	106	17
	Maximal Difference (mm)												
P1	x	10	2	11	2	11	2	7	1	7	1	7	1
	y	5	2	4	2	3	3	4	1	3	1	3	1
	z	3	1	3	1	3	1	3	0	3	1	3	1
	Objective Function (mm)	340	31	329	23	318	32	207	25	201	24	195	26
	Maximal Difference (mm)												
P2	x	4	1	4	1	3	1	3	1	3	1	3	1
	y	24	3	22	2	22	2	14	1	14	1	13	2
	z	13	1	10	1	11	1	7	1	7	1	7	1
	Objective Function (mm)	253	23	252	24	253	26	175	14	174	16	174	18
	Maximal Difference (mm)												
P3	x	15	2	15	1	15	2	10	1	10	1	11	1
	y	3	2	3	2	3	2	2	1	2	1	2	1
	z	10	1	10	1	10	1	8	1	8	1	7	1

Tableau 3.3 Article 1 Table 3 Indices of the initial, zero-gravity and final geometries after optimization ($\alpha = 1$) (all values in degrees)

			Geometry		
			Initial	Zero-gravity	Final
P1	Flexible	*Thoracic Cobb*	38	27	40
		Lumbar Cobb	22	14	24
		Kyphosis	12	1	13
		Lordosis	23	17	24
	Stiff	*Thoracic Cobb*	38	29	39
		Lumbar Cobb	22	16	23
		Kyphosis	12	1	12
		Lordosis	23	18	23
P2	Flexible	*Thoracic Cobb*	34	17	36
		Lumbar Cobb	14	7	16
		Kyphosis	9	2	9
		Lordosis	35	28	37
	Stiff	*Thoracic Cobb*	34	19	35
		Lumbar Cobb	14	9	16
		Kyphosis	9	2	9
		Lordosis	35	30	36
P3	Flexible	*Thoracic Cobb*	19	13	21
		Lumbar Cobb	30	18	32
		Kyphosis	49	26	51
		Lordosis	35	27	37
	Stiff	*Thoracic Cobb*	19	15	19
		Lumbar Cobb	30	22	30
		Kyphosis	49	27	49
		Lordosis	35	28	36

Tableau 3.4 Article 1 Table 4 Forces (N) and Moments (N.mm) acting on the vertebral endplates for the patient P1

	Flexible Spine						***Stiff Spine***					
Vertebrae	**Fz**	**Fy**	**Fx**	**Mz**	**My**	**Mx**	**Fz**	**Fy**	**Fx**	**Mz**	**My**	**Mx**
T1	-26	-63	28	28	-113	95	-32	-93	1	26	-149	137
T2	-26	-1	-5	-13	-60	60	-29	-1	-5	-16	-107	110
T3	-40	-5	-10	-40	173	88	-45	-5	-9	-31	124	137
T4	-52	3	-6	32	398	65	-59	3	-5	31	386	125
T5	-72	12	3	139	535	46	-81	14	4	153	574	86
T6	-90	23	-3	189	459	-155	-97	27	-1	247	587	-204
T7	-97	10	-15	172	439	-315	-104	14	-16	237	598	-472
T8	-98	2	-25	140	422	-302	-107	3	-27	213	567	-497
T9	-101	-6	-7	-24	383	-347	-112	-7	-7	-28	479	-577
T10	-114	-13	-23	-87	601	-174	-124	-14	-25	-83	733	-361
T11	-129	-37	-19	-262	231	220	-135	-38	-19	-302	343	90
T12	-140	-40	1	-351	560	330	-148	-45	2	-433	715	363
L1	-162	-15	-23	-154	713	301	-170	-19	-29	-194	863	432
L2	-172	-11	-33	-125	67	441	-178	-13	-41	-195	13	722
L3	-179	29	-29	-202	-585	907	-185	29	-35	-301	-743	1167
L4	-190	26	-11	-63	-1215	5	-198	28	-18	-150	-1603	134
L5	-199	12	43	-32	-879	-286	-208	16	44	-73	-1325	-231

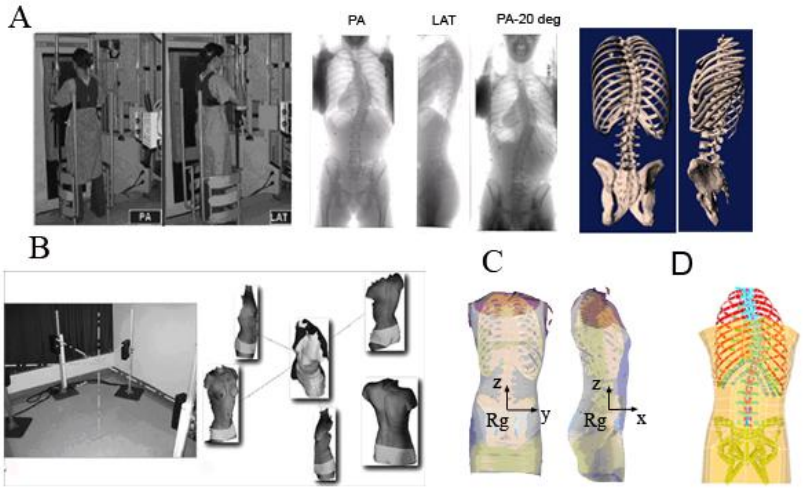

Figure 3.1 Article 1 Figure 1 A Acquisition of the internal geometry by a multi-view x-rays reconstruction technique B Acquisition of the external geometry by surface topography technique C Superimposition of the two geometries D Finite element model of the trunk

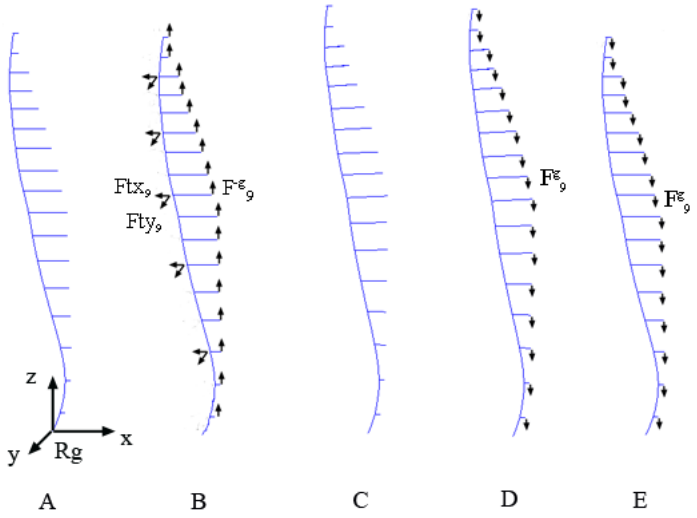

Figure 3.2 Article 1 Figure 2 Schematic representation of the spine and of the trunk slices gravity centers in the sagittal plane showing the different steps of the simulation process (A: Initial Geometry; B: Application of anti-gravitational forces; C: Zero-gravity geometry; D: Application of gravitational forces; E: Final geometry)

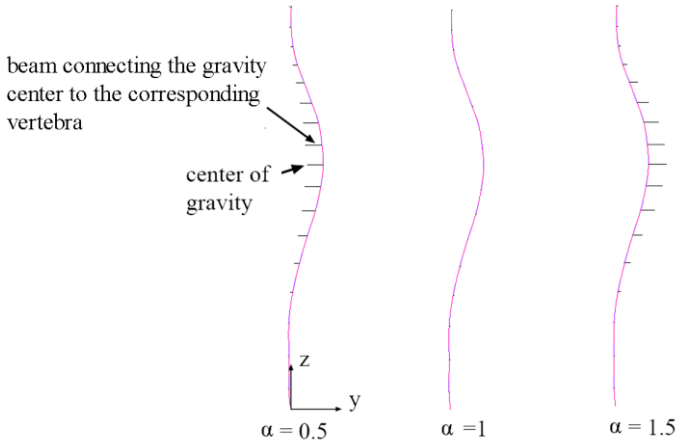

Figure 3.3 Article 1 Figure 3 Different positions of the centers of gravity of each trunk slice in the coronal plane (Patient P2)

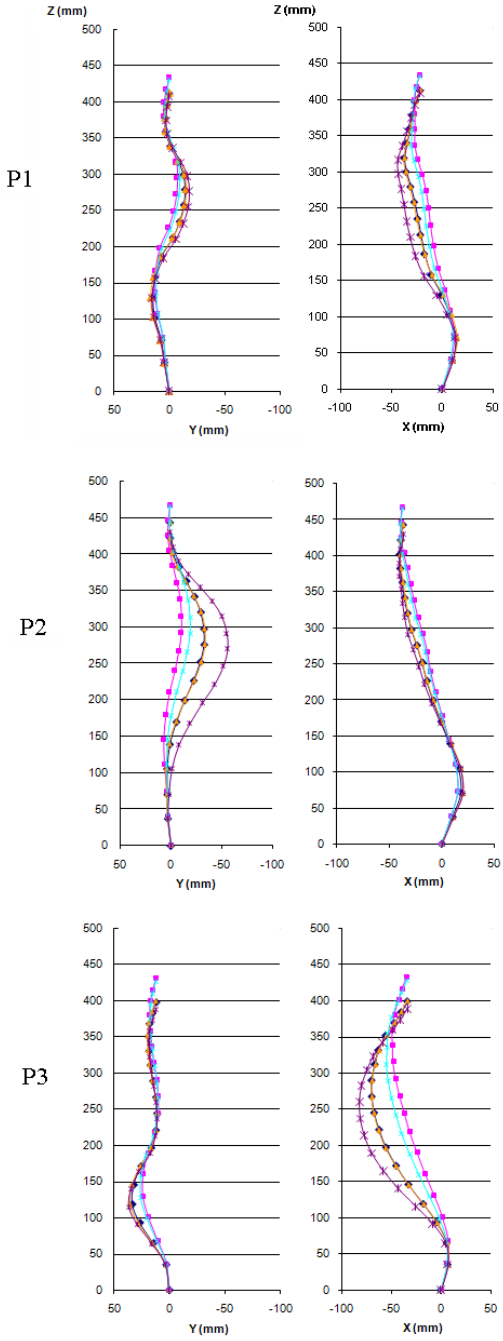

Figure 3.4 Article 1 Figure 4 Coronal and lateral views of the spine shape of the 3 patients in the initial geometry (◆), in the zero-gravity geometry before (×) and after the optimization process (▪), in the final geometry before (✳) and after (▲) the optimization process (α = 1, flexible spine model)

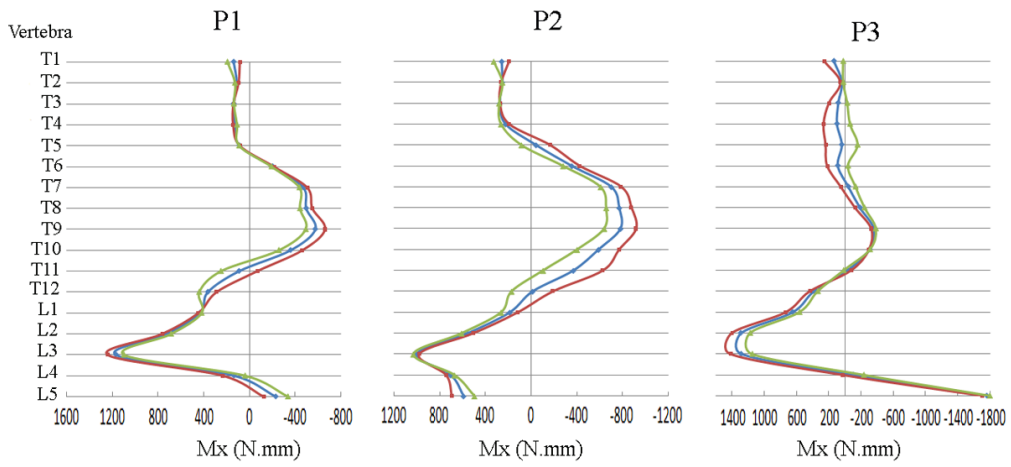

Figure 3.5 Article 1 Figure 5 Influence of the positions of the trunk slices gravity centers on the moment Mx exerted on the vertebral endplates (△ : α = 1.5, ◇ : α = 1, ▫ : α = 0.5) (stiff spine model)

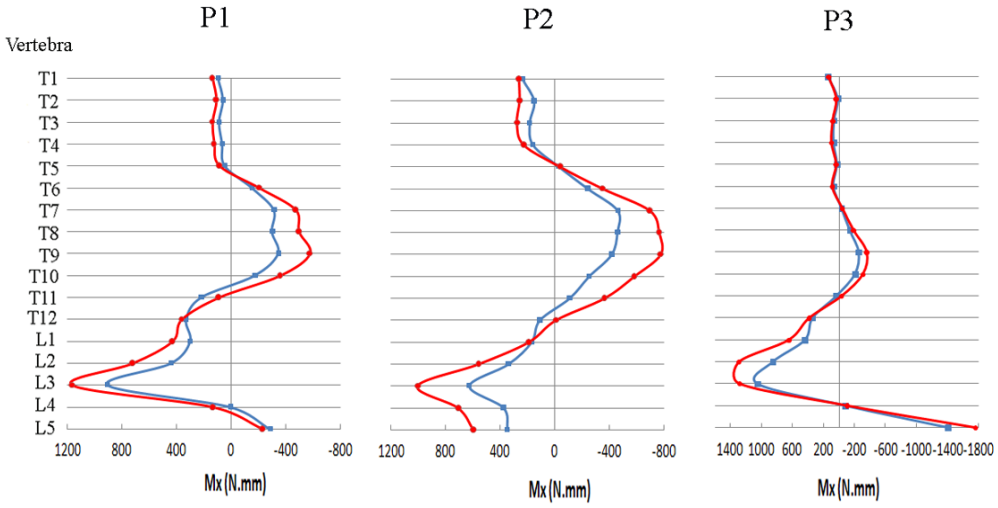

Figure 3.6 Article 1 Figure 6 Influence of the spine model stiffness on the moment Mx exerted on the vertebral endplates (▫ : flexible spine model, ○ : stiff spine model)

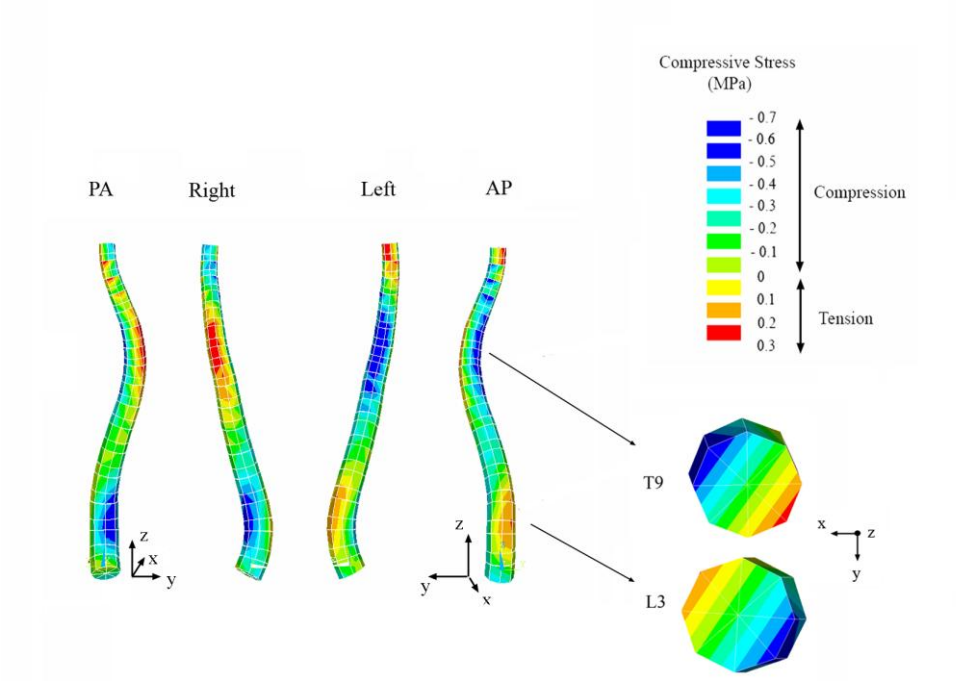

Figure 3.7 Article 1 Figure 7 Compressive stresses in the spine of P2 (α = 1, stiff spine model)

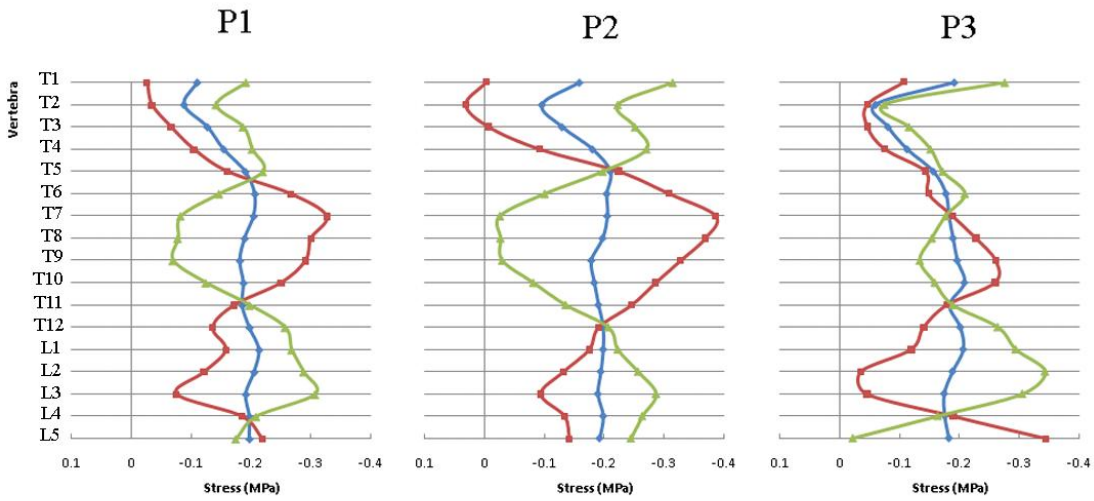

Figure 3.8 Article 1 Figure 8 Compressive stresses on the vertebral endplates (◇ : global mean stress, ▫ : mean stress on the left side , △ : mean stress on the right side) (α = 1, stiff spine model)

CHAPITRE 4 ÉVALUATION DE L'EFFET DE LA GRAVITÉ DANS LA SIMULATION DU TRAITEMENT DE LA SCOLIOSE PAR CORSET

4.1 Situation du deuxième article

L'article 1 a présenté une méthode permettant de modéliser les forces de gravité sur un modèle éléments finis du tronc scoliotique tout en respectant la géométrie du patient acquise par les radiographies. Les contraintes présentes dans la colonne vertébrale du fait des forces de gravité ont ainsi pu être calculées. Dans le deuxième article, cette méthode va être intégrée au processus de simulation du traitement par corset. L'influence de la présence de ces forces de gravité dans le modèle y est évalué. Pour ce faire deux processus de simulation, l'un incluant la méthode décrite à l'article 1 et l'autre n'intégrant pas les forces de gravité, sont utilisés et leurs résultats sont comparés. Une étude de validation préliminaire est également menée afin de montrer que le modèle est capable de reproduire les effets des corsets réels. Enfin l'action du corset sur les pressions asymétriques s'exerçant sur les plateaux vertébraux est quantifiée.

Cet article est intitulé : « Biomechanical modeling of brace treatment of scoliosis: Effects of gravitational loads », et a été soumis pour publication à la revue Medical and Biological Engineering and Computing en Janvier 2010. La contribution du premier auteur à la préparation et la rédaction de l'article est évaluée à 85%.

4.2 Article #2: Biomechanical modeling of brace treatment of scoliosis: Effects of gravitational loads

Biomechanical modeling of brace treatment of scoliosis: Effects of gravitational loads

Julien Clin[1,2], Carl-Éric Aubin[1,2], Stefan Parent[2], Hubert Labelle[2]

1- Dept. of Mechanical Engineering, École Polytechnique de Montréal

P.O. Box 6079, Station Centre-ville, Montréal, Québec, H3C 3A7, Canada

2- Sainte-Justine University Hospital Center

3175 Côte-Ste-Catherine Rd., Montréal, Québec, H3T 1C5, Canada

Address for notification, correspondence and reprints:

Carl-Eric Aubin, Ph.D., P.Eng.

Full Professor

Canada Research Chair 'CAD Innovation in Orthopedic Engineering' & NSERC-Medtronic industrial Research Chair in Spine Biomechanics

Ecole Polytechnique, Department of Mechanical Engineering

P.O. Box 6079, Station "Centre-ville", Montreal (Quebec), H3C 3A7 CANADA

E-mail: carl-eric.aubin@polymtl.ca

Phone: 1 (514) 340-4711 ext 2836; FAX: 1 (514) 340-5867

4.2.1 Abstract

The biomechanics of bracing in adolescent idiopathic scoliosis is still not fully understood. Finite element models (FEM) have been used but the gravity forces were not included and the production of spinal stresses not evaluated. An improved FEM to simulate brace treatment was thus developed. The 3D geometry of the spine, rib cage, pelvis and of the trunk external surface of five scoliotic patients was acquired using a multi-view x-ray technique and surface topography. A FEM of the patient's trunk including gravity forces was created. Custom-fit braces were modeled and their installation simulated. Immediate geometrical corrections and pressures were computed and validated. The resulting compressive loads on the vertebral endplates were quantified. The influence of the strap tension, spine stiffness and of the gravity forces was evaluated. Results showed that the brace biomechanical action was importantly to prevent the scoliotic spine from bending under the gravity forces. The immediate correction depended on the strap tension and spine stiffness. The distribution and amplitude of computed pressures were similar to those measured with the real braces. After the brace installation, the coronal asymmetrical compressive loading on the vertebral endplates was significantly reduced. In conclusion, the model developed presents improvements over previous models and could be used to better understand and optimize brace treatment.

Keywords *Scoliosis, Brace, Finite element model, Design, Gravity*

4.2.2 Introduction

Scoliosis is a complex deformity of the spine and entire torso. Up to moderate deformities, bracing is the most common treatment. However, its efficiency in preventing the progression of scoliotic deformities is still controversial [10, 18, 20, 32] and the biomechanics of brace treatment is still poorly understood. For instance, there is still no consensus about the optimal design of a brace [30]. The shape of the brace, the location of

pads and openings vary amongst orthotists [30]. The capacity of the braces to generate a real 3D correction of the scoliotic deformities has also been questioned. It appeared that the braces did not significantly correct the transverse plane deformities (rib hump and axial rotation) and in some cases tended to reduce the thoracic kyphosis (back flattening) [13]. Numerical finite element models (FEM) have thus been developed to better understand and optimize brace treatments. The brace treatment was mainly simulated by directly applying external forces on the rib cage and on the lumbar spine. Andriacchi et al [1] simulated the Milwaukee brace and Périé et al [27, 28] the Boston brace using such approach. Patwardhan et al. [22], Wynarsky et al. [37] and Gignac et al. [9] studied the optimal forces that a brace should exert but the optimization processes did not include many brace design parameters, such as the strap tension, the rigid shell geometry, or the shape of the pads. More recently, Périé et al [26] introduced an explicit FEM of the brace. Its installation on the patient was simulated using a contact interface between the trunk and the brace. Clin et al [5] introduced a parametric, custom-fit virtual brace model including the pads, openings and straps, and developed a more realistic simulation process. Gravity was however not included in all the previous models and hence the effect of brace treatment on the spine internal stresses could not be fully evaluated.

The aim of the present study was to develop a more complete way of simulating the brace treatment and to demonstrate the importance of explicitly representing gravity in the model in order to fully evaluate the effects of brace treatment. .

4.2.3 Methods

Trunk geometry

The geometry of the spine, rib cage and pelvis of five scoliotic patients (P1 to P5) with mean thoracic Cobb of 33˚ and mean lumbar Cobb of 25˚ (see Figure 4, Table 1) was acquired using a multiview radiographic self-calibration technique (Figure 1A) [6, 11]. On three radiographs (lateral, postero-anterior and postero-anterior with a 20˚ incidence) anatomical landmarks were digitized and reconstructed in 3D. An atlas of fully reconstructed vertebrae, ribs and pelvis along with a free-form interpolation technique were

used to obtain the final geometry. The accuracy of the reconstruction method was 3.3 mm on average (SD 3.8 mm) [6]. In addition the external trunk surface of the patient was digitized using 3-D surface topography (3-dimensional Capturor, Inspeck Inc., Montreal, Quebec, Canada)[23] (Figure 1B). The patient stood erect in the center of a setting of 4 cameras that acquired the surface of the patient trunk by analysing the deformation of a pattern of black and white narrow stripes. Using fiducial radiopaque landmarks visible on both the x-rays and the trunk surface, the internal and external geometries were then registered and superimposed using a point-to-point least squares algorithm (Figure 1C) [7].
A global coordinate system Rg, with the origin at the center of the first sacral vertebra S1, was associated with this geometry such that the z-axis was directed vertically upwards, x-axis was postero-anterior and the y-axis was lateral (oriented from right to left) (Figures 1, 2).

FEM of the trunk

Based on this geometry, a personalized FEM of the patient's torso was built. The Ansys 11.0 FE package was used (Ansys Inc., Canonsburg, PA, USA). Main components of the model of the spine, rib cage and pelvis have been described elsewhere and are here summarized [2, 28] (Figure 2A). Thoracic and lumbar vertebrae, intervertebral discs, ribs, sternum and rib cartilages were represented by 3D elastic beam elements, the zygapophyseal joints by shells and surface-to-surface contact elements and the vertebral and intercostal ligaments by tension-only spring elements. The abdominal cavity was modeled by equivalent beam elements whose nodes were interpolated from the nodes of the rib cage, vertebrae and pelvis. The external nodes of this model were then projected on the external trunk surface of the patient and hexahedral solid elements were created to model the external soft tissues of the patient.
Mechanical properties of all the components of the model were taken from experimental and published data [2, 26, 28]. To evaluate the influence of the variable flexibility of the spine, which can be encountered in scoliotic patients [29], a "stiff" and a "flexible" spine

were tested (intervertebral disc stiffness multiplied and divided by a factor of 2 respectively).

Seventeen nodes representing the center of gravity of each trunk's slice were created and associated to each thoracic and lumbar vertebra [4]. Their position in the sagittal plane was derived from published values and scaled according to patient size [3, 15, 24, 25]. In the coronal plane, it was assumed that their position followed the scoliotic curve of the spine. Non-deformable beam elements connected these nodes to their relative vertebrae to transmit the gravity forces to the spine.

Brace model

A custom-fit brace model was created over the already generated FEM of the patient's trunk. It was based on 10 generative curves defined by 8 control points (Figure 2B). As each of the control points had 3 coordinates (x_i, y_i, z_i, i =1..8), the shape of each generative curve was controlled by 24 parameters computed on the external surface of the trunk of the patient. They could then be modified to test different brace designs. A surface interpolating these ten generative curves was created. It was divided into 170 sub-surfaces. The brace openings were created by deleting sub-surfaces. The remaining sub-surfaces were then extruded outward to create a volumetric representation of the foam layer of the brace geometry. The pads were created by inwardly extruding sub-surfaces (Figure 2C).

For each of the five patients, a specific virtual brace was designed. The design of the virtual braces took into account the main features of the real Boston type braces of the patients. For instance, the virtual brace designed for the patient P1 is shown in Figure 2C. The external rigid shell was symmetric relatively to the sagittal plane. Pads were positioned inside the brace on the right thoracic, left lumbar, left anterior thoracic (derotational pad), and right trochanteric regions. Openings were cut in the right high thoracic, left thoracolumbar and left trochanteric regions.

The external rigid shell (located on the external surface of the volume representing the foam layer) was modeled by 4-node quadrilateral shell elements. The foam layer and pads were represented by 8-nodes hexahedral elements (Figure 2D). Element edge length was fixed to 30 mm. Material of the rigid shell was polyethylene (E=1500Mpa, ν=0.3), that of

foam layer was soft polyethylene foam (E=1MPa, ν=0.3), and that of pads was stiff polyethylene foam (E=10MPa, ν=0.3) [26, 33]. These materials were modeled as linear elastic as only the immediate effect at equilibrium was analyzed.

A non-linear surface-to-surface contact interface was created between the interior of the brace model and the exterior of the patient's trunk model. Its rigidity was fixed to 10^{-2} $N.mm^{-1}$. The penetration tolerance was 5 mm. These values, and the size of the mesh for the brace model, were fixed using a convergence study (criterion: variation of forces and displacements inferior to 5%) where a compromise was found between the computational time and the numerical precision of the simulation. Friction was taken into account in the contact interface using a Coulomb model (coefficient of friction = 0.6 [39]).

Simulation of the brace installation

Boundary conditions were applied on the FEM to mimic postural conditions of an in-brace patient. The pelvis was fixed in space and the translation of the first thoracic vertebra in the transverse plane (x and y directions) was blocked. The simulation of the brace installation on the patient was divided into 3 steps: (i) The gravitational forces were first applied on the nodes corresponding to the different centers of mass of the torso. Their magnitude was based on published data [3, 15, 24, 25] and was adapted to the patient specific weight (50kg). However, as the initial geometry of the patient was obtained while he was already standing and submitted to gravity forces, this step was divided into two -substeps. Forces were first applied vertically upward in order to find the zero-gravity geometry of the patient. The stresses were suppressed while the geometry was updated. Then the gravitational forces were applied vertically downward on the zero-gravity geometry and the geometry of the patient under gravity was obtained again but this time it included the stresses due to the presence of gravitational forces. It was verified that the simulated configuration with the gravitational forces corresponded to the geometry obtained from the x-rays. (ii) In the second step the brace was opened by applying displacements on four nodes located in its posterior part and was positioned on the patient. (iii) In the third step two sets of collinear forces representing thoracic and pelvic strap tensions (Figure 2E) were applied on the nodes corresponding to the strap fixations on the posterior part of the brace.

Two different strap tensions were tested: 20N and 60 N [16]. During the whole simulation process, non-linearities due to large deformations and changing status of elements due to contacts were taken into account using the Newton-Raphson method.

Influence of gravity

To evaluate the effect of introducing the gravity forces in the model, each of the brace simulations (2 strap tensions * 2 spinal stiffness) was done twice, one time without the gravity (the first step of the simulation process was omited), and one time with the gravity. A total of 8 simulations were thus done for each patient.

Validation of the brace simulation

To validate the model, the simulated in-brace spinal shape and the corrections of several 3D clinical indices (Cobb angles, kyphosis, lordosis, rib hump, axial rotation) were computed at the end of the simulations and compared to the spinal shape and to the 3D clinical indices of the patients in their actual braces. The pressures generated by the virtual braces on the torso of the patients were also evaluated and compared to the pressures exerted by their actual brace. These pressures were measured with a flexible pressure matrix composed of 192 thin pressure sensors worn under the brace [12, 16] and were visualized using a software dedicated to the design and adjustment of braces [12].

Study of brace biomechanics

The impact of the brace installation on the forces and moments acting on the vertebral endplates and on the compressive stresses in the spine was also evaluated. They were computed in a local coordinate system R_{local} for each vertebra. Origin of R_{local} was located at the vertebral body centroid. The z-axis was in the direction of the line joining the centers of the vertebral endplate centers. The x-axis was the projection of the global x-axis on the plane perpendicular to the z-axis. The y-axis was perpendicular to the x and z-axes. Because of its implication in the growth modulation process [34, 36], the asymmetrical

compressive loading of the vertebral endplates in the coronal plane was quantified using the resulting bending moment Mx at each level.

4.2.4 Results

Including the simulation of the gravity in the model had a great influence on the in-brace correction of the coronal and sagittal curves (Table 1, Figure 3). There was a 7° difference on average in the thoracic Cobb angle and a 3° difference in the lumbar Cobb angle between the simulations with and without gravity. The difference was of 5° on average for the thoracic kyphosis and for the lumbar lordosis. For instance, for the flexible model of patient P1, the difference in the apical vertebra translation was of 15 mm (Figure 3). The remainder results of this section will be with the model including gravity.

Increasing the strap tension from 20 to 60 N improved on average the correction of the thoracic and lumbar Cobb angles by 4° (Table 1). The spine stiffness influenced the correction of the coronal curves. For the flexible spine model, the mean percentage of correction of the thoracic and lumbar Cobb angles respectively was 53 % and 41 % for a strap tension of 60 N, while it was of 40 % and 29 % for the stiff spine model.

The spinal shapes of the 5 patients obtained after the virtual braces installation was simulated are shown in Figure 4. Results are given for the two spinal flexibility models and the two strap tensions tested. The simulated spinal shapes are compared to the spinal shapes of the patients in their real braces.

The pressures exerted on the torsos ranged between 0 and 30 kPa for both the real and simulated braces. Figure 5 shows the resulting pressures in details for the patient P1. Increasing the strap tension of the virtual brace resulted in increasing the pressures. The maximal pressure exerted on the right thoracic region increased of 45% when the strap tension was increased from 20 to 60N. Both the real brace and the brace model induced pressure zones on the patient's torso corresponding to their right thoracic pad (Figure 5A), their left lumbar pad (Figure 5B), their left and right iliac crest rolls (Figure 5C) and to their left thoracic extension (Figure 5D).

Before the brace installation, there was an asymmetrical compressive loading on the vertebral endplates in the coronal plane (Figures 6, 7): a slight tension appeared in the convexity of the thoracic and lumbar curves while a marked compression appeared in their concavity (Figure 6). Before the brace installation, the resulting bending moment Mx was maximal at the lumbar and thoracic curve apices and was greater for the stiff spine model than for the flexible spine model (Figure 7, Table 2). After the brace installation, Mx decreased globally (Figure 7). More specifically, it was reduced on average by 96% at the thoracic apex and by 85% at the lumbar apex. The simulated brace installation also induced a reduction of the total compressive forces Fz acting on the vertebrae because of the gravity. On average, the compressive force Fz on L5 decreased by 7% for a strap tension of 20 N and of 18% for a strap tension of 60 N.

4.2.5 Discussion

This study distinguishes from the previous brace studies using FEM [1, 5, 19, 27, 37] as it included explicitly the gravity and demonstrated its importance in the brace biomechanics. In scoliosis the brace must not be seen solely as a way of applying transverse corrective forces on the trunk of the patient but also as a mean of supporting the scoliotic spine and preventing it from bending under the gravitational forces. This role was confirmed by the reduction of the total compressive forces acting on the vertebrae (Fz) after the brace installation and of the bending moment Mx.

The developed model allows computing the asymmetrical compressive loading of the vertebrae in the coronal plane with and without the brace. This could be used to evaluate if the brace treatment would be able to stop the progression of scoliotic deformities. In the framework of the Hueter-Volkmann principle (compression slows growth, tension fastens growth), the reduction of the asymmetrical loading of the growth plates in the coronal plane generates a favorable condition to reduce the progression of the scoliotic deformities [34, 36]. In this study, it was demonstrated that the braces were able to reduce significantly the asymmetrical loading Mx (Table 2, Figure 7). In some cases they were even able to invert Mx, which proves that the brace treatment can theoretically stop the progression of the scoliotic deformities. However, in other cases, Mx was not inverted, which indicates an

optimal adjustment is still necessary and that more efficient designs are to be found. The growth modulation process is however still poorly understood and remains a subject of active research [8, 35]. For example it is not known if a 'neutral zone' exists, where a slight asymmetrical loading would not generate growth modulation. The growth modulation sensitivity to the stresses is also still unclear [30].

The model developed in this study allowed computing and visualizing the pressures exerted by the brace on the patients' torsos. The simulated distribution and magnitude of the pressures exerted by the brace agreed well with those measured on patients (Figure 5), which supports the validity of the model. The introduction of the true external surface of the patient's torso in the trunk model (Figures 1, 2) distinguishes itself from previous models [5]. It allows designing a brace for the patient custom-fit to the geometry of his torso, which is necessary in the long-term perspective of simulating and evaluating a brace design before fabricating it.

A few limitations due to the simplification hypotheses made for the trunk model should be taken into account when interpreting the results. Only the passive action of the brace was simulated as no muscles are present in the model. The active action (the patient would tend to self-correct his scoliotic deformities by escaping from the pressure points exerted by the brace) is however thought to be an important part of the brace action despite some controversies [21, 37, 38]. This active action could generate additional corrections to the passive effects modeled in this study. The muscles action also influences the spine stresses [17, 34]. Other alternatives to compute the spinal loading could be studied in future works to integrate the muscles contribution. For instance, a follower load could be used instead of pure vertical descending gravity forces [31]. The intervertebral disc model could be enhanced in order to refine the stresses computation. A true personalization of the mechanical properties could also be integrated using new methods to evaluate the flexibility of the patient [14].

4.2.6 Conclusion

An innovative simulation process for the brace treatment in adolescent idiopathic scoliosis was developed. It was demonstrated that one major biomechanical action of the brace was to prevent the scoliotic spine from bending under the gravity forces. The geometrical corrections and pressures found in this study are realistic against available measurements. The brace simulator developed using the FEM could be used to better understand the brace biomechanics and rationalize and optimize the treatment for the scoliotic patients.

Acknowledgements This study was funded by the Natural Sciences and Engineering Research Council of Canada.

4.2.7 References

1. Andriacchi TP, Schultz AB, Belytschko TB, Dewald R (1976) Milwaukee brace correction of idiopathic scoliosis. A biomechanical analysis and a restrospective study. J Bone Joint Surg Am 58:806-815

2. Aubin CE, Dansereau J, De Guise JA, Labelle H (1996) A study of biomechanical coupling between spine and rib cage in the treatment by orthosis of scoliosis. Ann Chir 50:641-650

3. Cheng CK, Chen HH, Chen CS, Chen CL, Chen CY (2000) Segment inertial properties of Chinese adults determined from magnetic resonance imaging. Clin Biomech (Bristol, Avon) 15:559-566

4. Clin J, Aubin C, Parent S, Ronsky J, Labelle H (2008) A new method to apply gravity on a scoliotic spine model and compute the spine internal forces and stresses. Submitted to Journal of Biomechanics

5. Clin J, Aubin CE, Labelle H (2007) Virtual prototyping of a brace design for the correction of scoliotic deformities. Med Biol Eng Comput 45:467-473

6. Delorme S, Petit Y, de Guise JA, Labelle H, Aubin CE, Dansereau J (2003) Assessment of the 3-d reconstruction and high-resolution geometrical modeling of the human skeletal trunk from 2-D radiographic images. IEEE Trans Biomed Eng 50:989-998

7. Fortin D, Cheriet F, Beausejour M, Debanne P, Joncas J, Labelle H (2007) A 3D visualization tool for the design and customization of spinal braces. Comput Med Imaging Graph 31:614-624

8. Frost HM (1990) Skeletal structural adaptations to mechanical usage (SATMU): 1. Redefining Wolff's law: the bone modeling problem. Anat Rec 226:403-413

9. Gignac D, Aubin CE, Dansereau J, Labelle H (2000) Optimization method for 3D bracing correction of scoliosis using a finite element model. Eur Spine J 9:185-190

10. Goldberg CJ, Moore DP, Fogarty EE, Dowling FE (2001) Adolescent idiopathic scoliosis: the effect of brace treatment on the incidence of surgery. Spine 26:42-47

11. Kadoury S, Cheriet F, Dansereau J, Labelle H (2007) Three-dimensional reconstruction of the scoliotic spine and pelvis from uncalibrated biplanar x-ray images. J Spinal Disord Tech 20:160-167

12. Labelle H, Bellefleur C, Joncas J, Aubin CE, Cheriet F (2007) Preliminary evaluation of a computer-assisted tool for the design and adjustment of braces in idiopathic scoliosis: a prospective and randomized study. Spine 32:835-843

13. Labelle H, Dansereau J, Bellefleur C, Poitras B (1996) Three-dimensional effect of the Boston brace on the thoracic spine and rib cage. Spine 21:59-64

14. Lamarre ME, Parent S, Labelle H, Aubin CE, Joncas J, Cabral A, Petit Y (2009) Assessment of spinal flexibility in adolescent idiopathic scoliosis: suspension versus side-bending radiography. Spine 34:591-597

15. Liu YK, Laborde JM, Van Buskirk WC (1971) Inertial properties of a segmented cadaver trunk: their implications in acceleration injuries. Aerosp Med 42:650-657

16. Mac-Thiong JM, Petit Y, Aubin CE, Delorme S, Dansereau J, Labelle H (2004) Biomechanical evaluation of the Boston brace system for the treatment of adolescent idiopathic scoliosis: relationship between strap tension and brace interface forces. Spine 29:26-32

17. Nachemson AL (1981) Disc pressure measurements. Spine 6:93-97

18. Nachemson AL, Peterson LE (1995) Effectiveness of treatment with a brace in girls who have adolescent idiopathic scoliosis. A prospective, controlled study based on data from the Brace Study of the Scoliosis Research Society. J Bone Joint Surg Am 77:815-822

19. Nie WZ, Ye M, Liu ZD, Wang CT (2009) The patient-specific brace design and biomechanical analysis of adolescent idiopathic scoliosis. J Biomech Eng 131:041007. DOI 10.1115/1.3049843

20. Noonan KJ, Weinstein SL, Jacobson WC, Dolan LA (1996) Use of the Milwaukee brace for progressive idiopathic scoliosis. J Bone Joint Surg Am 78:557-567

21. Odermatt D, Mathieu PA, Beausejour M, Labelle H, Aubin CE (2003) Electromyography of scoliotic patients treated with a brace. J Orthop Res 21:931-936

22. Patwardhan AG, Bunch WH, Meade KP, Vanderby R, Jr., Knight GW (1986) A biomechanical analog of curve progression and orthotic stabilization in idiopathic scoliosis. J Biomech 19:103-117

23. Pazos V, Cheriet F, Danserau J, Ronsky J, Zernicke RF, Labelle H (2007) Reliability of trunk shape measurements based on 3-D surface reconstructions. Eur Spine J 16:1882-1891

24. Pearsall DJ, Reid JG, Livingston LA (1996) Segmental inertial parameters of the human trunk as determined from computed tomography. Ann Biomed Eng 24:198-210

25. Pearsall DJ, Reid JG, Ross R (1994) Inertial properties of the human trunk of males determined from magnetic resonance imaging. Ann Biomed Eng 22:692-706

26. Perie D, Aubin CE, Lacroix M, Lafon Y, Labelle H (2004) Biomechanical modelling of orthotic treatment of the scoliotic spine including a detailed representation of the brace-torso interface. Med Biol Eng Comput 42:339-344

27. Perie D, Aubin CE, Petit Y, Beausejour M, Dansereau J, Labelle H (2003) Boston brace correction in idiopathic scoliosis: a biomechanical study. Spine 28:1672-1677

28. Perie D, Aubin CE, Petit Y, Labelle H, Dansereau J (2004) Personalized biomechanical simulations of orthotic treatment in idiopathic scoliosis. Clin Biomech (Bristol, Avon) 19:190-195

29. Petit Y, Aubin CE, Labelle H (2004) Patient-specific mechanical properties of a flexible multi-body model of the scoliotic spine. Med Biol Eng Comput 42:55-60

30. Rigo M, Negrini S, Weiss HR, Grivas TB, Maruyama T, Kotwicki T (2006) 'SOSORT consensus paper on brace action: TLSO biomechanics of correction (investigating the rationale for force vector selection)'. Scoliosis 1:11

31. Rohlmann A, Zander T, Rao M, Bergmann G (2009) Applying a follower load delivers realistic results for simulating standing. J Biomech 42:1520-1526. DOI S0021-9290(09)00191-2 [pii]
10.1016/j.jbiomech.2009.03.048

32. Rowe DE, Bernstein SM, Riddick MF, Adler F, Emans JB, Gardner-Bonneau D (1997) A meta-analysis of the efficacy of non-operative treatments for idiopathic scoliosis. J Bone Joint Surg Am 79:664-674

33. Sanders JE, Greve JM, Mitchell SB, Zachariah SG (1998) Material properties of commonly-used interface materials and their static coefficients of friction with skin and socks. J Rehabil Res Dev 35:161-176

34. Stokes IA (2007) Analysis and simulation of progressive adolescent scoliosis by biomechanical growth modulation. Eur Spine J 16:1621-1628

35. Stokes IA, Aronsson DD, Dimock AN, Cortright V, Beck S (2006) Endochondral growth in growth plates of three species at two anatomical locations modulated by mechanical compression and tension. J Orthop Res 24:1327-1334

36. Villemure I, Aubin CE, Dansereau J, Labelle H (2004) Biomechanical simulations of the spine deformation process in adolescent idiopathic scoliosis from different pathogenesis hypotheses. Eur Spine J 13:83-90

37. Wynarsky GT, Schultz AB (1991) Optimization of skeletal configuration: studies of scoliosis correction biomechanics. J Biomech 24:721-732

38. Wynarsky GT, Schultz AB (1989) Trunk muscle activities in braced scoliosis patients. Spine 14:1283-1286

39. Zhang M, Mak AF (1999) In vivo friction properties of human skin. Prosthet Orthot Int 23:135-141

4.2.8 Figures and Tables

Tableau 4.1 Article 2 Table 1 Geometrical indices before and after the brace simulation (Mean for the 5 patients)

Index (°)	Patient w/o brace	In-brace simulation								In Real Brace
		Without gravity				With gravity				
		Flexible Spine		Stiff Spine		Flexible Spine		Stiff Spine		
		Strap Tension		*Strap Tension*		*Strap Tension*		*Strap Tension*		
		20 N	*60 N*	*20 N*	*60 N*	*20 N*	*60 N*	*20 N*	*60 N*	
Thoracic Cobb	33	26	24	27	25	20	15	23	20	18
Lumbar Cobb	25	21	19	22	20	19	15	21	18	17
Kyphosis	26	21	20	21	20	16	15	18	16	12
Lordosis	42	37	36	38	37	32	30	34	33	30
Rib Hump	11	13	14	13	14	13	12	13	14	11
Axial Rotation	9	11	12	11	11	10	9	10	11	8

Tableau 4.2 Article 2 Table 2 Bending moment Mx on the apical vertebral endplates. Mx was calculated using the right-hand rule (+ve clockwise, -ve counter-clockwise).

Patient		Bending Moment Mx (N.mm)					
		Flexible Spine Model			Stiff Spine Model		
		w/o Brace	In Brace		w/o Brace	In Brace	
			Strap Tension			Strap Tension	
	Apex		20 N	60 N		20 N	60 N
P1	Thoracic	508	-2	-155	893	150	-36
	Lumbar	-764	-195	92	-1028	-515	-40
P2	Thoracic	235	-155	-324	432	-233	-515
	Lumbar	-477	222	530	-660	225	668
P3	Thoracic	244	184	167	376	295	296
	Lumbar	-771	-256	-3	-1061	-470	-88
P4	Thoracic	626	114	-52	1029	240	-23
	Lumbar	-1175	-290	-40	-1516	-366	18
P5	Thoracic	585	232	1	917	335	-52
	Lumbar	-1012	-700	-309	-1301	-919	-434

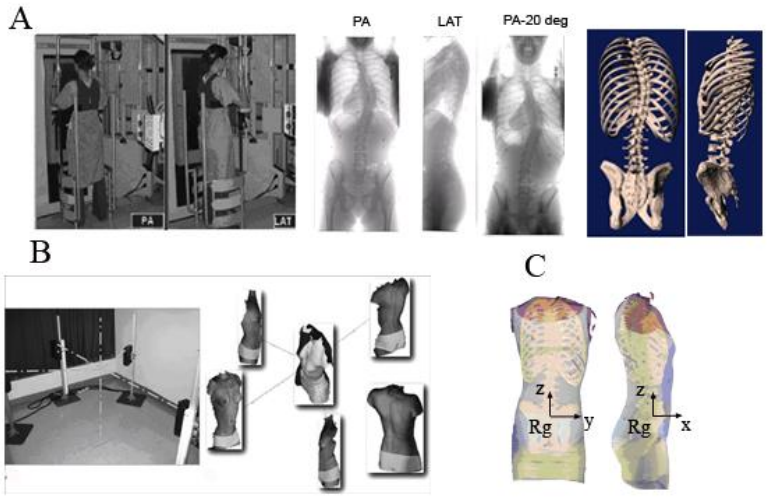

Figure 4.1 Article 2 Figure 1 A Acquisition of the internal geometry using the multi-view radiographic reconstruction technique; B Acquisition of the external geometry using surface topography; C Superimposition of the two geometries

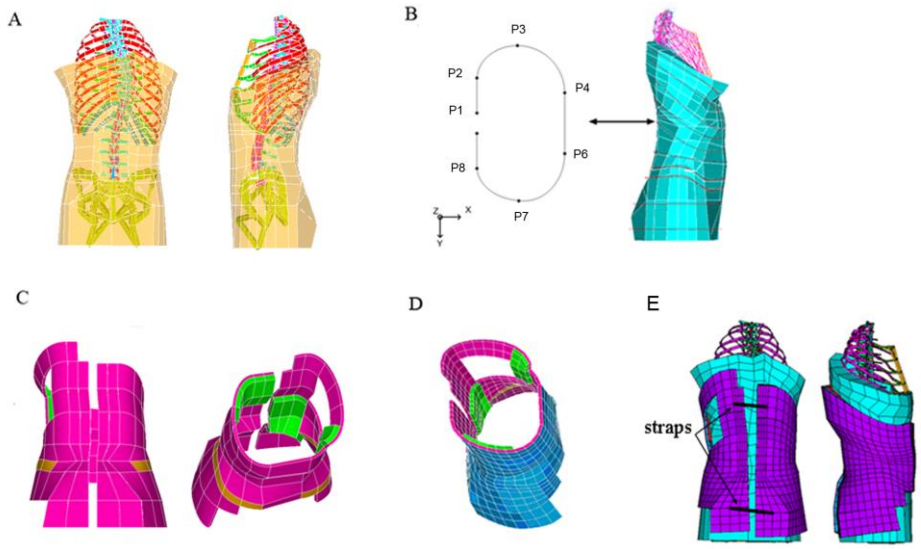

Figure 4.2 Article 2 Figure 2 A- Finite element model (FEM) of the trunk; B - Generative curves; C- Geometrical model of the brace; D- FEM of the brace; E- Brace installed on the patient

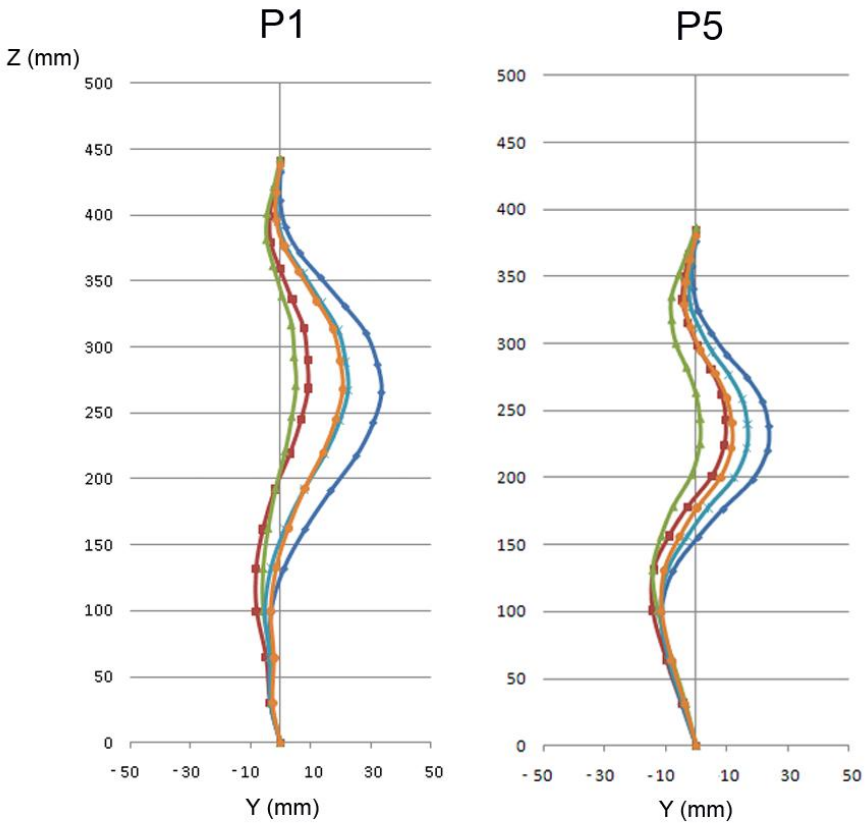

Figure 4.3 Article 2 Figure 3 Spine curve in the coronal plane of the patients P1 and P5: Without brace (), In brace, without gravity, for a strap tension of 20 N () and 60 N (), with gravity, for a strap tension of 20 N () and 60 N () (flexible spine model)

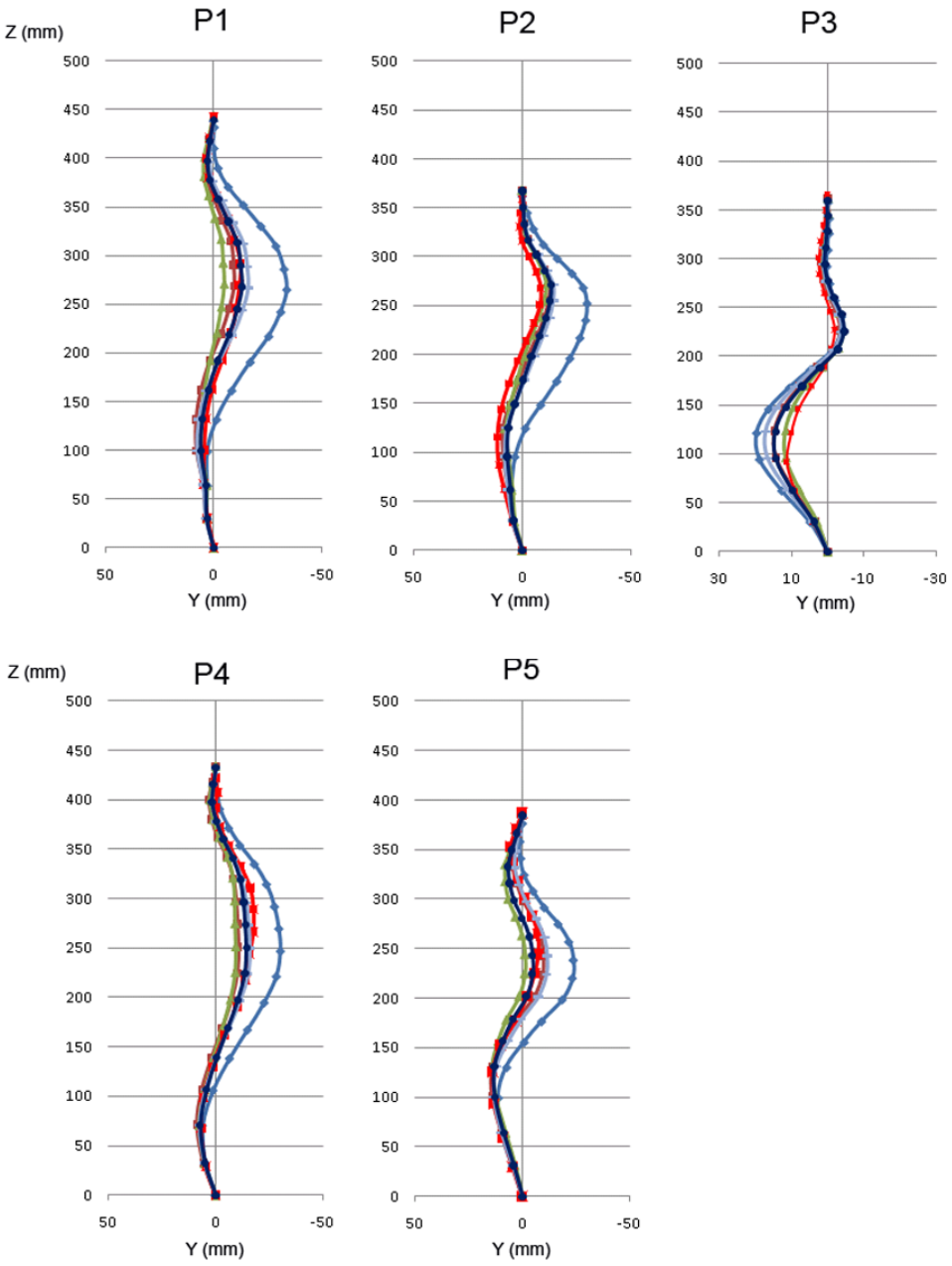

Figure 4.4 Article 2 Figure 4 Spine curve of the patients in the coronal plane: Before brace (), In virtual brace, with the flexible spine model, for a strap tension of 20 N () and 60 N (), with the stiff spine model, for a strap tension of 20 N () and 60 N (), and in the real brace ()

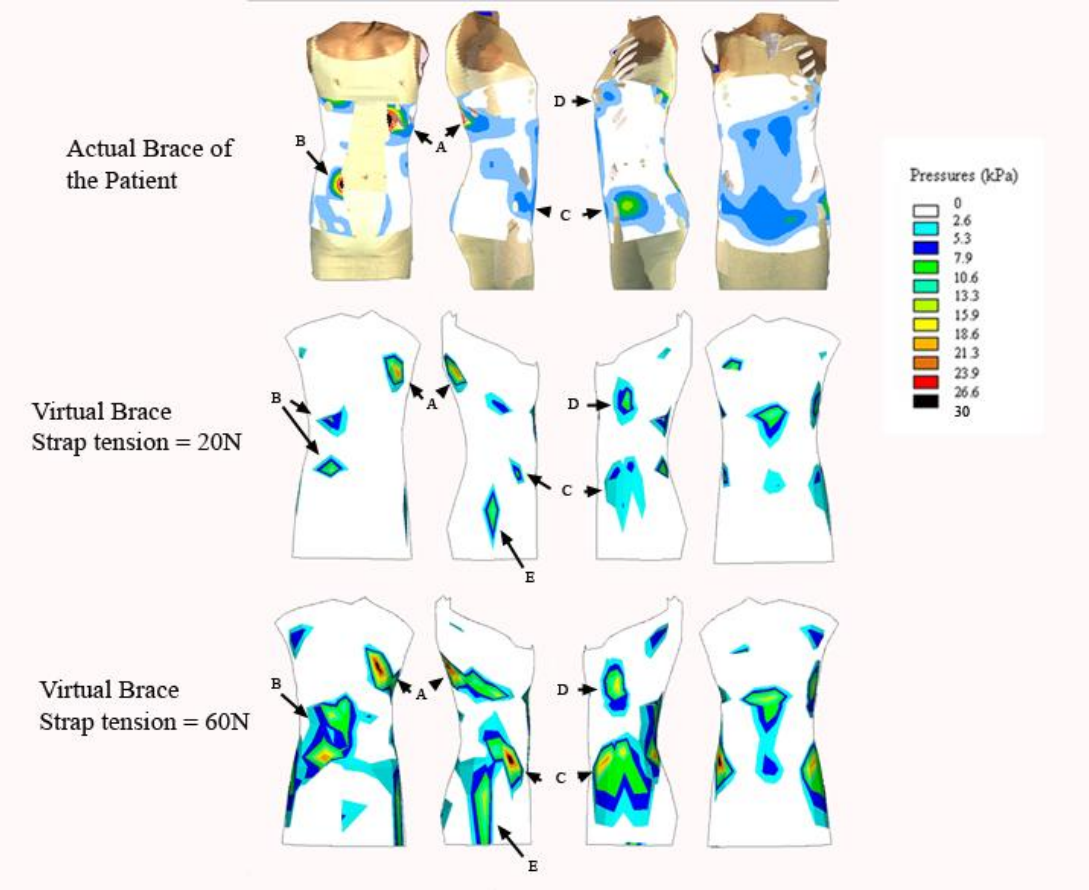

Figure 4.5 Article 2 Figure 5 Comparison of the measured pressures exerted by the actual brace of the patient P1 and the pressures from the simulated brace (A: Thoracic pad pressure, B: Lumbar pad, C: Iliac crest roll, D: Left anterior thoracic pad, E: Right trochanteric extension)

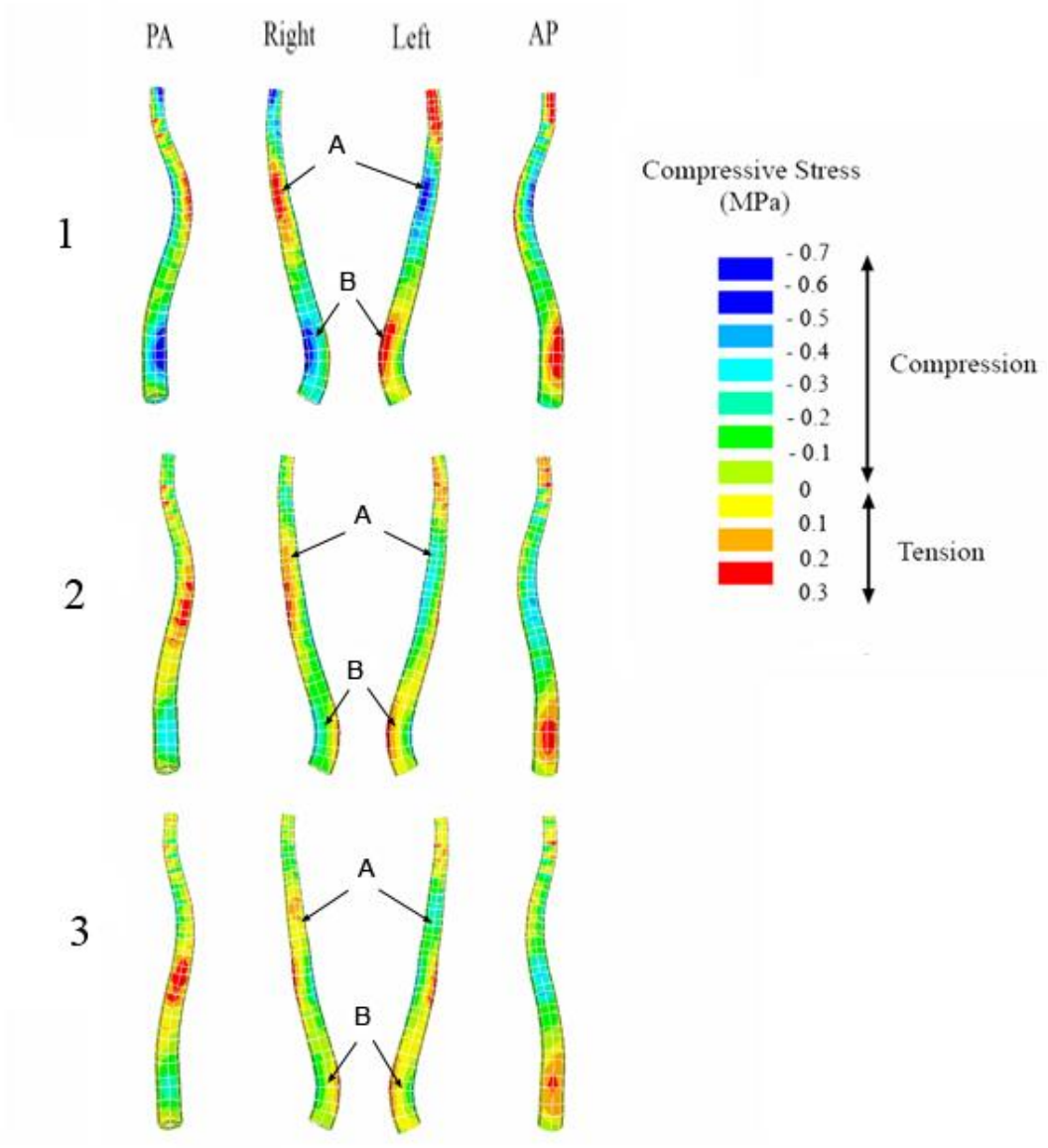

Figure 4.6 Article 2 Figure 6 Compressive stresses in the stiff spine model before and after the simulated brace installation on the FEM of patient P1 (1: before brace; 2: in-brace, strap tension =20 N; 3: in-brace, strap tension = 60 N, A: asymmetrical loading in the thoracic curve, B: asymmetrical loading in the lumbar curve)

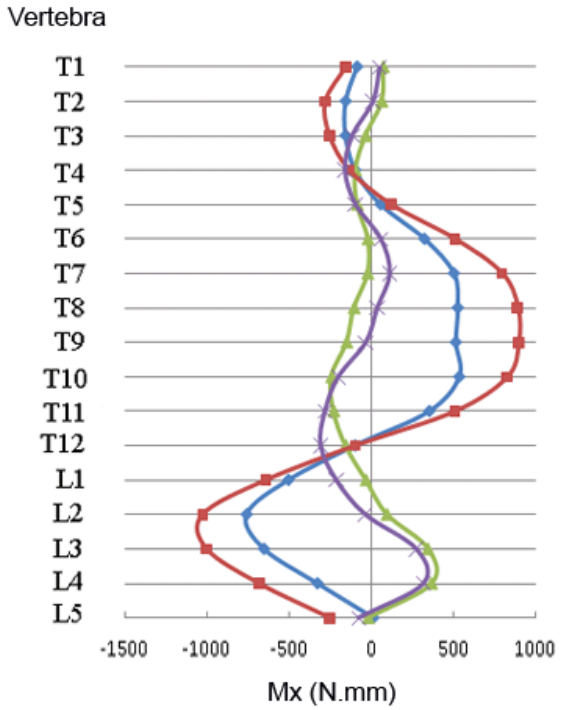

Figure 4.7 Article 2 Figure 7 Bending moment Mx acting on the vertebral endplates of patient P1 (flexible spine model: standing position without brace: , with brace for a strap tension of 60 N: ; stiff spine model: standing position without brace: , with brace for a strap tension of 60 N :)

4.3 Premier niveau d'évaluation de la validité du modèle

Les figures 4.8, 4.9 et 4.10 présentent pour 25 patients (P1 à P25) les résultats d'une évaluation de la validité du simulateur du traitement par corset prolongeant l'étude présentée dans l'article 2. Ces figures représentent la forme de la colonne vertébrale dans le plan frontal avant l'installation du corset (◆), après l'installation du corset réel sur le patient (▫), et après la simulation de l'installation du corset virtuel sur le patient (▲). Ne possédant pas la géométrie des corsets réels, les corsets virtuels ont été conçus selon une approche heuristique pour reproduire les résultats des corsets réels. La tension des courroies thoraciques et lombaires et la rigidité des disques intervertébraux ont également été ajustées selon une méthode heuristique afin d'optimiser l'adéquation entre la géométrie de la colonne vertébrale dans le corset réel et la géométrie simulée. La tension des courroies thoraciques et lombaires pouvait varier entre 20 et 70 N. La rigidité des disques intervertébraux pouvait être multipliée par un facteur K_{rigi} compris entre 0.5 et 2. Le tableau 4.3 indique les valeurs de ces paramètres utilisées pour chacun des patients.

Les figures 4.8, 4.9 et 4.10 montrent qu'en possédant des paramètres d'entrées appropriés pour le simulateur de corset, il est possible d'obtenir un effet immédiat dans le plan frontal très semblable aux corsets réels. En considérant la moyenne sur les 25 patients, la différence maximale entre la position frontale des vertèbres dans le corset réel et le corset simulé était de 3.5 mm (min: 2 mm; max: 5.1 mm).

Tableau 4.3: Tensions des courroies et facteur de rigidité spinale utilisés pour chacun des patients

Patient	Tension de Courroie (N)		Facteur de rigidité
	Thoracique	Lombaire	spinale K_{rigi}
P1	60	60	0.5
P2	60	60	1
P3	70	70	0.5
P4	20	20	1
P5	20	20	1
P6	60	60	1
P7	20	20	1
P8	70	70	0.5
P9	20	20	1
P10	20	20	0.5
P11	60	60	0.5
P12	20	20	1
P13	20	20	1
P14	40	40	1
P15	20	20	1
P16	20	20	1
P17	40	40	0.5
P18	60	60	0.5
P19	20	20	1
P20	60	60	1
P21	40	40	1
P22	60	60	0.5
P23	60	60	1
P24	60	60	0.5
P25	60	60	1

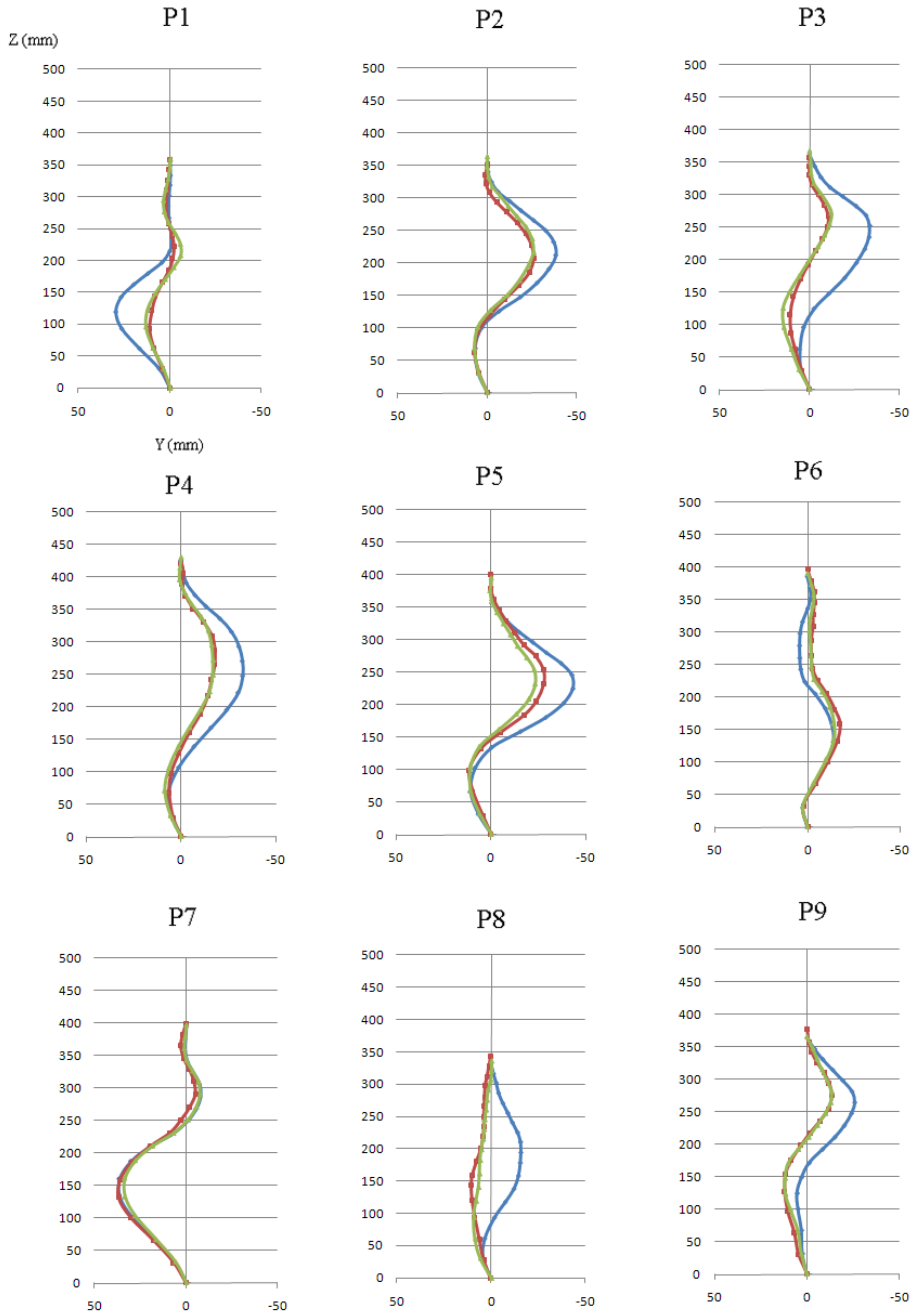

Figure 4.8: Géométrie du rachis (plan frontal) avant l'installation du corset (◆), après l'installation du corset réel sur le patient (◘), et après la simulation de l'installation du corset virtuel sur le patient (▲) (Patients P1 à P9)

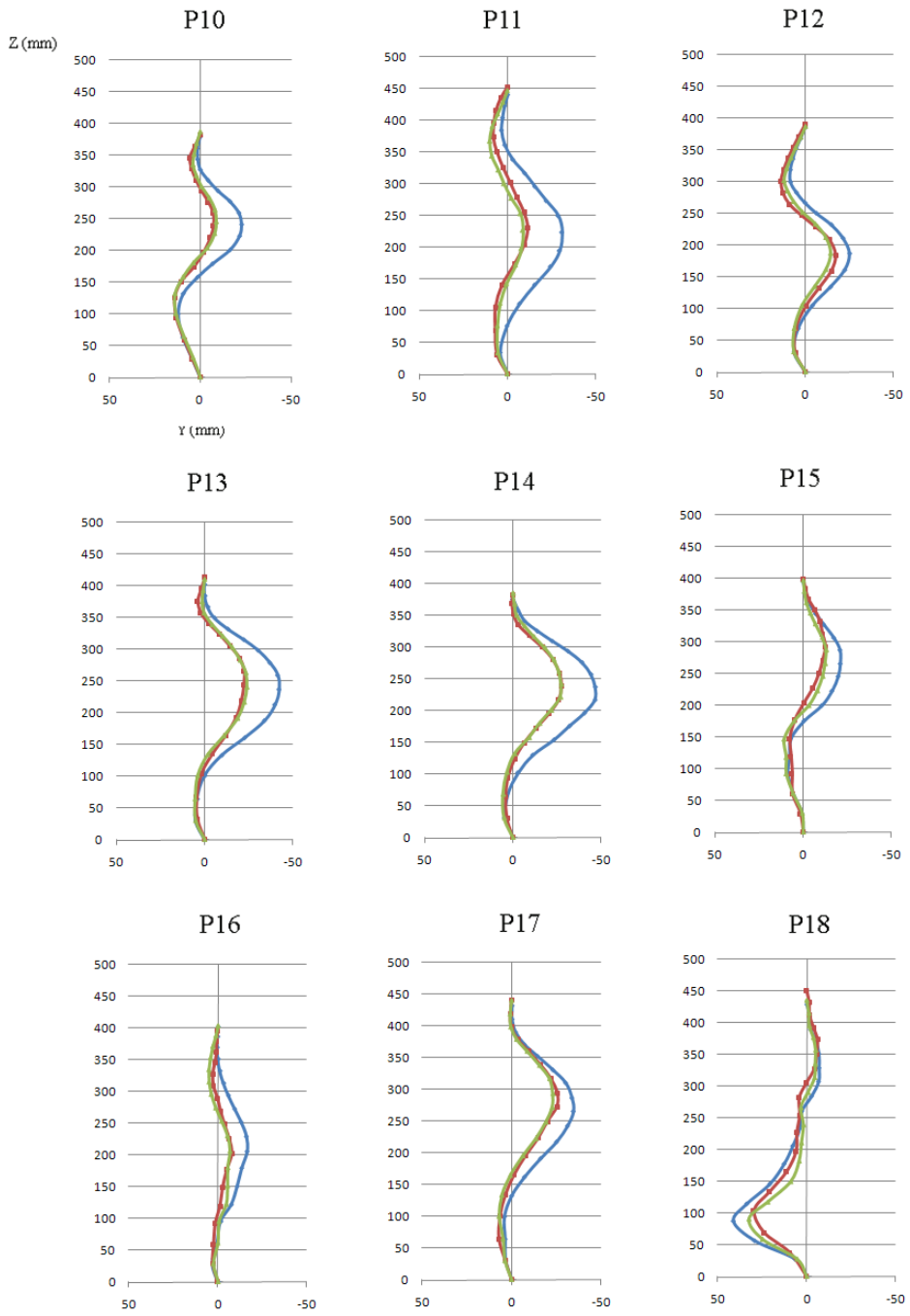

Figure 4.9: Géométrie du rachis (plan frontal) avant l'installation du corset (•), après l'installation du corset réel sur le patient (▫), et après la simulation de l'installation du corset virtuel sur le patient (▲) (Patients P10 à P18)

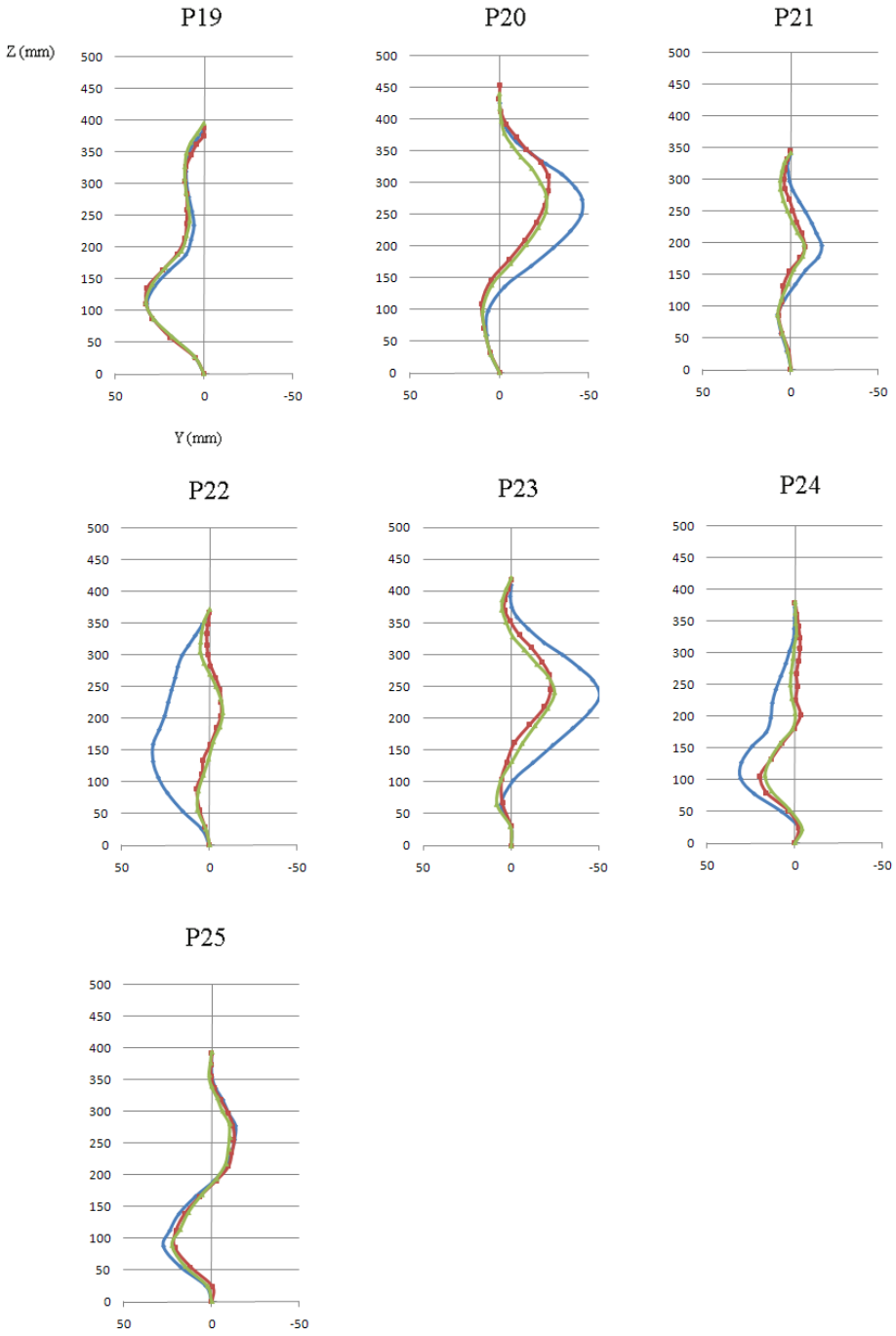

Figure 4.10**:** Géométrie du rachis (plan frontal) avant l'installation du corset (◆), après l'installation du corset réel sur le patient (▫), et après la simulation de l'installation du corset virtuel sur le patient (▲) (Patients P19 à P25)

CHAPITRE 5 ÉTUDE BIOMÉCANIQUE DU CORSET DE CHARLESTON

5.1 Situation du troisième article

L'article 2 présenté dans le chapitre précédent a décrit une nouvelle méthode de simulation d'un corset de type Boston. Grâce à l'inclusion des forces de gravité dans le processus de simulation, l'effet du corset sur les contraintes internes à la colonne vertébrale a pu être quantifié et analysé. Le troisième article présente un prolongement de cette étude biomécanique au corset de Charleston. Le corset de Charleston est un corset de type particulier. Il est porté uniquement de nuit, en position couchée et impose une inflexion latérale au patient. Dans l'article trois, une méthode de simulation du corset de Charleston est introduite. Les corrections géométriques produites par le modèle de sont calculées et comparées aux données de la littérature. Une analyse de l'effet du corset de Charleston sur l'asymétrie des contraintes en compression dans le rachis scoliotique est effectuée afin d'expliciter son principe de fonctionnement biomécanique.

Cet article est intitulé :« A biomechancial study of the Charleston brace for the treatment of scoliosis», et a été accepté pour publication dans la revue Spine en Novembre 2009. La contribution du premier auteur à la préparation et la rédaction de l'article est évaluée à 85%.

5.2 Article #3: A Biomechanical Study of the Charleston Brace for the Treatment of Scoliosis

A Biomechanical Study of the Charleston Brace for the Treatment of Scoliosis

Julien Clin, MSca [1,2], Carl-Éric Aubin, PhD [1,2], Stefan Parent, MD, PhD [2], Hubert Labelle, MD [2]

1- Dept. of Mechanical Engineering, École Polytechnique de Montréal

P.O. Box 6079, Station Centre-ville, Montréal, Québec, H3C 3A7, Canada

2- Sainte-Justine University Hospital Center

3175 Côte-Ste-Catherine Rd., Montréal, Québec, H3T 1C5, Canada

Address for notification, correspondence and reprints:
Carl-Eric Aubin, Ph.D. P.Eng., Full Professor
Canada Research Chair 'CAD Innovation in Orthopedic Engineering' & NSERC-Medtronic industrial Research Chair in Spine Biomechanics
Ecole Polytechnique, Department of Mechanical Engineering
P.O. Box 6079, Station "Centre-ville", Montreal (Quebec), H3C 3A7 CANADA
E-mail: carl-eric.aubin@polymtl.ca
Phone: 1 (514) 340-4711 ext 2836; FAX: 1 (514) 340-5867

Acknowledgements This study was funded by the Natural Sciences and Engineering Research Council of Canada. Special thanks to Dr Archana Sangole PhD for the careful revision of this manuscript

5.2.1 Abstract

Study Design. A biomechanical study of the Charleston brace.

Objective. To model the nighttime Charleston brace treatment and study its biomechanical action.

Summary of Background Data: The Charleston brace has been proposed as an alternative to the traditional daytime thoraco-lumbo-sacral orthosis (TLSO) for the treatment of moderate scoliotic deformities. It is worn at night and imposes a supine side-bending to reduce the major scoliotic curve. The biomechanics of the Charleston brace is still poorly understood.

Methods. The geometry of the spine, pelvis, rib cage and of the external trunk surface of two scoliotic patients were acquired using a 3D multiview x-ray reconstruction technique and surface topography. A finite element model of each patient's trunk was created. Two sets of mechanical properties (stiff and normal) of the spine were tested. For each case, the transition from standing to supine position was first simulated by modifying the direction of the gravity forces acting on the patients' spine. Supine bending was simulated by applying a lateral displacement on the first thoracic vertebra (T1). A custom-fit Charleston brace was modeled and positioned on the patient model. Tension was applied in the straps. Efficiency of the simulated Charleston braces was studied by computing geometrical corrections and effects on the internal stresses of the spine.

Results. The reduction of the major scoliotic curve varied between 58% and 97% and was in the range of published clinical data. Internal compressive stresses up to 1 MPa were generated on the convex side of the major scoliotic curve and tensile stresses up to 1 MPa on its concavity. In contrast, increased compressive stresses were exerted on the concavity of the secondary curves and added tensile stresses in their convexity.

Conclusion. This study quantified the Charleston brace biomechanical effect which consists in inverting the asymmetrical compressive loading in the major scoliotic curve. It also highlighted that the Charleston brace worsens the asymmetrical compressive loading in

the compensatory curves. The finite element model developed could help studying different brace designs and optimizing brace efficiency.

Keypoints:

- Charleston brace immediate effect can be simulated
- Charleston brace inverts the asymmetrical compressive loading in the major scoliotic curve
- Charleston brace worsens the asymmetrical compressive loading in the compensatory curve

5.2.2 Introduction

Scoliosis is a three-dimensional deformity of the spine and the rib cage. For small and moderate curves, bracing is the most common treatment. Different bracing systems exist, the most frequently used being the thoraco-lumbo-sacral orthoses (TLSO) that are generally worn almost full-time. The Boston brace in North-America and the Chêneau brace in Europe are examples of commonly used TLSO's. An alternative to the TLSO is the night time Charleston Brace, introduced in 1990 by Price [1]. Its action principle is to impose a supine side bending to the patient trunk in the direction of his major scoliotic curve in order to reduce it [2]. The clinical efficiency of the Charleston brace to prevent the progression of the scoliotic curves has been demonstrated [1,3,4], and compared to conventional TLSO's [5-7]. Katz [7] and Howard [6] concluded that the TLSO's were more efficient than the Charleston brace, while Gepstein [5] found no significant difference.

The Charleston brace designers have underlined that the factors contributing to the efficiency of night-time side-bending are unclear [2]. Stretching the concavity of the curvature and possibly a physiological contracture on the convexity appears to play a role, but that has not been proven. In theory, the brace should add opposite tensile and compression forces to the vertebral epiphyses compared to the forces acting in an upright posture.

To better understand the biomechanics of a TLSO, finite element models have been used. The Milwaukee brace [8] and the Boston brace [9,10] have been simulated by directly applying forces on a finite element model of the trunk. The optimal forces to correct scoliotic deformities have been studied [11-13]. Recently, a more realistic model to simulate a TLSO treatment has been proposed [14]. Instead of directly applying forces on a finite element model of the trunk, a TLSO was explicitly modeled and its action on the patient simulated using a contact interface.

The Charleston brace treatment however has never been simulated. Consequently, the aim of this study was to model the Charleston brace treatment in order to study its biomechanical action and to verify if it really adds opposite tensile and compression forces to the vertebral epiphyses compared to the forces acting in an upright posture.

5.2.3 Methods

Patient specific model geometry

The geometry of the spine, rib cage and pelvis of two scoliotic patients (P1 and P2) were acquired using a multiview self-calibrated radiography reconstruction technique [15-17] (Figure1A). On three radiographs (lateral, postero-anterior and postero-anterior with a 20˚ angled down incidence) anatomical landmarks (6 per vertebra, 11 per rib, 24 for the pelvis) were digitized and reconstructed in 3D. An atlas of detailed reconstructed vertebrae, ribs and pelvis along with a free-form interpolation technique were then used to obtain the final geometry [16]. The accuracy of this reconstruction method was 3.3 mm on average (SD 3.8 mm) [16]. In addition the external trunk surface of the patient was digitized using a 3-dimensionnal surface topography technique (3-dimensional Capturor, Inspeck Inc., Montreal, Quebec, Canada) [18] (Figure1B). Twelve markers were attached to the patient's torso and were visible on both the x-rays and the trunk surface. Internal and external geometries were superimposed by applying a point-to-point least square algorithm to the respective sets of 12 markers (Figure1C) [19]. A global coordinate system Rg, with origin at the center of the first sacral vertebra S1, was associated with this geometry such that the z-

axis was directed vertically upwards, x-axis was postero-anterior and the y-axis was lateral (oriented from left to right) (Figure1).

The two scoliotic patients had a right thoracic (Cobb: 36˚ and 20˚ respectively) and a left lumbar curve (Cobb: 16 and 33˚) (Figure 4).

Patient- specific finite element model of the trunk

Based on this geometry, a personalized finite element (FE) model of the patient's torso was built. The Ansys 11.0 FE package was used (Ansys Inc., Canonsburg, PA, USA). It has been presented in previous publications [9,14,20,21] (Figure 3A). The thoracic and lumbar vertebrae, intervertebral discs, ribs, sternum, cartilage and abdominal cavity were represented by 3D elastic beam elements, the zygapophyseal joints by shells and surface-to-surface contact elements, the vertebral and intercostal ligaments by tension-only spring elements and the external soft tissues by hexahedron elements.

Mechanical properties of all the components of the model were taken from experimental and published data [10,20,21]. To evaluate the influence of the flexibility of the spine, a "stiff" and a "flexible" spine were tested (intervertebral disc stiffness multiplied and divided by 2 respectively) [22].

Nodes representing the center of gravity of each trunk slice corresponding to a vertebral level were created. Their position in the sagittal plane was derived from the literature [23-26] and scaled according to patient size. In the coronal plane, it has been assumed that their position followed the scoliotic curve of the spine. Non-deformable beam elements connected these nodes to their relative vertebra to transmit the gravitational forces to the spine. The magnitude of the gravitational forces associated to each center of gravity node was scaled to the patients specific weight based on published values [23-26].

Supine bending Simulation

The initial geometry of the patients was acquired while they were standing (under gravity). A simulation was first done to compute the transition from standing to supine position (Figure 2). Forces directed vertically upwards were applied in order to find the zero-

gravity geometry (Figure 2B). During this step the pelvis was fixed in space and the translation of the first thoracic vertebrae in the transverse plane was blocked. An optimization process was developed to find the zero gravity geometry (stress free) that leads, when the vertical gravitational forces are reapplied, to the actual geometry of the patient in the standing position (Figure 2C). Gravitational forces were then applied in the antero-posterior direction in order to find the geometry of the patient in the supine position (Figure 2D). During this step the pelvis was fixed in space, the translation of the first thoracic vertebra in the transverse plane was blocked and the translation of the 7^{th} and 8^{th} ribs in the antero-posterior direction (x axis) was blocked (to simulate supine positioning on a horizontal surface).

From this supine position (Figure 3A), lateral bending was simulated by applying a displacement of 150 mm to the first thoracic vertebra (Figure 3B). For P1, the major curve is the right thoracic curve, so the bending was in the right direction, while for P2 the major curve is the left lumbar curve, so the bending was in the left direction.

Brace model

A custom-fit geometrical brace model following the Charleston brace system principles was created over the already generated FEM of the patient trunk (Figure 3C). It was based on ten generative curves whose shape was determined by 24 geometrical parameters computed on the external surface of the patient in the simulated supine bending position. A surface interpolating these ten generative curves was created. It was divided into 170 sub-surfaces. The brace openings were created by deleting some sub-surfaces. The remaining sub-surfaces were then extruded outward to create a volumetric representation of the foam layer of the brace geometry. The pads were created by inwardly extruding some sub-surfaces.

The modeled pads were positioned on the right thoracic region, on the left lumbar region and on the trochanter extension for both patients. For P1, the trochanteric extension was located on the left side while it was located on the right side for P2. The external rigid shell followed the sagittal curves of the patient in the sagittal plane.

The finite element model of the brace was then generated. An external rigid shell was located on the external surface of the volume representing the foam layer, and was modeled by 4-node quadrilateral shell elements. The foam layer and the pads were modeled by 8-nodes hexahedral elements (Figure 3D). The material of the rigid shell was polyethylene (E = 1500 Mpa, ν = 0.3), the foam layer was made of soft polyethylene foam (E = 1 MPa, ν = 0.3) and the pads were represented by stiff polyethylene foam (E = 10 MPa, ν = 0.3) [21,27]. These materials were modeled as linear elastic. A surface-to-surface contact interface taking friction into account (μ = 0.6 [28]) was created between the interior of the brace model and the exterior of the trunk model.

Simulation of the brace installation

The brace installation on the patient was simulated in 2 steps after that the supine bending position was obtained as described previously. In the first step, the brace was opened by applying displacements on four nodes located in its anterior part and was positioned on the patient. In the second step, three sets of collinear forces representing thoracic, lumbar and pelvic strap tensions of 60 N were applied on the nodes corresponding to the strap fixations on the anterior part of the brace (Figure 3E) [29]. Finally, the displacement initially applied to T1 was suppressed and the equilibrium state was computed.

Study of brace biomechanics

Once the simulation was completed several 3D clinical indices (Cobb angles, kyphosis, lordosis, rib hump, axial rotation) and the pressures generated by the brace on the patient's trunk were computed. The global forces and moments acting on the vertebral endplates and the axial compressive stresses in the spine were also evaluated in a local system R_{local} for each vertebra. The origin of R_{local} was located at the center of the vertebral body. The z-axis was in the direction of the line joining the centers of the vertebral endplate centers. The x-axis was the projection of the global x-axis on the plane perpendicular to the z-axis. The y-axis was perpendicular to the x and z-axes.

5.2.4 Results

The transition from an upright to supine position induced a mean 38% correction of the lumbar and thoracic Cobb (Figure 4 and Table 1). The transition from a straight supine position to a bent supine position in brace induced a further reduction (mean: 37%) of the major scoliotic curves (thoracic for P1 and lumbar for P2) but also increased the secondary curve (mean: 25%). The correction in the transverse plane was negligible (axial rotation of the apical vertebra and of the rib hump).

The simulated brace exerted pressure on the torsos of the patients against the left lumbar pad (Figure 5A), the right thoracic pad (Figure 5B), the trochanteric pads (Figure 5C) and the abdominal shell (Figure 5D). Brace-torso interface pressure ranged between 0 and 30 kPa.

The resulting local side bending moments (Mx) applied on the vertebra endplates in the standing and supine positions and in brace are shown in Figure 7. This bending moment quantifies the asymmetrical compressive loading of the vertebrae in the coronal plane shown in Figure 6. For the patients in an upright standing position, the compressive loading of the spine in the coronal plane is asymmetrical and maximal at the apical levels. The compressive loading is greater in the concavity of the scoliotic curves (compression up to 1 MPa for P1 and P2) than in their convexity (tension up to 0.5 MPa for P1 and 0.2 MPa for P2). A marked asymmetrical compressive pressure is also present at L5 for P2 with a greater compression on the left than on the right side.

In the supine position, this asymmetrical loading becomes almost null. In the Charleston brace, the side of the spine located in the direction of the bending (right for P1, left for P2) is subjected to compressive stresses (up to 1 MPa) while the other side is subjected to tensile stresses (up to 1 MPa). Consequently, the Charleston brace induced an inverted bending moment on the major scoliotic curve compared to the upright standing position. It however generated bending moments on the secondary curve similar to those present in the upright standing position. For P1 this side effect was equivalent in magnitude to the effect on the major curve. For P2 it remained inferior (Figure 7).

5.2.5 Discussion

The resulting geometrical corrections given by the model corresponded to the expected clinical behavior and to the published experimental data. The transition from standing to supine position induced a correction of the scoliotic curves (Table 1, Figure 4) due to the suppression of gravity forces along the spine longitudinal axis and the interaction with the horizontal surface. The amount of reduction of the coronal curves is similar to the mean reduction of 37% found by Delorme [30] in prone position of surgical patients. The relative correction of the major scoliotic curve obtained in-brace (between 58% and 92% for P1, between 58% and 97% for P2 compared to the standing position) is similar to published data (mean correction of 73-83 % for the primary curve with the Charleston brace system [1,7]).

The distribution of the pressures exerted by the braces on the patients' trunk (Figure 5) corresponded to what was expected considering the positioning of the pads. The pressure, between 10 and 30 kPa, corresponded to experimental measures reported by Mac-Thiong et al. [29] with the Boston brace system. The action of the thoracic, lumbar and trochanteric pads was clearly visible. The pressures are the results of force-reaction due to the interaction of two deformable bodies with their specific stiffness (patient's trunk and brace system) and should not be interpreted as external forces applied on the torso [20].

Globally, the biomechanical action of the Charleston brace on the asymmetrical compressive loading of the vertebrae in the coronal plane corresponded to what was assumed by its designers [2]. For the major curve the Charleston brace induced an asymmetrical loading of the vertebral endplates in the coronal plane inverted relatively to the standing position (Figures 6 and 7), with compressive stresses in the convexity of the curve and tensile stresses in the concavity. According to the Hueter-Volkmann principle [31] (compressive stresses slow growth while tensile stresses fasten growth) it should invert the growth deformation process of the major scoliotic curve. However, the Charleston brace also generated negative effects for the compensatory curves (especially for P1). Asymmetrical loads of the vertebrae were similar to those in the standing position. This could aggravate the deformation process of the secondary curves. It confirms the assertions

of Price [1,3] who recommended to carefully follow the evolution of the compensatory curves when using the Charleston brace.

The interpretation of growth modulation effects should be done with caution. The growth sensitivity to mechanical stresses and mechanoregulation are still not well understood and the subject of active research [32-36]. It is not well known if there exists a threshold load that could trigger the growth modulation process, or what is the most efficient load condition (static vs dynamic) [35,36]. The circumdiurnal effectiveness of the growth modulation process is also questioned, but Stokes [37] concluded there was no difference in growth modulation between diurnal and nocturnal periods.

When interpreting the results of the present study, the model limits should also be taken into account. The trunk model did not include muscles. However, their role is probably passive during the night while the patient is asleep. With the model it was possible to maintain the supine bending position with very low forces at the boundary condition sites in the coronal and sagittal planes. The intervertebral discs and vertebrae were represented by beam elements without taking into account the hydrostatic behavior of the nucleus, which might affect the load distribution on the growth plates. Future work should focus on using a more detailed model of the spine to analyze this effect. Even if the results are quite plausible compared to published literature [32,38], there is still no data about the stress distribution in a scoliotic spine, which makes the validation quite difficult [38,39].

The next step of this project will be to validate more thoroughly the model by simulating the Charleston brace effect on a larger cohort of patients that actually wear a Charleston brace (and compare the simulation results to the in-brace correction). Supine and bending x-rays acquisition and calibrated flexibility tests could also be included in the protocol to personalize the mechanical properties of the spine model for each patient and to validate the intermediate steps of the simulation process [22,40].

5.2.6 Conclusion

The present study showed the feasibility of simulating the Charleston brace and the value of the model in providing insights into its biomechanical action. It confirmed the working

principle of the brace assumed by its designers [2] which consists of inverting the asymmetrical compressive loading at the level of the major scoliotic curve. It also highlighted a shorthcoming of the supine side-bending principle which is to worsen the asymmetrical compressive loading in the compensatory curves. The finite element model developed could help studying different brace designs and to optimize brace efficiency.

5.2.7 Figures and Tables Captions

Tableau 5.1 Article 3 Table 1: Geometrical indices of the patients in different positions

			Flexible Spine		Stiff Spine	
		Standing	Supine	In Brace	Supine	In Brace
P1	Thoracic Cobb (°)	36	15	6	21	13
	Lumbar Cobb (°)	16	7	12	10	17
	Kyphosis (°)	9	1	1	3	4
	Lordosis (°)	37	25	22	30	29
	Rib Hump (°)	20	18	21	18	21
	Axial Rotation (°)	10	10	10	10	10
P2	Thoracic Cobb (°)	20	14	15	17	21
	Lumbar Cobb (°)	33	19	1	25	9
	Kyphosis (°)	49	29	31	36	38
	Lordosis (°)	37	23	26	28	30
	Rib Hump (°)	9	9	9	9	9
	Axial Rotation (°)	10	9	11	10	11

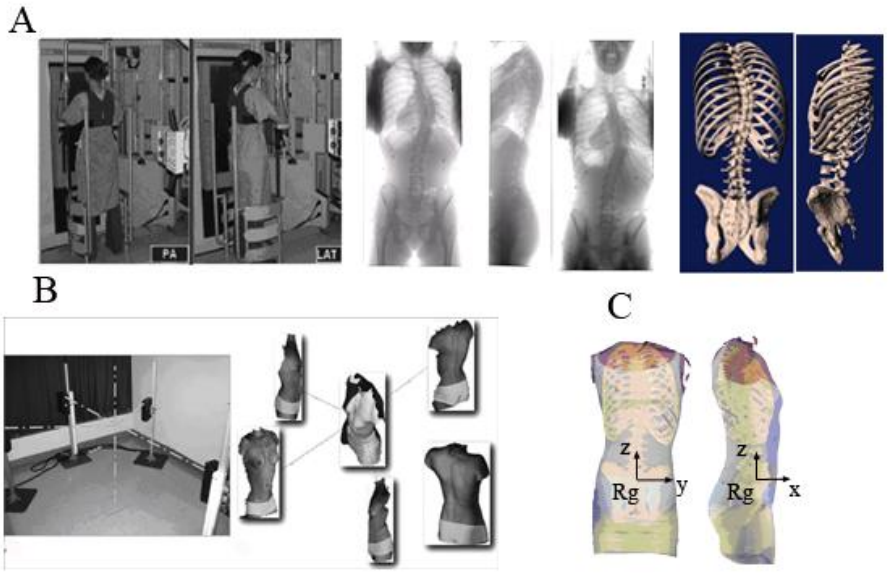

Figure 5.1 Article 3 Figure 1: A Acquisition of the internal geometry using the multi-view radiographic reconstruction technique; B Acquisition of the external geometry using topography technique; C Superimposition of the two geometries

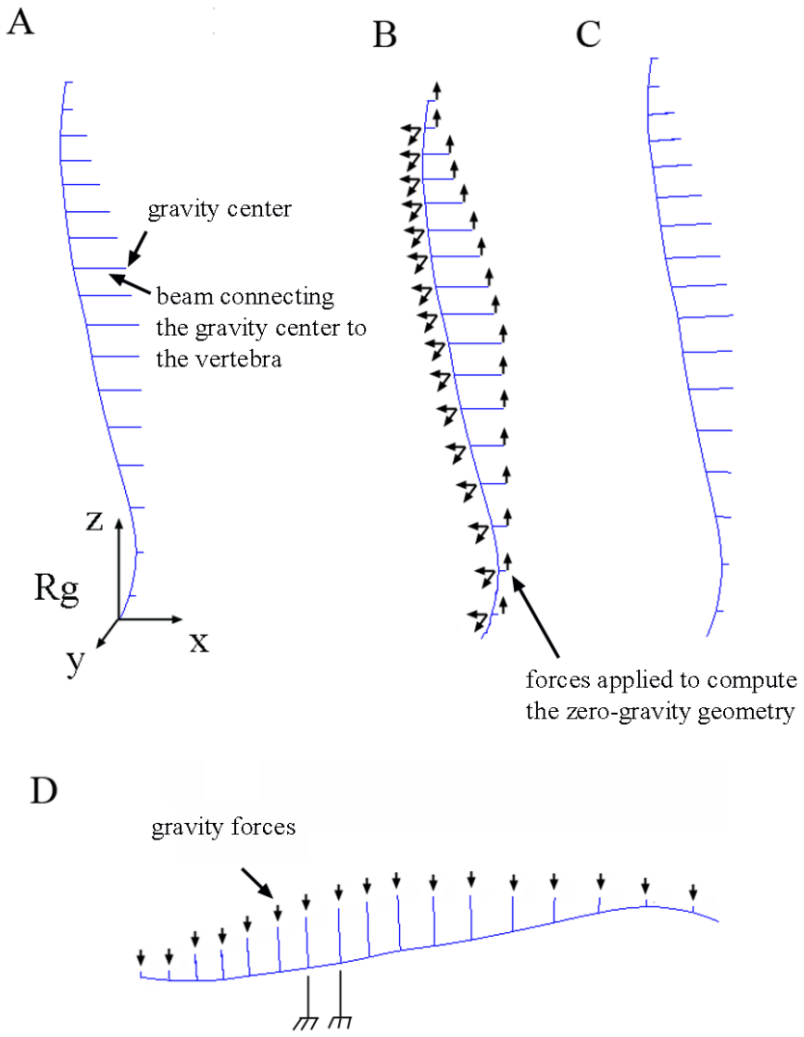

Figure 5.2 Article 3 Figure 2: Simulation of the supine position (A: Initial geometry of the patient's spine in the standing position, B: Computation of the zero-gravity geometry, C: Zero-gravity geometry, D: Computation of the supine position)

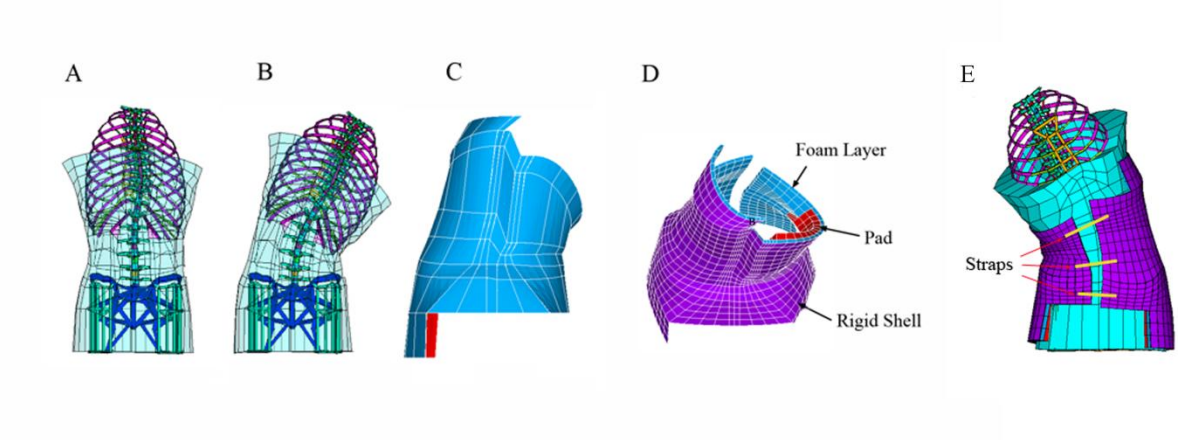

Figure 5.3 Article 3 Figure 3: A- FEM of the patient (P1) in the supine position; B- FEM in the supine bending position; C- Geometrical Model of the brace; D- FEM of the brace; E- Resulting FEM (brace installed on the patient)

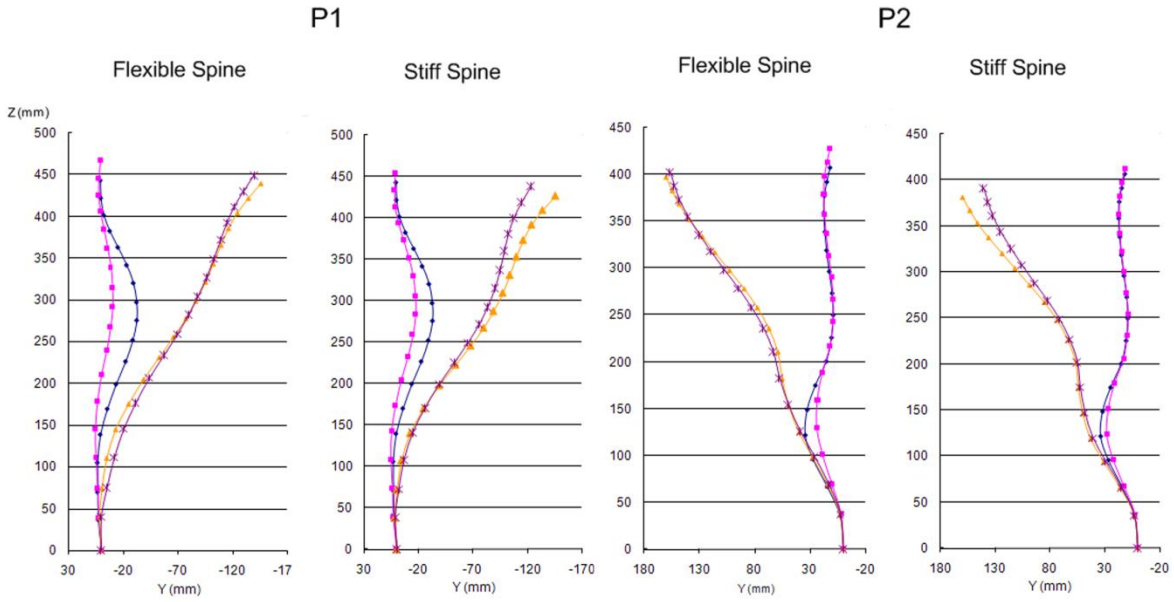

Figure 5.4 Article 3 Figure 4: Spine curves of the patients in the coronal plane: Initial standing position (◆), Simulated supine position (■), Simulated supine bending (▲), Simulated In brace (✳)

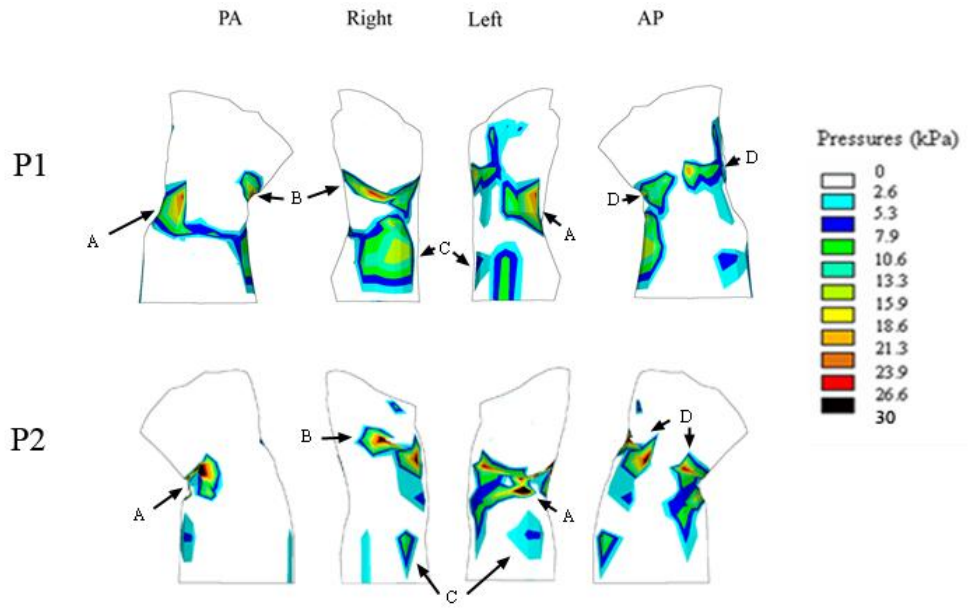

Figure 5.5 Article 3 Figure 5: Simulated pressures exerted by the braces on the patient torsos

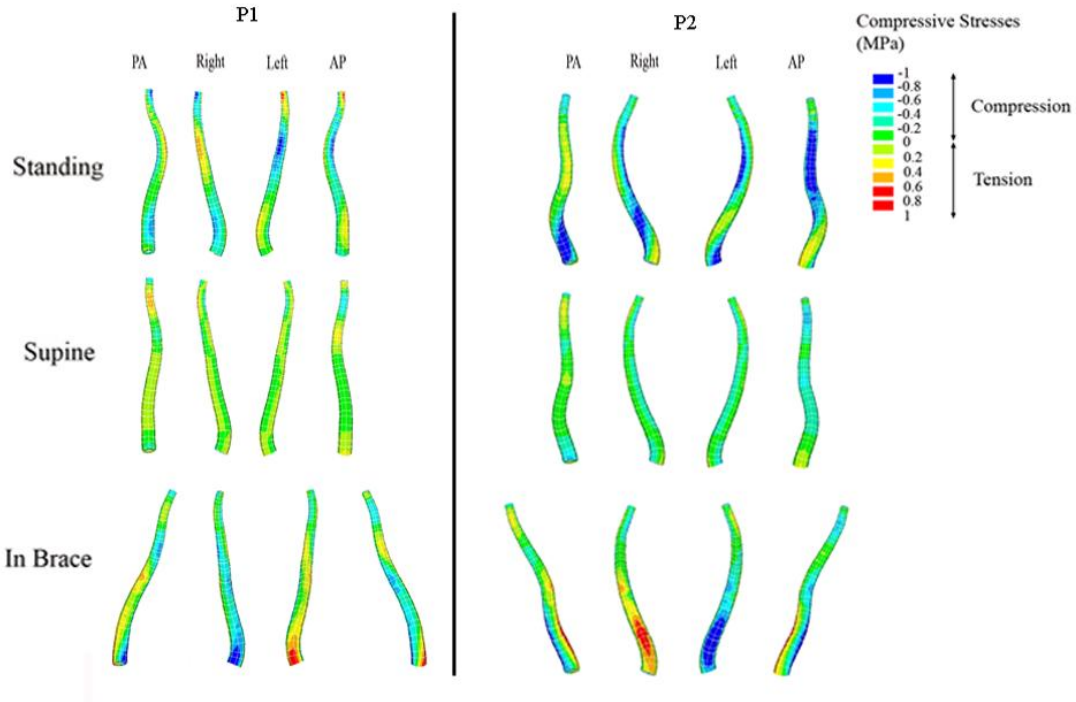

Figure 5.6 Article 3 Figure 6: Compressive stresses in the spine models (stiff spine model)

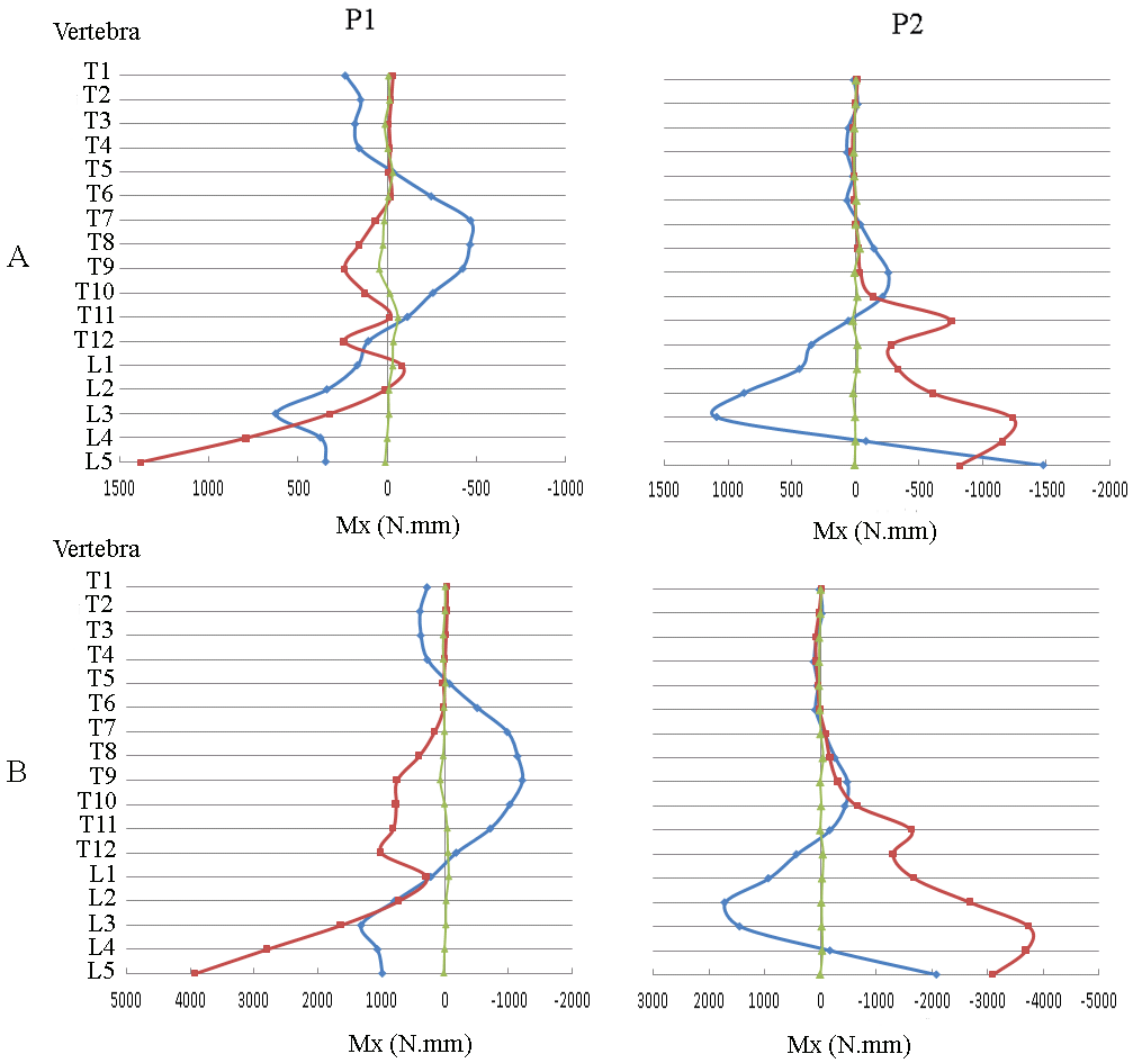

Figure 5.7 Article 3 Figure 7: Resulting bending moment Mx on the vertebral endplates (◇: initial standing position, △: simulated supine position, ▫: simulated supine position wearing the brace) (A: Flexible spine; B: Stiff spine)

5.2.8 References

1. Price CT, Scott DS, Reed FE, Jr., et al. Nighttime bracing for adolescent idiopathic scoliosis with the Charleston bending brace. Preliminary report. *Spine* 1990;15:1294-9.

2. Hooper R, Reed F, Price C. The Charleston Brace. *SRS bracing manual (http://www.srs.org/professionals/bracing_manuals/)* 2003.

3. Price CT, Scott DS, Reed FR, Jr., et al. Nighttime bracing for adolescent idiopathic scoliosis with the Charleston Bending Brace: long-term follow-up. *J Pediatr Orthop* 1997;17:703-7.

4. Trivedi JM, Thomson JD. Results of Charleston bracing in skeletally immature patients with idiopathic scoliosis. *J Pediatr Orthop* 2001;21:277-80.

5. Gepstein R, Leitner Y, Zohar E, et al. Effectiveness of the Charleston bending brace in the treatment of single-curve idiopathic scoliosis. *J Pediatr Orthop* 2002;22:84-7.

6. Howard A, Wright JG, Hedden D. A comparative study of TLSO, Charleston, and Milwaukee braces for idiopathic scoliosis. *Spine* 1998;23:2404-11.

7. Katz DE, Richards BS, Browne RH, et al. A comparison between the Boston brace and the Charleston bending brace in adolescent idiopathic scoliosis. *Spine* 1997;22:1302-12.

8. Andriacchi TP, Schultz AB, Belytschko TB, et al. Milwaukee brace correction of idiopathic scoliosis. A biomechanical analysis and a restrospective study. *J Bone Joint Surg Am* 1976;58:806-15.

9. Perie D, Aubin CE, Petit Y, et al. Boston brace correction in idiopathic scoliosis: a biomechanical study. *Spine* 2003;28:1672-7.

10. Perie D, Aubin CE, Petit Y, et al. Personalized biomechanical simulations of orthotic treatment in idiopathic scoliosis. *Clin Biomech (Bristol, Avon)* 2004;19:190-5.

11. Gignac D, Aubin CE, Dansereau J, et al. Optimization method for 3D bracing correction of scoliosis using a finite element model. *Eur Spine J* 2000;9:185-90.

12. Patwardhan AG, Bunch WH, Meade KP, et al. A biomechanical analog of curve progression and orthotic stabilization in idiopathic scoliosis. *J Biomech* 1986;19:103-17.

13. Wynarsky GT, Schultz AB. Optimization of skeletal configuration: studies of scoliosis correction biomechanics. *J Biomech* 1991;24:721-32.

14. Clin J, Aubin CE, Labelle H. Virtual prototyping of a brace design for the correction of scoliotic deformities. *Med Biol Eng Comput* 2007;45:467-73.

15. Aubin CE, Descrimes JL, Dansereau J, et al. [Geometrical modeling of the spine and the thorax for the biomechanical analysis of scoliotic deformities using the finite element method]. *Ann Chir* 1995;49:749-61.

16. Delorme S, Petit Y, de Guise JA, et al. Assessment of the 3-d reconstruction and high-resolution geometrical modeling of the human skeletal trunk from 2-D radiographic images. *IEEE Trans Biomed Eng* 2003;50:989-98.

17. Kadoury S, Cheriet F, Dansereau J, et al. Three-dimensional reconstruction of the scoliotic spine and pelvis from uncalibrated biplanar x-ray images. *J Spinal Disord Tech* 2007;20:160-7.

18. Pazos V, Cheriet F, Danserau J, et al. Reliability of trunk shape measurements based on 3-D surface reconstructions. *Eur Spine J* 2007;16:1882-91.

19. Fortin D, Cheriet F, Beausejour M, et al. A 3D visualization tool for the design and customization of spinal braces. *Comput Med Imaging Graph* 2007;31:614-24.

20. Aubin CE, Dansereau J, De Guise JA, et al. [A study of biomechanical coupling between spine and rib cage in the treatment by orthosis of scoliosis]. *Ann Chir* 1996;50:641-50.

21. Perie D, Aubin CE, Lacroix M, et al. Biomechanical modelling of orthotic treatment of the scoliotic spine including a detailed representation of the brace-torso interface. *Med Biol Eng Comput* 2004;42:339-44.

22. Petit Y, Aubin CE, Labelle H. Patient-specific mechanical properties of a flexible multi-body model of the scoliotic spine. *Med Biol Eng Comput* 2004;42:55-60.

23. Cheng CK, Chen HH, Chen CS, et al. Segment inertial properties of Chinese adults determined from magnetic resonance imaging. *Clin Biomech (Bristol, Avon)* 2000;15:559-66.

24. Liu YK, Laborde JM, Van Buskirk WC. Inertial properties of a segmented cadaver trunk: their implications in acceleration injuries. *Aerosp Med* 1971;42:650-7.

25. Pearsall DJ, Reid JG, Livingston LA. Segmental inertial parameters of the human trunk as determined from computed tomography. *Ann Biomed Eng* 1996;24:198-210.

26. Pearsall DJ, Reid JG, Ross R. Inertial properties of the human trunk of males determined from magnetic resonance imaging. *Ann Biomed Eng* 1994;22:692-706.

27. Sanders JE, Greve JM, Mitchell SB, et al. Material properties of commonly-used interface materials and their static coefficients of friction with skin and socks. *J Rehabil Res Dev* 1998;35:161-76.

28. Zhang M, Mak AF. In vivo friction properties of human skin. *Prosthet Orthot Int* 1999;23:135-41.

29. Mac-Thiong JM, Petit Y, Aubin CE, et al. Biomechanical evaluation of the Boston brace system for the treatment of adolescent idiopathic scoliosis: relationship between strap tension and brace interface forces. *Spine* 2004;29:26-32.

30. Delorme S, Labelle H, Poitras B, et al. Pre-, intra-, and postoperative three-dimensional evaluation of adolescent idiopathic scoliosis. *J Spinal Disord* 2000;13:93-101.

31. Roaf R. Vertebral growth and its mechanical control. *J Bone Joint Surg Br* 1960;42-B:40-59.

32. Stokes IA, Aronsson DD, Dimock AN, et al. Endochondral growth in growth plates of three species at two anatomical locations modulated by mechanical compression and tension. *J Orthop Res* 2006;24:1327-34.

33. Villemure I, Chung MA, Seck CS, et al. Static compressive loading reduces the mRNA expression of type II and X collagen in rat growth-plate chondrocytes during postnatal growth. *Connect Tissue Res* 2005;46:211-9.

34. Villemure I, Cloutier L, Matyas JR, et al. Non-uniform strain distribution within rat cartilaginous growth plate under uniaxial compression. *J Biomech* 2007;40:149-56.

35. Frost HM. Skeletal structural adaptations to mechanical usage (SATMU): 3. The hyaline cartilage modeling problem. *Anat Rec* 1990;226:423-32.

36. Frost HM. Skeletal structural adaptations to mechanical usage (SATMU): 1. Redefining Wolff's law: the bone modeling problem. *Anat Rec* 1990;226:403-13.

37. Stokes IA, Gwadera J, Dimock A, et al. Modulation of vertebral and tibial growth by compression loading: diurnal versus full-time loading. *J Orthop Res* 2005;23:188-95.

38. Meir AR, Fairbank JC, Jones DA, et al. High pressures and asymmetrical stresses in the scoliotic disc in the absence of muscle loading. *Scoliosis* 2007;2:4.

39. Meir A, McNally DS, Fairbank JC, et al. The internal pressure and stress environment of the scoliotic intervertebral disc--a review. *Proc Inst Mech Eng [H]* 2008;222:209-19.

40. Lamarre ME, Parent S, Labelle H, et al. Assessment of spinal flexibility in adolescent idiopathic scoliosis: suspension versus side-bending radiography. *Spine* 2009;34:591-7.

.

CHAPITRE 6 ÉTUDE DE L'INFLUENCE DES PARAMÈTRES DE CONCEPTION D'UN CORSET

6.1 Situation du quatrième article

Les articles deux et trois ont décrit de nouvelles méthodes de simulation des corsets de type Boston et Charleston. Dans le quatrième article, la méthode de simulation du corset de type Boston décrite dans l'article 2 est utilisée afin d'étudier l'influence des paramètres de conception des corsets. Un grand nombre de corsets différents sont testés sur 3 patients et leurs effets immédiats sur les corrections géométriques 3D sont comparés afin de détecter quels sont les paramètres de conception les plus influents.

Cet article est intitulé :« Comparison of the biomechanical 3D efficiency of different brace designs for the treatment of scoliosis using a finite element model», et a été publié dans la revue European Spine Journal en Janvier 2010. La contribution du premier auteur à la préparation et la rédaction de l'article est évaluée à 85%.

6.2 Article #4: Comparison of the biomechanical 3D efficiency of different brace designs for the treatment of scoliosis using a finite element model

Comparison of the biomechanical 3D efficiency of different brace designs for the treatment of scoliosis using a finite element model

Julien Clin[1,2], Carl-Éric Aubin[1,2], Stefan Parent[1,2], Archana Sangole[1,2], Hubert Labelle[2]

1- Dept. of Mechanical Engineering, École Polytechnique de Montréal

P.O. Box 6079, Station Centre-ville, Montréal, Québec, H3C 3A7, Canada

2- Sainte-Justine University Hospital Center

3175 Côte-Ste-Catherine Rd., Montréal, Québec, H3T 1C5, Canada

Address for notification, correspondence and reprints:

Carl-Eric Aubin, Ph.D., P.Eng., Full Professor

Canada Research Chair 'CAD Innovation in Orthopedic Engineering'

& NSERC-Medtronic industrial Research Chair in Spine Biomechanics

Ecole Polytechnique, Department of Mechanical Engineering

P.O. Box 6079, Station "Centre-ville", Montreal (Quebec), H3C 3A7 CANADA

E-mail: carl-eric.aubin@polymtl.ca

Phone: 1 (514) 340-4711 ext 2836; FAX: 1 (514) 340-5867

Acknowledgements This study was funded by the Natural Sciences and Engineering Research Council of Canada.

6.2.1 Abstract: The biomechanical influence of thoraco-lumbo-sacral bracing, a commonly employed treatment in scoliosis, is still not fully understood. The aim of this study was to compare the immediate corrections generated by different virtual braces using a patient-specific finite element model (FEM) and to analyze the most influential design factors. The 3D geometry of 3 patients presenting different types of curves was acquired with a multi-view x-ray technique and surface topography. A personalized FEM of the patients' trunk and a parametric model of a virtual custom-fit brace were then created. The installation of the braces on the patients was simulated. The influence of 15 design factors on the 3D correction generated by the brace was evaluated following a design of experiments simulation protocol allowing computing the main and two-way interaction effects of the design factors. A total of 12,288 different braces were tested. Results showed a great variability of the braces effectiveness. Of the fifteen design factors investigated, according to the 2 modalities chosen for each one, the 5 most influential design factors were the position of the brace opening (posterior vs anterior), the strap tension, the trochanter extension side, the lordosis design and the rigid shell shape. The position of the brace opening modified the correction mechanism. The trochanter extension position influenced the efficiency of the thoracic and lumbar pads by modifying their lever arm. Increasing the strap tension improved corrections of coronal curves. The lordosis design had an influence in the sagittal plane but not in the coronal plane. This study could help to better understand the brace biomechanics and to rationalize and optimize their design.

Keywords Scoliosis; Brace; Finite element model; Design; Optimization

6.2.2 Introduction

Scoliosis is a three-dimensional deformity of the spine and of the rib cage. For moderate deformities, bracing is the most common treatment. However, its efficiency in preventing the progression of scoliotic deformities is still controversial [14, 19-21, 30]. Many questions remain about what could be the best brace design. For instance it is unclear where

the pads and openings should be positioned and how they should be shaped. Rigo [29] found significant variability in the brace designs that were recommended by 21 brace specialists for the same patient (right thoracic curve scoliosis with a minor lumbar curve). There was no consensus about whether the thoracic pad should be positioned below, at or above the apical rib, the optimal shape of the pads, the inclusion of an anterior derotationnal thoracic pad and the shape of the pelvis section (side of trochanteric extension and location of pads). Van Rhijn [33] compared the immediate effect of lumbar and thoracic braces on coronal curves and found that lumbar braces, relative to thoracic braces, significantly improved the correction of the lumbar curve and allowed spontaneous correction in the thoracic curve through improved balance of the spine. To our knowledge, this study was the only one that compared the efficiency of different brace designs on the same given patient.

A numerical model based analysis of brace biomechanics overcomes the experimental limitation of multiple radiographic exposures required to test the effect of multiple brace designs on the same patient. A common method is to generate a finite element model (FEM) of a patient's trunk and to simulate brace treatment by applying the forces exerted by the brace on the FEM [1, 13, 22, 27, 34]. Andriacchi [1] simulated the Milwaukee brace immediate effect and concluded that it was efficient in correcting coronal curves. Wynarsky [34] and Gignac [13] tried to find the optimal location and amplitude of the corrective forces generated by a brace. The method however has several limitations. The corrective forces applied on the trunk FEM were not necessarily balanced and equilibrium was obtained using restrictive boundary conditions. Furthermore, the optimization process cannot include many brace design parameters, such as the strap tension, the rigid shell geometry, or the pads shape. In our previous studies (Perié [26] and Clin [8]), we presented a new method wherein a single brace with all its components (rigid shell, pads, openings, straps, foam layer) was explicitly modeled for one patient. Its installation was simulated using a contact interface between the patient's trunk and brace models. The method is a more realistic representation of the actual procedure of fitting a brace onto a patient's torso.

This study uses the previously developed simulation process to test multiple brace designs on given patients and to compare their immediate corrections of the 3D scoliotic deformities. The aim was to detect the most influential brace design factors and to quantify their influence on the immediate 3D corrections.

6.2.3 Methods

Simulation of the brace installation

The geometry of the spine, rib cage and pelvis of three scoliotic patients (thoracic and lumbar Cobb: P1 (38˚, 23˚); P2 (36˚, 16˚); P3: (20˚, 33˚)) was reconstructed in 3D using a multiview radiographic self-calibration technique [4, 7, 15, 16] (Figures 1A, 2). The accuracy of this reconstruction method was 3.3 mm on average (SD 3.8 mm) [9]. In addition the external trunk surface of the patient was digitized using a 3-dimensionnal range sensing technique (3-dimensional Capturor, Inspeck Inc., Montreal, Quebec, Canada) [23-25] (Figure 1B). Using fiducial radiopaque landmarks visible on both the x-rays and the trunk surface, the internal and external geometries were then superimposed using a point-to-point least square algorithm (Figure 1C) [12]. A global coordinate system Rg, with the origin at the center of the first sacral vertebra S1, was associated with this geometry such that the z-axis was directed vertically upwards, x-axis was postero-anterior and the y-axis was lateral (oriented from right to left).

Based on this geometry, a personalized finite element model (FEM) of the patient's torso was built [3, 27] (Figure 3) using Ansys 11.0 FE package (Ansys Inc., Canonsburg, PA, USA). In brief, the thoracic and lumbar vertebrae, intervertebral discs, ribs, sternum, rib cartilages and abdominal cavity were represented by 3D elastic beam elements, the zygapophyseal joints by shells and surface-to-surface contact elements, the vertebral and intercostal ligaments by tension-only spring elements and the external soft tissues by hexahedral elements. Mechanical properties of all the components of the model were taken from experimental and published data [3, 26, 27]. The influence of the spine flexibility ("stiff" and "flexible" spines) was tested (intervertebral disc stiffness multiplied and divided by 2 respectively) [28].

A custom-fit geometrical brace model was created over the already generated FEM of the patient's trunk (Figure 4A, B, C). It included the external rigid shell, the foam layer, the openings and the pads. The external rigid shell was modeled by 4-node quadrilateral shell elements. The foam layer and the pads were modeled by 8-nodes hexahedral elements. The material of the rigid shell was polyethylene (E=1500 Mpa, ν=0.3), that of the foam layer was soft polyethylene foam (E=1 MPa, ν=0.3) and that of the pads was stiff polyethylene foam (E=10 MPa, ν=0.3) [26, 31]. A surface-to-surface contact interface was created between the interior of the brace model and the exterior of the trunk model.

Boundary conditions were applied on the trunk model to mimic an in-brace patient. The pelvis was fixed in space and translation of the first thoracic vertebra in the transverse plane (x and y directions) was blocked. Brace installation on the patient was simulated. The simulation process was divided into 2 steps: *(i)* The brace was opened by applying displacements on four nodes and was positioned on the patient. *(ii)* Forces representing strap tensions were applied on the nodes corresponding to the strap fixations. At the end of the simulation, the virtual brace was consequently installed on the patient (Figure 4D).

On completion of the simulation, corrections in 3D clinical indices (Cobb angles, kyphosis, lordosis, rib hump, axial rotation) were computed.

Design of experiments

For each patient, with either the flexible or stiff spine model, a Box, Hunter & Hunter fractional design of experiments [5] was used to evaluate the effects of 15 brace design factors: strap number and tension, type of brace, thoracic pad position in the transverse and vertical planes, lumbar, anterior thoracic and trochanteric pads presence, iliac crest roll design, lordosis design, height of lumbar pad, rigid shell symmetry, trochanteric extension side, brace size and opening position. Each factor had two modalities. Table 1 lists the two modalities that were tested for each of the 15 factors illustrated in Figure 5. The modalities for each design factor were chosen based on previous published studies [10, 29] and according to the recommendations of orthotists.

Using the fractional design of experiments, for each patient, with either the flexible or stiff spine model, 2048 ($2^{(15-4)}$) virtual braces were tested (total of 12,288: 3 patients*2 flexibility models*2048 braces). It allowed evaluating the main and two-way interaction effects of the tested design factors on the 3D corrections generated by the brace. For example, the main effect of the strap tension on the correction of the thoracic curve Cobb angle is the mean change of correction (for all the tested braces) of the thoracic curve Cobb angle when the strap tension increases from 20 N to 60 N. The interaction effect of the strap tension and the brace type on the correction of the thoracic curve Cobb angle is the difference of effect of the strap tension on the correction of the thoracic curve Cobb angle between the lumbar braces and the thoracic braces. Likewise for every design factor, the main effect and its interaction with the remaining factors were evaluated.

6.2.4 Results

The immediate correction in all the tested braces was quite variable, especially when the thoracic and lumbar Cobb angles, the kyphosis and the lordosis parameters were considered (Table 2). For instance, for P1 with a flexible spine, the thoracic Cobb in-brace varied between 6° and 54°. There was little correction on average in the transverse plane (axial rotation and rib hump). Relatively more correction in the coronal plane was obtained for the flexible spine as compared to the stiff spine model. For instance, the mean in-brace thoracic Cobb angle for P1 was 24° with a flexible spine and 31° with a stiff spine.

An interaction was found between the position of the brace opening (anterior or posterior) and the other design factors, which revealed that the effect of the design factors was quite different if the opening was anterior or posterior. For instance, in case of P1, when a brace with a posterior opening was used, the four influential parameters that impacted most thoracic Cobb angle were strap tension, trochanter extension side, brace symmetry and the number of straps. For the same case, when a brace with an anterior opening was used, the four influential parameters were the brace type, brace symmetry, trochanter extension side and brace size.

For both types of brace openings (anterior and posterior), the main effects on the 3D geometrical indices of the most influential brace design factors are presented in Table 3. As an example, in the case of P1, when a brace with a posterior opening was used, changing the position of the trochanter extension from right to left increased the in-brace thoracic Cobb angle by 5° (1st row, 2nd factor, Table 3). For the same case, when a brace with an anterior opening was used, an increase of 3.6° was obtained (7th row, 3rd factor, Table 3). Results of only the flexible spine models are listed in Table 3. For the stiff spine models, although the most influential design factors were identical for all indices, the resulting effects were weaker due to smaller corrections.

Increasing strap tension and using 3 straps instead of 2 gave a better correction in the coronal plane (Table 3). Introducing an asymmetry relative to the sagittal plane in the rigid shell also gave better correction. The 'lumbar brace' type improved the correction of the lumbar curve relatively to the 'thoracic brace'. The trochanter extension side had an important effect on the coronal curves. Positioning it on the right (side of the thoracic curve for the patients in this study) improved the correction of both the thoracic and lumbar Cobb angles. Figure 6 shows the spinal shape of the patients in the coronal plane before the brace installation and the same after two different braces installation, both of which were identical except for the trochanter extension side. When the trochanter extension side was on the right (■), the brace pushed the spine more to the left. For patients P1 and P3, even if it increased the reduction of the thoracic and lumbar Cobb angles, it also aggravated the decompensation of the trunk to the left.

In the sagittal plane, the most influential factor was the lordosis design. When the sagittal curve of the brace rigid shell was reduced, it decreased both the lordosis and the kyphosis (for instance 5° on average for P1 with a flexible spine) (Table 3). However it did not generate a significant reduction of the coronal curves. An increase of the strap tension reduced the sagittal curves while an asymmetry in the rigid shell increased them. The presence of the lumbar pad, positioned posteriorly, had a lordotic effect. When the thoracic pad was positioned posteriorly rather than laterally, aside from decreasing the kyphosis and lordosis, it also reduced rib hump and apical axial rotation. No distinct tendency for the

other design factors was observed in the transverse plane (rib hump and vertebral axial rotation).

6.2.5 Discussion

Simulating brace treatment allowed testing a large number of virtual braces (12,288). Such numerical simulations allow the comparison of immediate in-brace corrections obtained using different brace designs for the same patient. It also provides a versatile tool to examine the impact of varying specific design parameters and the relative interaction between them. Such comparisons and evaluations on patients are very difficult to do with real braces.

The trochanter extension side significantly impacted the correction of the coronal curves and the global balance of the trunk. Mechanically, it acts as a lever arm. If positioned on the right side, it enhances the action of the right thoracic pad and the trunk is pushed globally to the left. If positioned on the left side, it enhances the action of the left lumbar pad but the effect is less because the lever arm is shorter (see figure 6). The brace lordosis design influenced the sagittal curves. The trunk shape tended to conform to the brace shape. When the thoracic pad was placed in a more posterior position, it pushed the right rib hump forward, which reduced the transverse plane deformity (vertebral axial rotation, rib hump) but also induced a reduction in the kyphosis. Aubin et al. [2] also observed this effect. In a similar way, the presence of the posterior lumbar pad, that pushes the abdomen forward, had a lordotic effect. These results corroborate with empirical observations [6-8].

The thoracic and lumbar pads upper limit had limited effects of the scoliotic coronal curves, and the current study is not supporting the general recommendation of brace manufacturers to place the thoracic and lumbar pads below the curve apex [8]. No correlation was found between the reduction of the lordosis and the correction of the coronal curves, even if this is one of the principles of the Boston brace system [10]. The reduction of the lordotic profile of the brace had only a negative effect on sagittal curves (hypo-kyphosising and hypo-lordosing). An asymmetric rigid shell was more efficient to correct the coronal curves than

a symmetric one. A more thorough optimization study of the rigid shell shape could help better understand these results.

The interaction effect between the opening position and the other design factors reveals that braces like for instance the Boston brace (posterior opening) and the Chêneau brace (anterior opening) have quite different working mechanisms. The anterior or posterior position of the straps influences the force transmission from the brace to the torso and modifies the efficiency of the pads. It can be explained mechanically by the fact that the pressures exerted by the pads on the torso result from the tension applied to the straps. Changing the opening position and hence the straps location modifies the moment created by the strap force on the pads location and consequently it modifies the action of the pads on the torso. The optimal opening position could be an interesting future direction to investigate.

Fifteen design factors were examined in this study to limit the already extensive number of simulations. Other design factors could also be considered, e.g. position of the lumbar pad in the transverse plane (posterior or postero-lateral position), the presence of an abdominal pad, the shape of the pads, and other configurations of openings. It should also be noted that the ranking of the design factors by their effects magnitude (Table 3) is dependant from the two modalities that were chosen for each factor in the design of experiments (Table 1). Other modalities could be investigated in the future. The present study, as it detected some of the key brace design parameters, could be the basis of an optimization process. It could notably help to choose the optimization variables. An objective function representing appropriately the orthotist definition of an efficient brace treatment should also be defined.

The present model has, as any numerical models, its limitations and the results should therefore be interpreted with caution. Given the boundary conditions, the pelvis was not allowed to tilt, which could have modified notably the effect of the brace lordosis design. The first thoracic vertebra was only free to move along the vertical axis and the effect of the brace on the patient decompensation could not be evaluated. The intervertebral discs and the ligaments were modeled as linear elastic. These limitations were thoroughly discussed by Clin and Périé [8, 26, 27].

Only the passive action of the brace was simulated as no muscles were present in the model. It could be reasonable however to assume that the active action, if any, would be concomitant, complementary, to the passive action and that it would amplify the brace design factors effects generated by the passive action. For instance, it might be that greater strap tension increases the passive effect as studied here, and also increases the discomfort, thereby encouraging an 'active' response. More generally, to model the muscular contribution is complex and a great challenge to be undertaken in the future.

The present study focused on the immediate action of braces but the aim of brace treatment is to stop the progression of scoliotic deformities in a long-term perspective. It was however remarked that the immediate efficiency of a brace is a good predictor of the outcome of the treatment [6, 11, 32], which justifies to focus mainly on this immediate action.

Different studies were done to evaluate the brace model validity [8, 26, 27]. Périé [27] compared the spinal geometries obtained after simulation and in the real brace and found differences in Cobb angles inferior to eight degrees. Differences in positions of vertebrae in coronal and sagittal planes were inferior to 6 mm and 9.8 mm respectively. The pressures exerted by the virtual brace on the patients' torsos FE models were also computed and compared to pressures measured experimentally. They were found to be in the same range (0-30 kPa). The validation process will however continue, by integrating personalized mechanical properties for instance.

The model used in this study is an improvement over the previous methods used to simulate brace treatment because the brace is explicitly modeled, all its components are included (pads, openings, foam layer, straps) and the simulation process represents adequately the installation of the brace on the patient (opening, positioning, tightening of straps) [8].

6.2.6 Conclusion

By using a finite element model to simulate brace treatment, it was possible to compare the efficiency of multiple brace designs on specific patients. Results showed great variability of the 3D corrections generated by the braces according to their design. The most influential

design factors were identified. The importance of strap tension, trochanter extension side, rigid shell shape and lordosis design was notably detected. The position of the opening, posterior or anterior, changed the working mechanism of the brace. The present study provides a better understanding of brace biomechanics and gives insights for an objective assessment of the bracing treatment.

6.2.7 References

1. Andriacchi TP, Schultz AB, Belytschko TB, Dewald R (1976) Milwaukee brace correction of idiopathic scoliosis. A biomechanical analysis and a restrospective study. J Bone Joint Surg Am 58:806-815

2. Aubin CE, Dansereau J, de Guise JA, Labelle H (1997) Rib cage-spine coupling patterns involved in brace treatment of adolescent idiopathic scoliosis. Spine 22:629-635

3. Aubin CE, Dansereau J, De Guise JA, Labelle H (1996) A study of biomechanical coupling between spine and rib cage in the treatment by orthosis of scoliosis. Ann Chir 50:641-650

4. Aubin CE, Descrimes JL, Dansereau J, Skalli W, Lavaste F, Labelle H (1995) Geometrical modeling of the spine and the thorax for the biomechanical analysis of scoliotic deformities using the finite element method. Ann Chir 49:749-761

5. Box GEP, Hunter JS (2000) 2k-p fractional factorial designs. Part I. Technometrics 42:28-47

6. Castro FP, Jr. (2003) Adolescent idiopathic scoliosis, bracing, and the Hueter-Volkmann principle. Spine J 3:180-185

7. Cheriet F, Remaki L, Bellefleur C, Koller A, Labelle H, Dansereau J (2002) A new X-ray calibration/reconstruction system for 3D clinical assessment of spinal deformities. Stud Health Technol Inform 91:257-261

8. Clin J, Aubin CE, Labelle H (2007) Virtual prototyping of a brace design for the correction of scoliotic deformities. Med Biol Eng Comput 45:467-473

9. Delorme S, Petit Y, de Guise JA, Labelle H, Aubin CE, Dansereau J (2003) Assessment of the 3-d reconstruction and high-resolution geometrical modeling of the human skeletal trunk from 2-D radiographic images. IEEE Trans Biomed Eng 50:989-998

10. Emans JB (2003) Boston Brace. srs bracing manual (http://wwwsrsorg/professionals/bracing_manuals/)

11. Emans JB, Kaelin A, Bancel P, Hall JE, Miller ME (1986) The Boston bracing system for idiopathic scoliosis. Follow-up results in 295 patients. Spine 11:792-801

12. Fortin D, Cheriet F, Beausejour M, Debanne P, Joncas J, Labelle H (2007) A 3D visualization tool for the design and customization of spinal braces. Comput Med Imaging Graph 31:614-624

13. Gignac D, Aubin CE, Dansereau J, Labelle H (2000) Optimization method for 3D bracing correction of scoliosis using a finite element model. Eur Spine J 9:185-190

14. Goldberg CJ, Moore DP, Fogarty EE, Dowling FE (2001) Adolescent idiopathic scoliosis: the effect of brace treatment on the incidence of surgery. Spine 26:42-47

15. Kadoury S, Cheriet F, Dansereau J, Labelle H (2007) Three-dimensional reconstruction of the scoliotic spine and pelvis from uncalibrated biplanar x-ray images. J Spinal Disord Tech 20:160-167

16. Kadoury S, Cheriet F, Laporte C, Labelle H (2007) A versatile 3D reconstruction system of the spine and pelvis for clinical assessment of spinal deformities. Med Biol Eng Comput 45:591-602

17. Katz DE, Durrani AA (2001) Factors that influence outcome in bracing large curves in patients with adolescent idiopathic scoliosis. Spine 26:2354-2361

18. Labelle H, Dansereau J, Bellefleur C, Poitras B (1996) Three-dimensional effect of the Boston brace on the thoracic spine and rib cage. Spine 21:59-64

19. Lenssinck ML, Frijlink AC, Berger MY, Bierman-Zeinstra SM, Verkerk K, Verhagen AP (2005) Effect of bracing and other conservative interventions in the treatment of idiopathic scoliosis in adolescents: a systematic review of clinical trials. Phys Ther 85:1329-1339

20. Nachemson AL, Peterson LE (1995) Effectiveness of treatment with a brace in girls who have adolescent idiopathic scoliosis. A prospective, controlled study based on data from the Brace Study of the Scoliosis Research Society. J Bone Joint Surg Am 77:815-822

21. Noonan KJ, Weinstein SL, Jacobson WC, Dolan LA (1996) Use of the Milwaukee brace for progressive idiopathic scoliosis. J Bone Joint Surg Am 78:557-567

22. Patwardhan AG, Bunch WH, Meade KP, Vanderby R, Jr., Knight GW (1986) A biomechanical analog of curve progression and orthotic stabilization in idiopathic scoliosis. J Biomech 19:103-117

23. Pazos V, Cheriet F, Danserau J, Ronsky J, Zernicke RF, Labelle H (2007) Reliability of trunk shape measurements based on 3-D surface reconstructions. Eur Spine J 16:1882-1891

24. Pazos V, Cheriet F, Labelle H, Dansereau J (2002) 3D reconstruction and analysis of the whole trunk surface for non-invasive follow-up of scoliotic deformities. Stud Health Technol Inform 91:296-299

25. Pazos V, Cheriet F, Song L, Labelle H, Dansereau J (2005) Accuracy assessment of human trunk surface 3D reconstructions from an optical digitising system. Med Biol Eng Comput 43:11-15

26. Perie D, Aubin CE, Lacroix M, Lafon Y, Labelle H (2004) Biomechanical modelling of orthotic treatment of the scoliotic spine including a detailed representation of the brace-torso interface. Med Biol Eng Comput 42:339-344

27. Perie D, Aubin CE, Petit Y, Labelle H, Dansereau J (2004) Personalized biomechanical simulations of orthotic treatment in idiopathic scoliosis. Clin Biomech (Bristol, Avon) 19:190-195

28. Petit Y, Aubin CE, Labelle H (2004) Patient-specific mechanical properties of a flexible multi-body model of the scoliotic spine. Med Biol Eng Comput 42:55-60

29. Rigo M, Negrini S, Weiss HR, Grivas TB, Maruyama T, Kotwicki T (2006) SOSORT consensus paper on brace action: TLSO biomechanics of correction (investigating the rationale for force vector selection). Scoliosis 1:11

30. Rowe DE, Bernstein SM, Riddick MF, Adler F, Emans JB, Gardner-Bonneau D (1997) A meta-analysis of the efficacy of non-operative treatments for idiopathic scoliosis. J Bone Joint Surg Am 79:664-674

31. Sanders JE, Greve JM, Mitchell SB, Zachariah SG (1998) Material properties of commonly-used interface materials and their static coefficients of friction with skin and socks. J Rehabil Res Dev 35:161-176

32. Upadhyay SS, Nelson IW, Ho EK, Hsu LC, Leong JC (1995) New prognostic factors to predict the final outcome of brace treatment in adolescent idiopathic scoliosis. Spine 20:537-545

33. van Rhijn LW, Veraart BE, Plasmans CM (2003) Application of a lumbar brace for thoracic and double thoracic lumbar scoliosis: a comparative study. J Pediatr Orthop B 12:178-182

34. Wynarsky GT, Schultz AB (1991) Optimization of skeletal configuration: studies of scoliosis correction biomechanics. J Biomech 24:721-732

6.2.8 Figures and Tables Captions

Tableau 6.1 Article 4 Table 1: Brace design factors tested with the design of experiments

Design Factor	Modality 1	Modality 2	Ref. (Fig.5)
1: Brace type	Thoracic brace	Lumbar brace	A, B
2: Number of straps	2	3	K
3: Strap tension	20 N	60 N	
4: Sagittal profile	Follows the sagittal curves	Sagittal curves reduced	C
5: Thoracic pad position	Lateral	Posterior	D
6: Thoracic pad upper limit	Rib of the thoracic apex	2 ribs above	I
7: Anterior derotational thoracic pad	Absent	Present	L
8: Lumbar pad	Absent	Present	E
9: Upper limit of the lumbar pad	Lumbar curve apex vertebra	2 vertebrae above	E
10: Trochanter extension side	Right	Left	F
11: Trochanter pad	Absent	Present	G
12: Iliac crest roll presence	Absent	Present	H
13: Rigid shell symmetry (coronal plane)	Symmetric	Asymmetric (10% reduction of thoracic and lumbar parts)	J
14: Brace size	5% too tight	5% too large	
15: Brace opening position	Posterior	Anterior	M

Tableau 6.2 Article 4 Table 2: Geometrical indices of the models before and after the simulation of the brace installation (all values are in degrees)

	Index (°)	Initial	In Brace											
			Flexible Spine						Stiff Spine					
			Posterior opening			Anterior opening			Posterior opening			Anterior opening		
			Mean	Max	Min	Mean	Max	Min	Mean	Max	Min	Mean	Max	Min
P1	Thoracic Cobb	37	24	35	6	29	54	17	31	36	23	33	39	26
	Lumbar Cobb	23	13	20	1	16	24	9	19	22	14	20	24	17
	Kyphosis	18	13	23	0	14	25	1	15	21	4	15	22	9
	Lordosis	25	21	27	7	21	28	11	23	26	17	23	27	19
	Rib Hump	17	16	26	11	16	32	11	16	23	12	15	27	11
	Axial Rotation	22	22	32	15	21	35	14	22	28	18	21	29	12
P2	Thoracic Cobb	39	29	40	14	28	36	17	36	40	30	35	38	31
	Lumbar Cobb	17	11	17	2	11	16	4	15	17	12	15	17	13
	Kyphosis	9	7	16	0	5	15	0	7	12	0	6	11	0
	Lordosis	35	33	38	25	32	37	25	34	36	30	33	36	30
	Rib Hump	22	24	33	18	20	33	14	25	33	19	22	27	17
	Axial Rotation	13	12	17	9	9	19	5	13	17	10	11	15	7
P3	Thoracic Cobb	20	12	23	0	15	28	4	17	21	10	19	22	14
	Lumbar Cobb	30	22	30	9	25	32	18	28	31	23	29	31	25
	Kyphosis	53	48	54	37	49	58	42	51	55	44	51	56	47
	Lordosis	37	34	38	27	35	41	28	36	38	32	36	39	33
	Rib Hump	9	8	11	6	9	15	6	9	11	7	9	11	7
	Axial Rotation	11	11	14	9	11	18	9	11	13	9	11	12	9

Tableau 6.3 Article 4 Table 3: Effects of the most influential design factors (flexible spine models, all values are in degrees). Example: for P1, using brace with a posterior opening, changing the position of the trochanter extension from right to left increased the in-brace thoracic Cobb angle by 5° (1st row, 2nd factor), increasing the strap tension from 20 to 60 N decreased the in-brace thoracic Cobb angle by 5.2° (1st row, 1st factor)

	Opening Position	Index (°)	1st Factor	2nd Factor	3rd Factor	4th Factor	5th Factor
P1	Posterior	*Thoracic Cobb*	Strap Tension -5.2	Troch. Ext. Side 5.0	Brace Symmetry -3.9	Strap Number -2.5	Brace Size 2.0
		Lumbar Cobb	Strap Tension -4.9	Brace Type -3.4	Brace Symmetry -2.8	Strap Number -2.1	Troch. Ext. Side 1.4
		Kyphosis	Lordosis Design -5.9	Strap Tension -4.7	Thor. Pad Position -2.9	Brace Symmetry 2.8	Lumbar Pad 2.6
		Lordosis	Lordosis Design -5.7	Strap Tension -2.5	Brace Symmetry 1.8	Thor. Pad Position -1.6	Lumbar Pad 1.5
		Rib Hump	Brace Type -3.7	Thor. Pad Position -1.5	Brace Size -1.2	Strap Tension 0.6	Counter-Thor. Pad -0.5
		Axial Rotation	Brace Type -4.2	Brace Size -1.5	Thor. Pad Position -1.4	Troch. Ext Side -0.8	Brace Symmetry 0.5
	Anterior	*Thoracic Cobb*	Brace Type 4.6	Brace Symmetry -3.6	Troch. Ext. Side 3.6	Brace Size 2.9	Strap Tension -2.0
		Lumbar Cobb	Brace Symmetry -3.2	Brace Size 2.2	Strap Tension -2.1	Troch. Ext Side 1.1	Thor. Pad Position 1.1
		Kyphosis	Lordosis Design -4.6	Lumbar Pad 2.6	Thor. Pad Position -1.8	Strap Tension -1.7	Brace Symmetry 1.5
		Lordosis	Lordosis Design -4.6	Strap Tension -2.1	Brace Symmetry 1.6	Lumbar Pad 1.6	Thor. Pad Position -1.0
		Rib Hump	Brace Size 2.7	Lordosis Design -1.1	Troch. Ext. Side 0.9	Brace Type -0.8	Strap Tension 0.8
		Axial Rotation	Brace Size 2.6	Lordosis Design -1.3	Strap Tension 0.9	Brace Type -0.8	Troch. Ext. Side 0.7
P2	Posterior	*Thoracic Cobb*	Troch. Ext. Side 4.2	Brace Symmetry -4.0	Brace Size 2.9	Thor. Pad Height -1.4	Brace Type -1.3
		Lumbar Cobb	Brace Type -2.3	Brace Symmetry -2.2	Troch. Ext. Side 1.6	Thor. Pad Height -1.2	Brace Size 1.2
		Kyphosis	Lordosis Design -3.8	Strap Tension -3.4	Brace Size -2.2	Brace Symmetry 1.7	Thor. Pad Height 1.3
		Lordosis	Lordosis Design -3.5	Strap Tension -2.0	Brace Type 1.6	Brace Symmetry 1.2	Thor. Pad Position -0.9
		Rib Hump	Brace Type -2.6	Brace Size -1.9	Strap Tension 0.9	Thor. Pad Position -0.8	Thor. Pad Height 0.5
		Axial Rotation	Brace Type -1.2	Brace Size -1.1	Thor. Pad Position -0.5	Brace Symmetry -0.4	Lumbar Pad -0.3
	Anterior	*Thoracic Cobb*	Troch. Ext. Side 4.4	Brace Symmetry -2.9	Brace Size 2.2	Strap Tension -2.0	Thor. Pad Height -0.9
		Lumbar Cobb	Brace Symmetry -2.3	Brace Type -1.9	Strap Tension -1.8	Troch. Ext. Side 1.6	Thor. Pad Height -0.9
		Kyphosis	Lordosis Design -5.0	Brace Symmetry 1.9	Lumbar Pad 1.9	Strap Tension -1.2	Brace Size 1.2
		Lordosis	Lordosis Design -3.6	Strap Tension -1.4	Brace Symmetry 1.4	Lumbar Pad 1.2	Thor. Pad Position -0.8
		Rib Hump	Thor. Pad Position -0.9	Brace Symmetry 0.9	Troch. Ext. Side 0.6	Lordosis Design -0.5	Brace Type -0.3
		Axial Rotation	Lordosis Design -0.5	Strap Tension -0.5	Brace Symmetry 0.4	Thor. Pad Position -0.4	Thor. Pad Height -0.3
P3	Posterior	*Thoracic Cobb*	Strap Tension -7.5	Troch. Ext. Side 3.3	Brace Size -3.0	Strap Number -2.4	Brace Symmetry -2.3
		Lumbar Cobb	Strap Tension -5.9	Brace Symmetry -2.9	Troch. Ext. Side 2.4	Strap Number -2.2	Brace Type -1.7
		Kyphosis	Lordosis Design -3.8	Strap Tension -3.8	Lumbar Pad 1.7	Thor. Pad Position -1.5	Strap Number -1.4
		Lordosis	Lordosis Design -3.8	Strap Tension -2.0	Thor. Pad Position -1.0	Brace Symmetry 0.9	Lumbar Pad 0.9
		Rib Hump	Troch. Ext. Side 0.9	Brace Symmetry -0.8	Strap Tension -0.8	Thor. Pad Position 0.5	Counter-Thor. Pad 0.3
		Axial Rotation	Troch. Ext. Side -0.8	Strap Tension 0.6	Brace Type 0.6	Brace Symmetry 0.6	Thor. Pad Position -0.2
	Anterior	*Thoracic Cobb*	Brace Type 2.5	Strap Tension -2.5	Brace Symmetry -2.4	Thor. Pad Height 0.8	Iliac Crest Roll -0.4
		Lumbar Cobb	Strap Tension -2.4	Troch. Ext. Side 2.4	Lumbar Pad -0.5	Lordosis Design 0.4	Counter-Thor. Pad 0.4
		Kyphosis	Brace Type 2.0	Lumbar Pad 1.9	Brace Size 1.1	Thor. Pad Position -1.0	Lumb. Pad Height -0.9
		Lordosis	Lumbar Pad 1.4	Brace Type 1.4	Brace Symmetry 1.2	Strap Tension -1.2	Thor. Pad Position -0.9
		Rib Hump	Strap Tension -0.6	Troch. Ext. Side 0.5	Brace Symmetry -0.4	Thor. Pad Position 0.4	Strap Number -0.2
		Axial Rotation	Strap Tension 0.5	Brace Size 0.5	Brace Symmetry 0.4	Brace Type 0.3	Thor. Pad Height 0.3

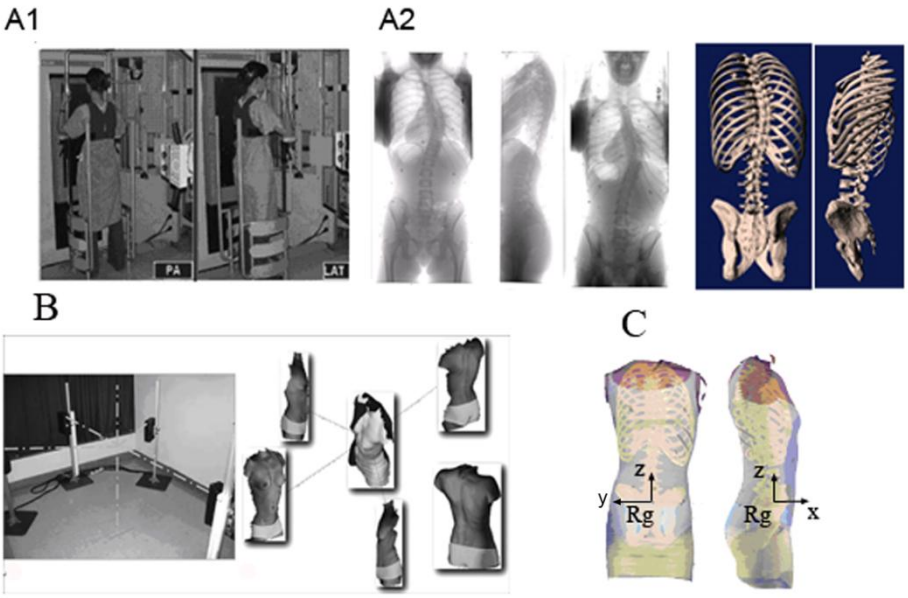

Figure 6.1 Article 4 Figure 1: A Acquisition of the internal geometry using the multi-view radiographic reconstruction technique: A1- Postero-anterior (PA) and lateral acquisition; A2- PA, lateral, and PA with an incidence of 20° radiographs; A-3 3D reconstruction; B Acquisition of the external geometry using the range sensor topography technique; C Superimposition of the two geometries (Rg: Global reference system).

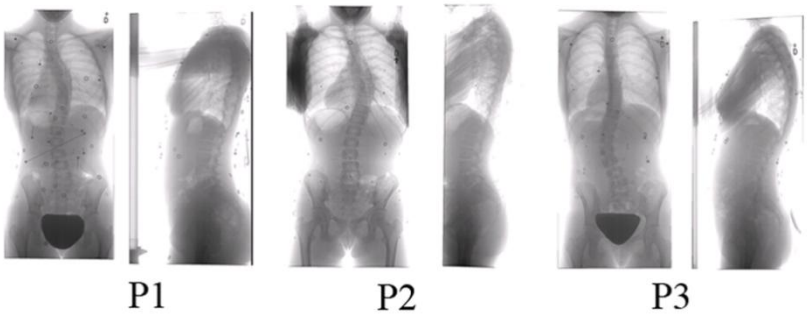

Figure 6.2 Article 4 Figure 2: Postero-anterior and lateral radiographs of the patients

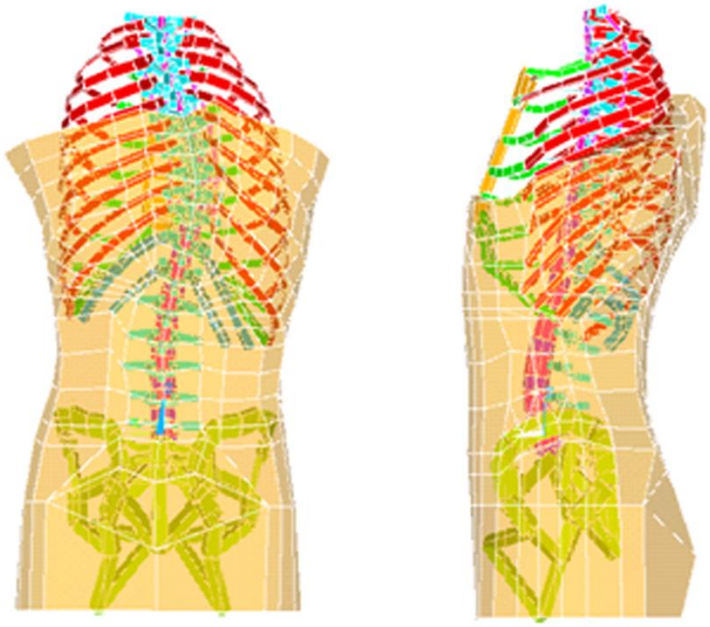

Figure 6.3 Article 4 Figure 3: Trunk FEM of the patient P2 (intercostal ligaments and abdominal beams are not shown for clarity)

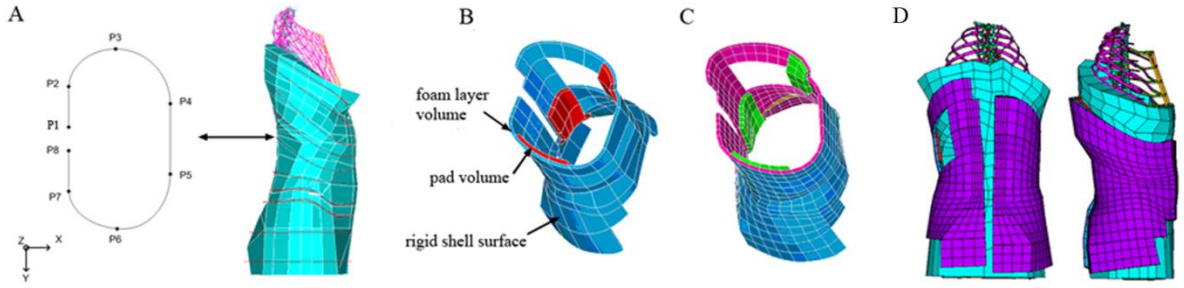

Figure 6.4 Article 4 Figure 4: A- Generative curves; B Geometrical model of the brace; C Finite element model of the brace; D FEM Brace installed on the patient

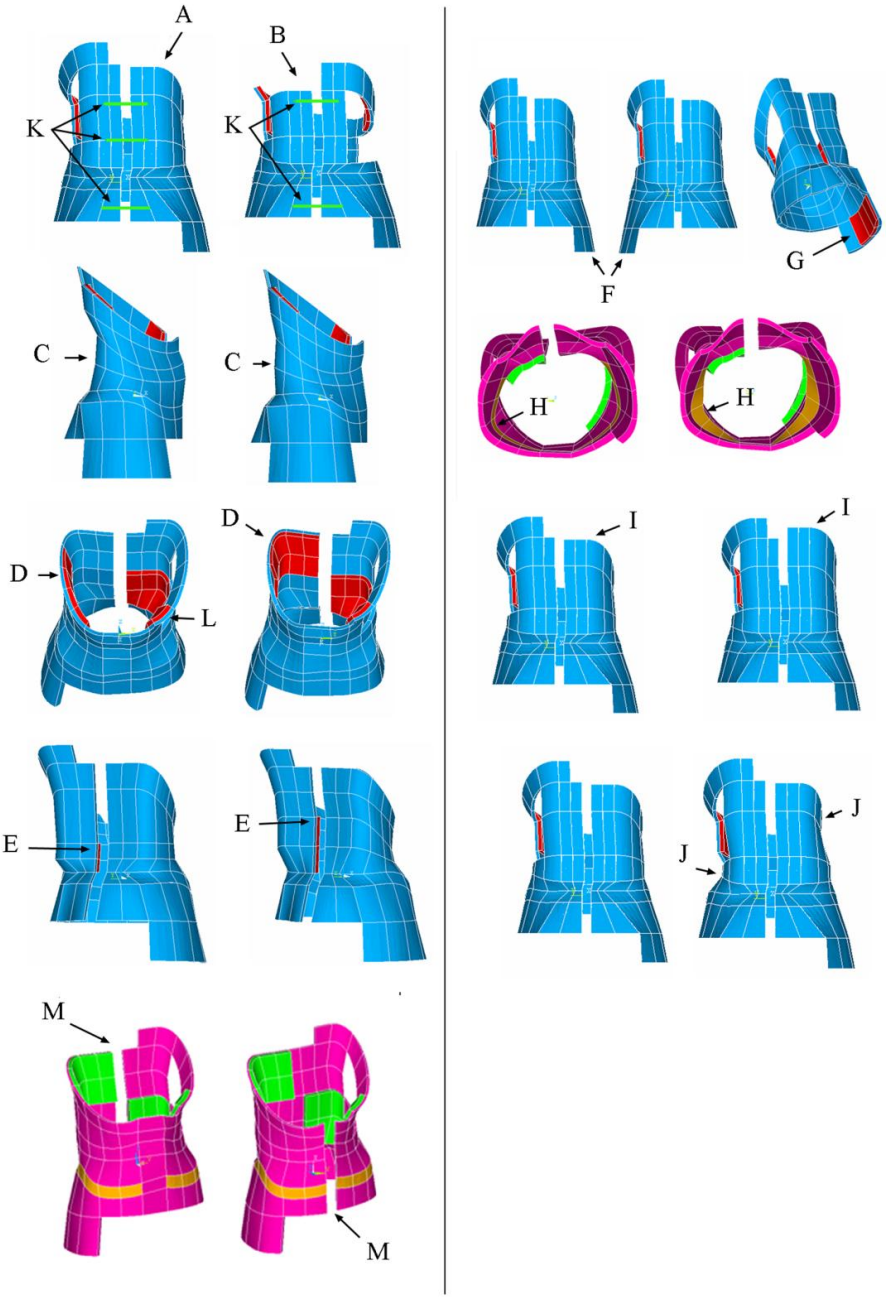

Figure 6.5 Article 4 Figure 5: Brace design factors (A and B: Brace type; C: Lordosis design; D: Thoracic pad position; E: Lumbar pad height; F: Trochanter extension side; G: Trochanter pad; H: Iliac Crest Roll Design; I: Thoracic pad height; J: Shell symmetry; K: Number of straps; L; Counter-thoracic pad; M: Opening position)

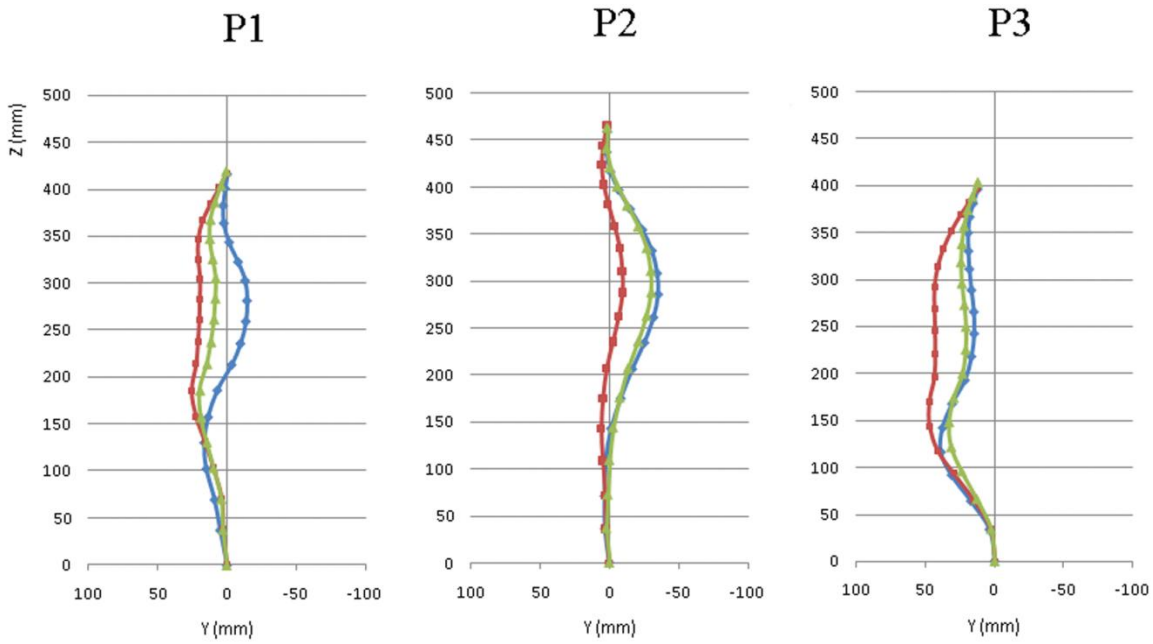

Figure 6.6 Article 4 Figure 6: Effect of the position of the trochanter extension side on the spine shape of the three patients P1, P2, P3 in the coronal plane (postero-anterior view) (◆: without brace , ■ : in brace with the trochanter extension on the right side, ▲ : in brace with the trochanter extension on the left side)

CHAPITRE 7 ÉTUDE DE LA CORRECTION IMMÉDIATE DES COURBURES CORONALES ET DU CHARGEMENT ASYMÉTRIQUE DES VERTÈBRES

7.1 Situation du cinquième article

Dans le quatrième article, un plan d'expériences a été utilisé afin d'évaluer les effets des paramètres de conception des corsets sur les corrections géométriques. Ces corrections géométriques étaient "immédiates". Elles sont générées lors de la première installation du corset. Afin d'étudier le potentiel de correction à long-terme des corsets, le cinquième article porte sur une étude de corrélation entre la correction immédiate des courbures frontales et la correction du chargement asymétrique des vertèbres. Dans cet article, il est démontré biomécaniquement que plus la correction immédiate des courbures frontales est importante, plus l'asymétrie des contraintes en compression à l'apex des courbures scoliotiques est réduite. Le niveau de correction immédiate nécessaire pour annuler cette asymétrie des contraintes est également évalué.

Cet article est intitulé :« Correlation between immediate in-brace correction and biomechanical effectiveness of brace treatment in adolescent idiopathic scoliosis» et a été accepté pour publication dans la revue Spine en Novembre 2009. La contribution du premier auteur à la préparation et la rédaction de l'article est évaluée à 85%.

7.2 Article #5: Correlation between immediate in-brace correction and biomechanical effectiveness of brace treatment in Adolescent Idiopathic Scoliosis

Correlation between immediate in-brace correction and biomechanical effectiveness of brace treatment in Adolescent Idiopathic Scoliosis

Julien Clin[1,2], Carl-Éric Aubin[1,2], Archana Sangole[1,2], Hubert Labelle[2], Stefan Parent[1,2]

1- Dept. of Mechanical Engineering, École Polytechnique de Montréal

P.O. Box 6079, Station Centre-ville, Montréal, Québec, H3C 3A7, Canada

2- Sainte-Justine University Hospital Center

3175 Côte-Ste-Catherine Rd., Montréal, Québec, H3T 1C5, Canada

Address for notification, correspondence and reprints:

Carl-Eric Aubin, Ph.D., P.Eng., Full Professor

Canada Research Chair 'CAD Innovation in Orthopedic Engineering' & NSERC-Medtronic industrial Research Chair in Spine Biomechanics

Ecole Polytechnique, Department of Mechanical Engineering

P.O. Box 6079, Station "Centre-ville", Montreal (Quebec), H3C 3A7 CANADA

E-mail: carl-eric.aubin@polymtl.ca

Phone: 1 (514) 340-4711 ext 2836; FAX: 1 (514) 340-5867

Acknowledgements This study was funded by the Natural Sciences and Engineering Research Council of Canada.

7.2.1 Abstract

Study Design: Multiple brace designs were simulated using a finite element model and their biomechanical effect was evaluated.

Objective: To study correlations between immediate in-brace correction of coronal curves and bending moments acting on the apical vertebrae.

Summary of Background Data: Immediate in-brace correction has often been deemed as fundamental to long-term brace effect but the biomechanical explanation is unclear.

Methods: Three-dimensional geometry of 3 patients was acquired using multi-view x-rays and surface topography techniques. A finite element model of the patients' trunk including gravitational forces and a parametric brace model were created. Two sets of mechanical properties of the spine (stiff and flexible) were tested. Installation of the brace on the patients was simulated. Using an experimental design framework including fourteen design factors, 1024 different virtual braces were tested for each patient. For each brace, immediate in-brace correction of the coronal Cobb angles and the bending moment acting on the apical vertebrae were computed and their correlation was studied.

Results: Immediate correction of coronal curves and corresponding impact on the apical vertebrae bending moments were linearly correlated (mean $R^2 = 0.88$). The amount of immediate correction necessary to nullify the bending moment ranged between 19% and 61% with average 48% (flexible spine model) and 27% (stiff spine model). The braces corrected the apical vertebrae bending moment more in the flexible spine model. In the framework of the Hueter-Volkmann principle, the correlation between coronal immediate in-brace correction and corresponding apical bending moment can be interpreted as a correlation between immediate in-brace correction and long-term treatment outcome. The amount of immediate correction necessary to invert the bending moments, and in theory counteract the progression of the scoliotic deformity, depends on spine stiffness and spine segment.

Conclusion: This study confirms the importance of immediate in-brace correction to predict long-term outcome of the treatment and provides insights in the understanding of brace biomechanics.

Keywords: Scoliosis; Brace; Finite element model; Growth modulation

Keypoints:

- Immediate correction of coronal curves and corresponding impact on the apical vertebrae bending moments are linearly correlated.
- In the framework of the Hueter-Volkmann principle, it can be interpreted as a correlation between immediate in-brace correction and long-term treatment outcome
- The amount of immediate correction necessary to invert the bending moments, and in theory counteract the progression of the scoliotic deformity, depends on spine stiffness and spine segment.

7.2.2 Introduction

Scoliosis is defined by a three-dimensional deformity of the spine and the rib cage. Conventionally, bracing is adopted as the treatment for moderate curves. In the past, factors influencing the long-term outcome of this treatment have been investigated in retrospective or prospective studies. Results of such analyses suggest that immediate in-brace correction of scoliotic curves is recognized to influence the treatments long-term effect [1-6]. As a rule-of-thumb, orthotists frequently consider that approximately 50% initial correction in the Cobb angle is necessary to expect a positive outcome [6,7]. However, very few studies have investigated this aspect biomechanically. Patwardhan et al. [8] used a biomechanical model where the scoliotic spine was represented as a vertical beam buckling under gravitational force. They evaluated the effect of the corrective forces provided by the brace on the stability of the spine and concluded that immediate in-brace correction of scoliotic curves was correlated with spinal stability in the brace and, consequently, with the efficiency of the treatment. However, their model did not take into account recent biomechanical studies [9-11] stipulating that compressive asymmetrical loading of the growth plates in the coronal

plane could be responsible for the progression of scoliotic deformities (Hueter-Volkmann principle). In the framework of this theory, brace treatments should invert the asymmetrical loading present in a scoliotic spine in order to prevent further progression and augmentation of the deformity.

In support of this theory, Castro [7] investigated initial and final follow-up coronal vertebral wedging in bracing. A correlation was found between immediate in-brace correction and the reduction of vertebral wedging following the treatment. However, as wedging was measured only on 2D postero-anterior x-rays and not in 3D, it was difficult to identify whether the apparent effect was truly due to reduced coronal plane wedging and was not an artifact of vertebral derotation. This emphasizes the need for a 3D evaluation of this wedging effect.

Numerical models have been used for the 3D evaluation of the biomechanical influence of braces [12-16]. Recently, a new method for simulating brace treatment was introduced [12] that enables the evaluation of brace treatments within the 3D scoliotic deformities. In addition such model allows the interpretation of the coronal asymmetrical loading of the spine due to gravity.

Using the aforementioned model, this study seeks to examine the correlation between immediate in-brace correction of scoliotic curves and the corresponding correction in coronal asymmetrical compressive loading of the spine.

7.2.3 Methods

Patient-Specific Modeling of the Spine and Torso and Simulation of the brace installation

A multi-view self-calibrated radiography reconstruction technique was used to acquire the 3D geometry of the spine, rib cage and pelvis of three scoliotic patients (P1, P2, P3) [17-20] (Figure 1A), within an accuracy of 3.3 mm ±3.8 mm (1.2 ±0.8 mm for the vertebral body corners and 1.6 ±1.1 mm for the pedicles) [21]. The external trunk surface was digitized using a 3-dimensional surface topography technique [22,23] (Inspeck Inc., Montreal, Quebec, Canada) (Figure 1B). Twelve fiducial markers were attached to the patient's torso and used to align the internal and external geometries using a point-to-point least square algorithm

(Figure 1C) [24]. A global coordinate system Rg, was defined with its origin at the center of the first sacral vertebra S1, the z-axis directed vertically upwards, x-axis pointing postero-anteriorly and the y-axis directed laterally (from left to right) (Figures 1, 3). The thoracic and lumbar Cobb angles of the three scoliotic patients included in the study respectively were - P1: 38˚, 23˚; P2: 36˚, 16˚; P3: 20˚, 33˚ (Figure 2).

A personalized finite element model of the patient's torso was created (Figure 3) using ANSYS 11.0 FE (Ansys Inc., Canonsburg, PA, USA) [12,14,15]. Thoracic and lumbar vertebrae, intervertebral discs, ribs, sternum, cartilage and abdominal cavity were represented by 3D elastic beam elements, the zygapophyseal joints by shells and surface-to-surface contact elements, the vertebral and intercostal ligaments by tension-only spring elements and the external soft tissues by hexahedral elements.

Mechanical properties of all the components of the model were taken from experimental and published data [14,25,26]. To evaluate the influence of spine flexibility on the results discussed herein, a "stiff" and a "flexible" spine were tested. For the 'stiff spine', the intervertebral disc stiffness (force divided by the deformation it produces) based on published and experimental data was multiplied by 2. For the 'flexible' spine' it was divided by 2 [27].

Seventeen nodes representing the center of gravity of the trunk slice at each vertebral level were created. Their position in the sagittal plane was derived from the literature [28-31] while their location with respect to the coronal plane was assumed to follow the scoliotic curve of the spine. Non-deformable beam elements connected these nodes to their relative vertebrae in order to transmit the gravitational forces to the spine. The magnitudes of the gravitational forces associated to each center of gravity node were taken from the literature [28-31] and were adjusted to the specific weight of the patients.

A custom-fit geometrical brace model inspired by the Boston brace system principles, including the external rigid shell of the brace, the foam layer, the openings and the pads was fitted over the already generated FEM of the patient's trunk (Figure 4A, B, C). The external rigid shell was modeled with 4-node quadrilateral shell elements, the foam layer and the pads were represented with 8-node hexahedral elements. The materials associated

to each brace division were: polyethylene for the rigid shell (E=1500 Mpa, ν=0.3), soft polyethylene foam for the foam layer (E=1 MPa, ν=0.3) and stiff polyethylene foam for the pads (E=10 MPa, ν=0.3) [14,32]. These materials were modeled with linear elastic properties. A surface-to-surface contact interface taking friction into account (coefficient of friction fixed to 0.6 [33]) was created between the interior of the brace model and the exterior of the trunk model.

Appropriate boundary conditions were applied on the trunk model to represent the overall behavior of the isolated torso model. The pelvis was fixed in space while translations of the first thoracic vertebrae were blocked in the transverse plane (x and y directions). Installation of the brace on the patient was simulated using 3 steps: (i) Gravitational forces were applied on the nodes corresponding to the different centers of mass. This step was divided into two substeps because the configuration of the patient acquired from the x-rays is already a configuration where the gravitational forces are present. Forces resulting from an optimization process were first applied vertically upward in order to find the zero-gravity geometry of the patient. Gravitational forces were then applied vertically downward on this zero-gravity geometry and the configuration of the patient under gravity was obtained again but this time it included the stresses due to the presence of gravitational forces. It was verified that the simulated configuration with the gravitational forces corresponded to the configuration obtained from the x-rays; (ii) The brace was opened by applying displacements to the four nodes located in its posterior part and was positioned on the patient; (iii) The brace then closed due to the restoration of the elastic energy from the previous opening step, and forces representing strap tensions were applied on the nodes corresponding to strap fixations. Following these steps, the virtual brace was thus installed on the patient (Figure 4D).

Upon completion of the brace fitting simulation, 3D clinical indices (Cobb angles, kyphosis, lordosis, rib hump, axial rotation at the apical vertebrae) of the corrected spine were computed. For the 3D reconstruction of the initial spine geometry, the intra and inter-observer variability for the Cobb angles was respectively 0.4° and 0.8° for the thoracic curve, and 1.7° and 1.8° for the lumbar curve [21]. In addition, this reconstructed geometry

was used as initial geometry for the model. In all the simulations, the computation of the Cobb angles is using the same nodes of the resulting simulations. Thus, no supplementary variability was introduced in the computation of the Cobb angles. Asymmetrical compressive loads on the apical vertebrae were quantified as the bending moment Mx calculated using the right-hand rule (+ve clockwise, -ve counter-clockwise). Mx was evaluated locally (vertebral body reference system: R_{local}) for each vertebra with the origin of R_{local} located at the center of the vertebral body. The z-axis was in the direction of the line joining the centers of the vertebral endplate centers. The x-axis was the projection of the global x-axis on the plane perpendicular to the z-axis. The y-axis was perpendicular to the x and z-axes.

Correlation analysis

Correlations between immediate in-brace correction of the thoracic and lumbar Cobb angles and the reduction of asymmetrical compressive loads acting on the apical endplates(quantified by the bending moment Mx) were examined using both flexible and stiff spine models for each of the 3 patients. A Box, Hunter & Hunter fractional experimental design [34] was employed to simulate 1024 virtual braces for each patient. The experimental design framework included 14 brace design factors: number of straps and strap tension, type of brace, thoracic pad position in the transverse and vertical planes, the lumbar, anterior thoracic and trochanter pads presence, iliac crest roll design, lordosis design, height of the lumbar pad, rigid shell symmetry, trochanter extension side, brace size. Table 1 provides the two modalities for each of the 14 factors as illustrated in Figure 5.

Finally, for every patient the bending moment Mx in the coronal plane for the thoracic and lumbar apical vertebrae were plotted against the immediate in-brace Cobb angle correction. These plots were quantified for both types of spine models (stiff and flexible spine). A linear correlation coefficient (R^2) was then computed. In additional, the amount of immediate in-brace correction required to nullify the apical bending moment (due to asymmetrical loading) was identified as the % correction (x-axis) corresponding to 0 Mx on the regression line.

7.2.4 Results

The immediate correction of the lumbar and thoracic Cobb angles and the resulting bending moment Mx acting on the apical vertebrae were linearly correlated with a mean R^2=0.88 (Figures 6-8). On Figures 6-8 each point represents one of the 1024 tested braces. The symbol ● corresponds to the bending moment Mx present before installation of the brace.

The minimum amount of immediate coronal Cobb angle correction necessary to invert the apical bending moment Mx (vertical green line in Figures 6-8) varied between 19% and 61% (Mean: 48% for the flexible spine models and 27% for the stiff spine models). These results varied according to the spine stiffness and spine segment (thoracic or lumbar) (Table 2).

Table 3 lists the mean bending moments (Mx) measured, before bracing and in-brace, for both spine models (flexible and stiff) in all three patients. The mean in-brace bending moment Mx (for the 1024 tested braces) at the apex of the scoliotic curves was greater in the stiff spine models than in the flexible spine models. Paired student t-tests showed a significant difference in all patients and both spine segments (thoracic or lumbar) ($p<0.0001$ for all cases). In general, although the immediate in-brace correction required to nullify Mx was smaller for the stiffer spine model, the percentage of explored brace designs succeeding in inverting Mx was lower when compared to the flexible model (Table 4). For example, analysis of the thoracic segment in P1 suggested that 51% of the tested brace designs could succeed in inverting the apical bending moment for the flexible spine model (35% immediate in-brace correction required) but only 19% succeeded when using the stiff spine model (22% immediate in-brace correction required).

The 1024 tested braces impacted weakly on the transverse plane deformities of the 3 cases, with a mean 3% reduction of the rib hump angle at the apex of the deformity and a mean 4% reduction of the apical axial rotation. The 1024 tested braces for each of the 3 cases had a general flattening effect in the sagittal plane where the thoracic kyphosis and lumbar lordosis decreased respectively by 17% and 7% on average. There was no correlation

between the immediate correction obtained in the coronal plane and the immediate correction obtained in the transverse and sagittal planes.

7.2.5 Discussion

In the scoliotic spine, gravitational forces induce coronal asymmetrical compressive loading of the vertebrae [10]. These compressive forces are greater on the concavity of scoliotic curves than on their convexity and the intensity of this phenomenon reaches a maximum at the apex of the curves. As a result, this asymmetrical compressive loading creates a bending moment Mx over the vertebrae which, in turn, can be used to quantify its magnitude. In the framework of the Hueter-Volkmann principle the bending moment Mx , that is generating more compression loads in the concave side of the scoliotic curve, could be responsible for the progression of scoliotic deformities [10,35]. Consequently, the effect of brace installation on the bending moment Mx could be a good predictor of the long-term outcome of the treatment. Theoretically, in order to stop the progression of the scoliotic deformity, the brace should nullify the initial moment Mx (present prior to bracing). The strong correlations between immediate in-brace correction in the scoliotic curves and the apical bending moment Mx, evident in Figures 6-8, confirm that immediate in-brace correction is a good predictor of the long-term outcome of the treatment.

Variability between the three patients was observed pertaining to the amount of immediate correction necessary to nullify the bending moment Mx which, if achieved, could potentially stop scoliotic progression. Thus, the findings neither confirm nor refute the 50% rule-of-the-thumb sometimes adopted by orthotists. The percentage of braces to successfully invert the apical bending moment was higher for the flexible spine model. This finding is in agreement with the accepted notion that brace treatments are more efficient when spinal curves are flexible [6,36].

However, interpretation of the asymmetrical compressive loading Mx as a predictor of the evolution of the scoliotic deformities should be made with caution. It is still unknown whether there exists a ‘neutral zone’ where a slight asymmetrical loading will not generate

growth modulation [37,38]. Sensitivity of growth modulation to compressive stresses is still an active area of research [9,39].

The brace effect on asymmetrical loading purely due to gravity was studied and the model did not take into account muscle contribution. At times, a patient may tend to self-correct the scoliotic deformity by adjusting their in-brace posture such that the torso moves away from the pressure points of the brace. The trunk muscles play role in this brace active action [40,41]. Muscle contributions responsible for maintaining a stable posture is also an essential consideration even in a static standing position [42]. To model such muscular contributions is complex and poses great challenge to be undertaken in the future.

The main objective of this study was to analyze the correlations between immediate in-brace correction in the thoracic and lumbar Cobb angles and the correction in the asymmetrical compressive loads acting on the endplates of the apical vertebrae. But in the future the model could also identify what is the best brace design, once the concept of 'best brace' has been defined (i.e. clarification of the appropriate objective function [13,16]). In this study, the brace design factors that influenced the most the geometrical corrections in the coronal plane were the tension of the straps, the trochanteric extension position and the rigid shell symmetry (Table 1, Figure 5). The tested braces did not significantly correct the transverse plane deformities (rib hump and axial rotation). Other brace designs should be tested in the future to analyze more thoroughly the biomechanical influence of the brace in those planes.

The discussed results are based on three patients with different scoliotic curves, which is a limitation to the conclusions and generalizations that may be drawn. Although the explored findings are limited to these cases due to computational time (approximately 80 hours per case), this paper shows a sizeable proof of concept of a rationalized method to analyze the corrective outcome of different brace designs. The next step is to apply these methods of simulation to a larger cohort of scoliotic patients to fully validate this approach before further exploiting the potential of the simulator as a method to optimizing the brace design process. The model could also be adapted to predict if the brace of a given patient would stop the progression of the scoliotic deformities (i.e. if the immediate correction provided

by the brace is producing a moment superior to the one necessary to nullify the pathologic bending moment in the coronal plane). Further improvements to the brace simulator include the model refinement to account for the patient-specific mechanical properties of the spine [27] and the representation of the growth modulation process [10,35] to account for the time effect of the brace.

7.2.6 Conclusion

This study showed there was a correlation between immediate in-brace correction and the compressive asymmetrical loading of the spine in the frontal plane due to gravity. According to the Hueter-Volkmannn principle, this relationship should then lead to a correlation between immediate in-brace correction and long-term outcome of the treatment. These findings indicate that the stiffness of the spine is an important factor that determines the positive outcome related to immediate in-brace correction. This study highlights the biomechanical impact of bracing scoliotic spines and provides insights for a better understanding of this treatment.

7.2.7 Figures and Tables Captions

Tableau 7.1 Article 5 Table 1: Design factors tested with the design of experiments

Design Factor	*Modality 1*	*Modality 2*	*Ref. (Fig.5)*
1: Brace type	Thoracic brace	Lumbar brace	A, B
2: Number of straps	2	3	K
3: Strap tension	20 N	60 N	
4: Sagittal profile	Follows sagittal curves	Sagittal curves reduced	C
5: Thoracic pad position	Lateral	Posterior	D
6: Thoracic pad upper limit	Apical rib	2 ribs above	I
7: Anterior derotational thoracic pad	Absent	Present	L
8: Lumbar pad	Absent	Present	E
9: Upper limit of lumbar pad	Lumbar curve apex	2 vertebrae above	E
10: Trochanteric extension	Right	Left	F
11: Trochanter pad	Absent	Present	G
12: Iliac crest roll	Absent	Present	H
13: Rigid shell symmetry (coronal plane)	Symmetric	Asymmetric (10% reduction of thoracic and lumbar parts)	J
14: Brace size	5% too tight	5% too large	

Tableau 7.2 Article 5 Table 2: Amount of immediate in-brace correction necessary to nullify the asymmetrical loading of the vertebrae in the coronal plane (Mx)

Patient	Curve	Immediate Correction Threshold	
		Flexible spine	*Stiff Spine*
P1	Thoracic	35%	22%
	Lumbar	52%	21%
P2	Thoracic	60%	37%
	Lumbar	59%	30%
P3	Thoracic	21%	19%
	Lumbar	61%	30%

Tableau 7.3 Article 5 Table 3: Mean in-brace bending moment Mx in the coronal plane (in N.mm) at the apices of the scoliotic curves for the 1024 tested braces

Patient	Curve	Mean Bending Moment at Apex			
		Flexible Spine		*Stiff Spine*	
		Before Brace	*In Brace*	*Before Brace*	*In Brace*
P1	Thoracic	-319	18	-950	-220
	Lumbar	714	90	1258	141
P2	Thoracic	-746	-462	-1883	-1436
	Lumbar	1111	450	2204	1411
P3	Thoracic	-174	138	-548	-52
	Lumbar	999	548	1873	1249

Tableau 7.4 Article 5 Table 4: Percentage of the 1024 tested braces that succeeded in inverting the bending moment Mx on the apical vertebrae

Patient	Curve	Percentage of the tested braces that inverted Mx	
		Flexible spine	*Stiff Spine*
P1	Thoracic	51%	19%
	Lumbar	69%	66%
P2	Thoracic	0.3%	0%
	Lumbar	7%	0%
P3	Thoracic	72%	36%
	Lumbar	2%	0%

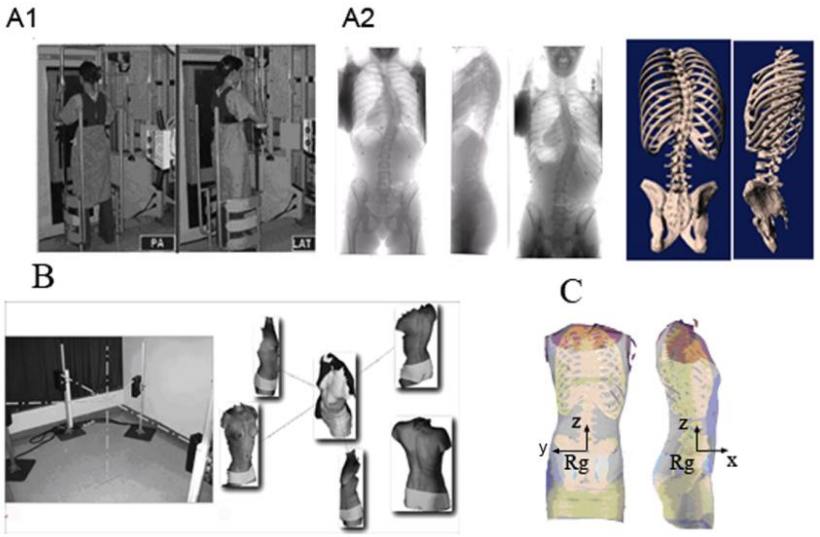

Figure 7.1 Article 5 Figure 1: A Acquisition of the internal geometry using the multi-view radiographic reconstruction technique: A1- PA and lateral acquisition; A2- PA, PA with an incidence of 20°, and lateral radiographs; A-3 3D reconstruction) ; B Acquisition of the external geometry using the range sensor topography technique; C Superimposition of the two geometries.

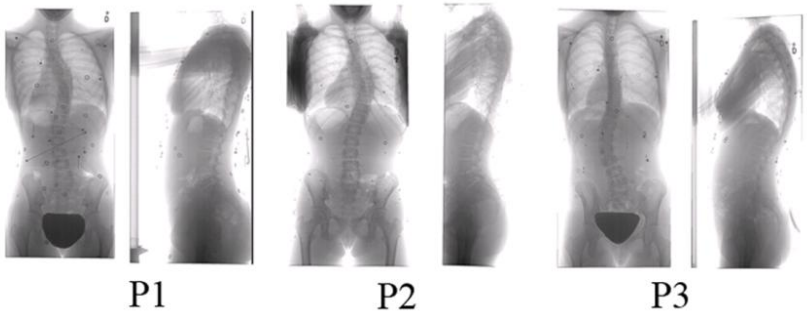

Figure 7.2 Article 5 Figure 2: Postero-anterior and lateral radiographs of the patients

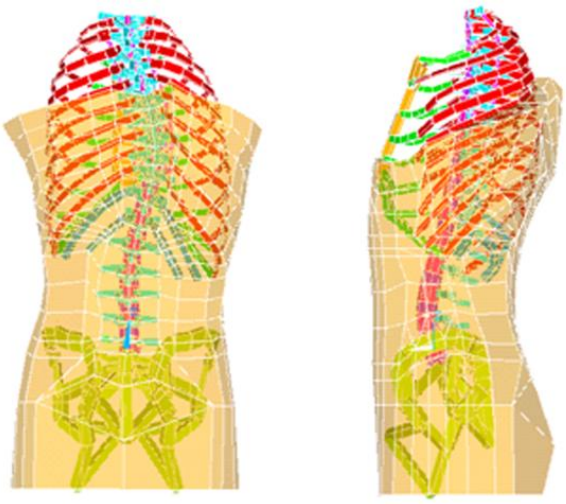

Figure 7.3 Article 5 Figure 3: Trunk FEM (intercostal ligaments and abdominal beams and are not shown for clarity)

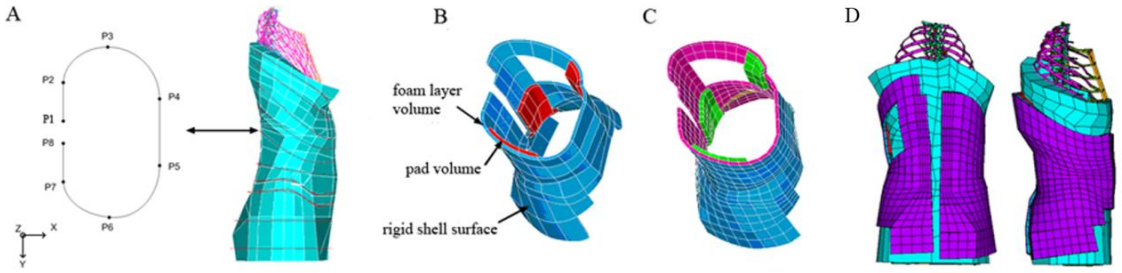

Figure 7.4 Article 5 Figure 4: A Generative curves (in red) B Geometrical model of the brace C Finite element model of the brace D Brace installed on the patient

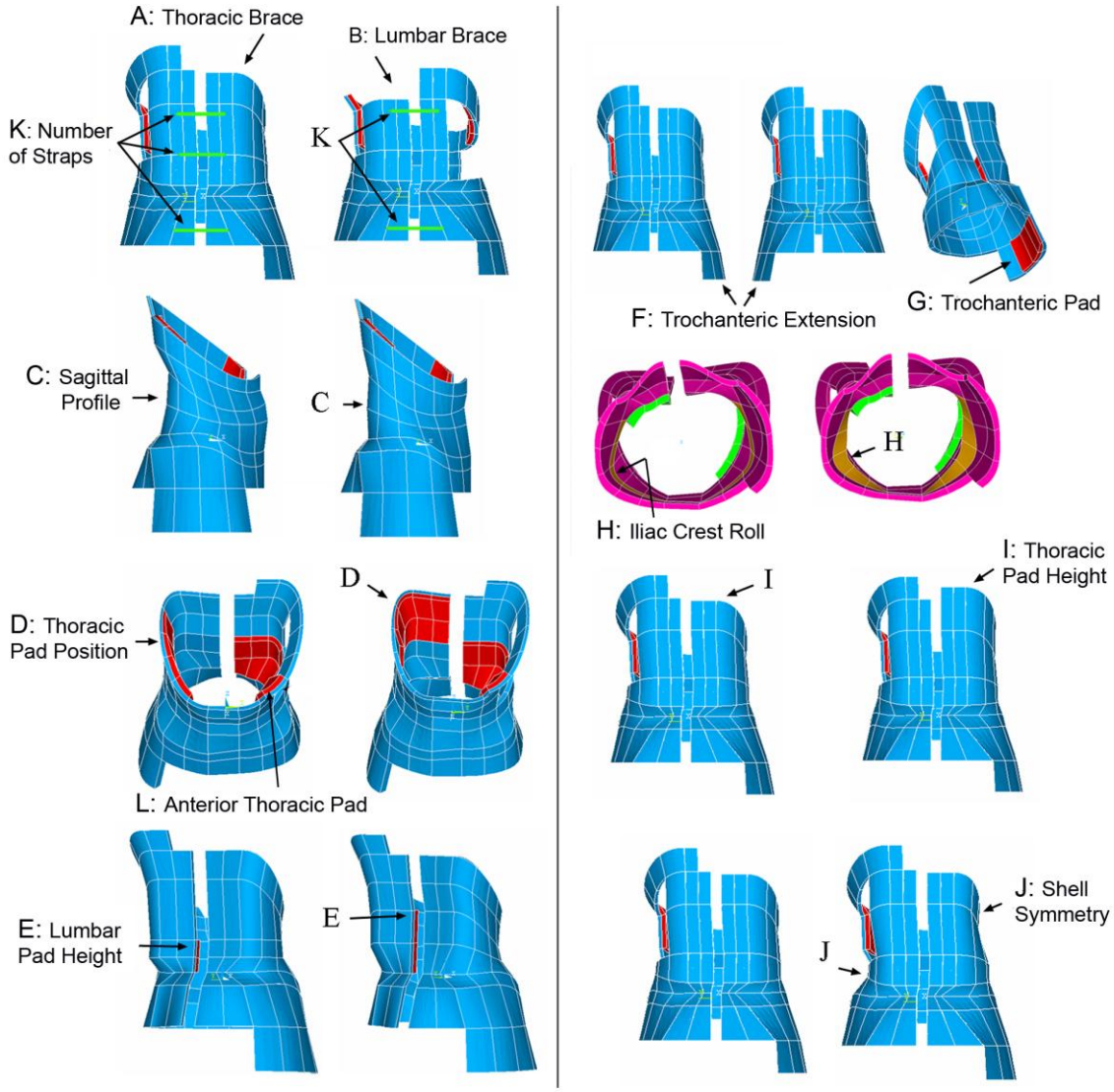

Figure 7.5 Article 5 Figure 5: Brace design factors, see Table 1 for details (A and B: Brace type; C: Lordosis design; D: Thoracic pad position; E: Lumbar pad height; F: Trochanteric extension side; G: Trochanter pad; H: Iliac Crest Roll Design; I: Thoracic pad height; J: Shell symmetry; K: Number of straps; L: Anterior Thoracic Pad)

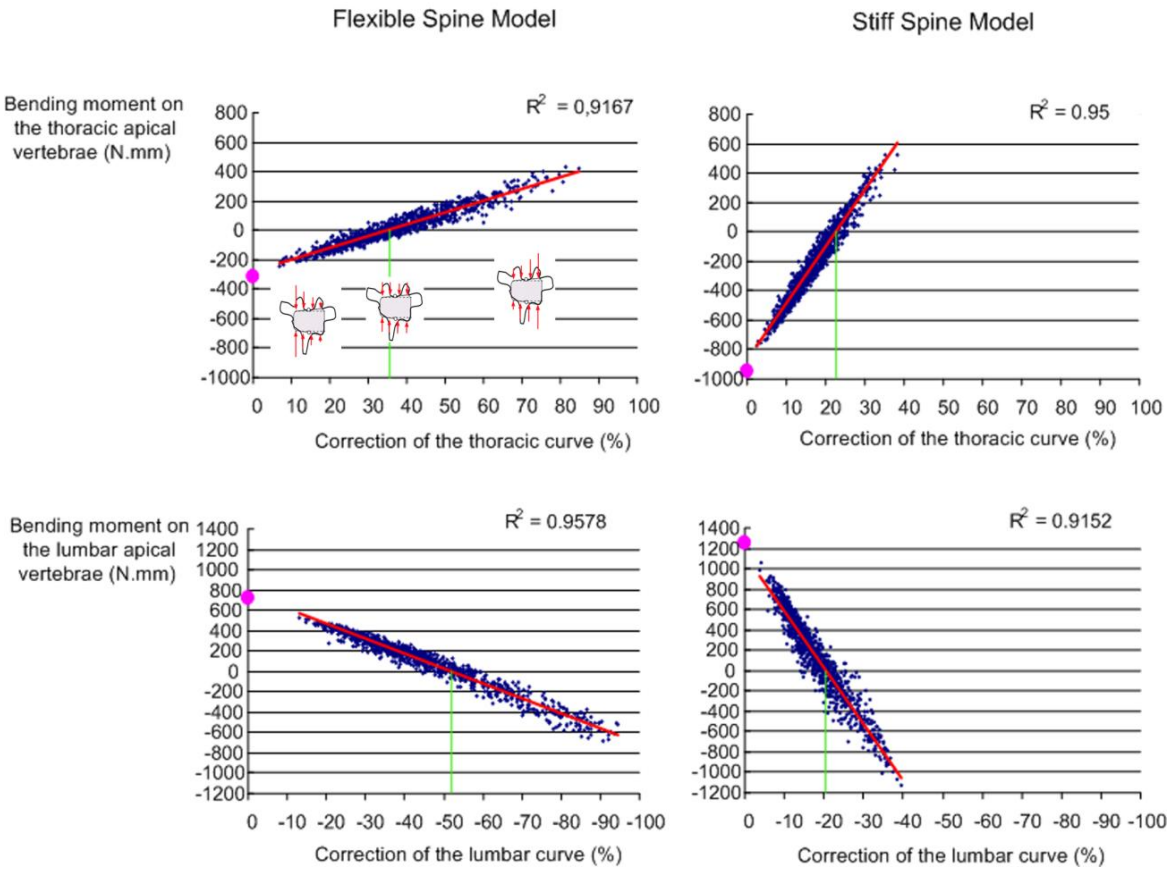

Figure 7.6 Article 5 Figure 6: Correlation between the immediate in-brace correction and the bending moment at the coronal curves apices for P1. A schematic of apical vertebral loading is illustrated in top left graph.

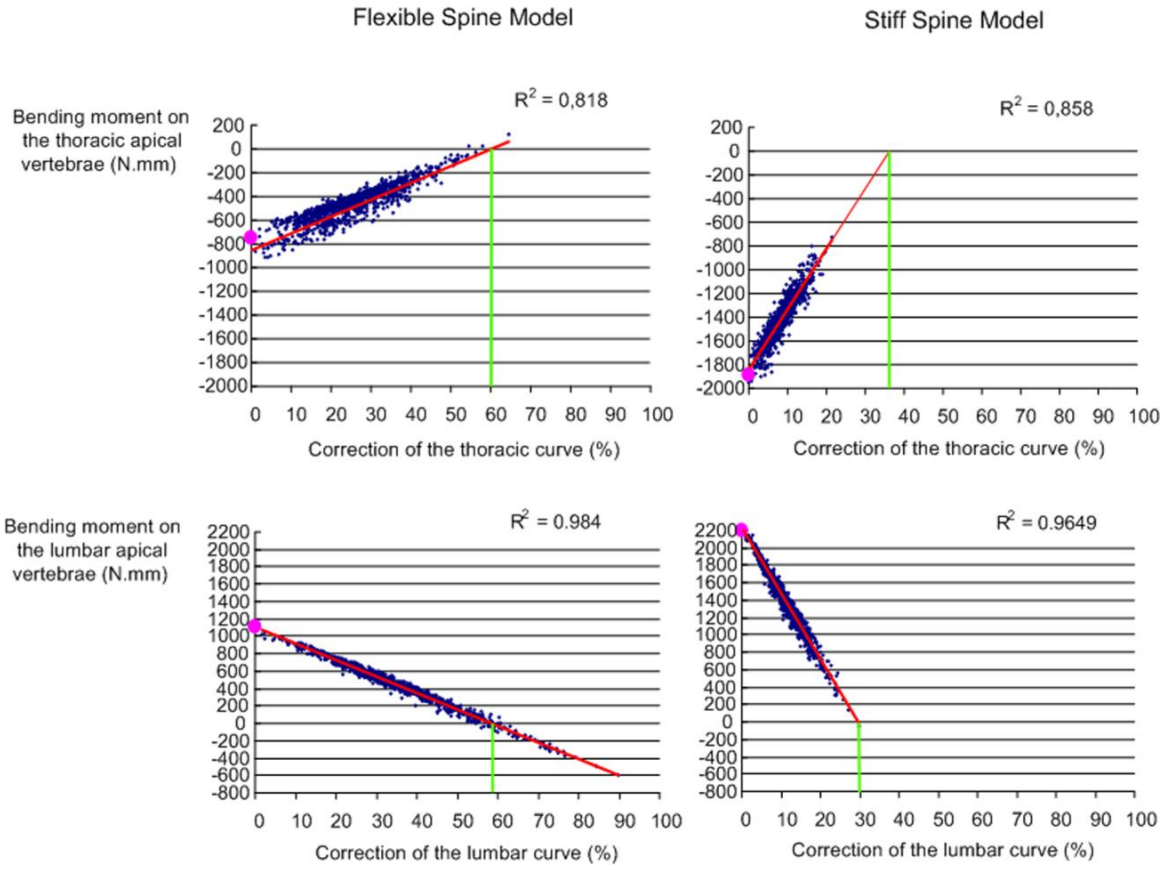

Figure 7.7 Article 5 Figure 7: Correlation between the immediate in-brace correction and the bending moment at the coronal curves apices for P1

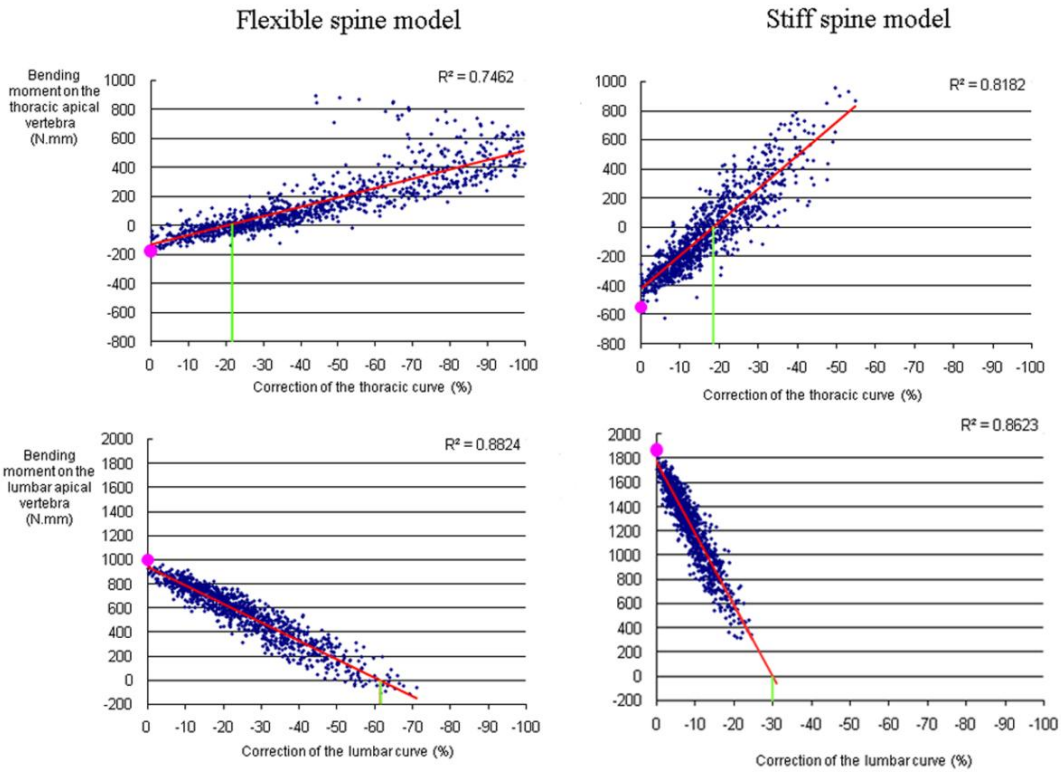

Figure 7.8 Article 5 Figure 8: Correlation between the immediate in-brace correction and the bending moment at the coronal curves apices for P3

7.2.8 References

1. Katz DE, Durrani AA. Factors that influence outcome in bracing large curves in patients with adolescent idiopathic scoliosis. *Spine* 2001;26:2354-61.

2. Landauer F, Wimmer C, Behensky H. Estimating the final outcome of brace treatment for idiopathic thoracic scoliosis at 6-month follow-up. *Pediatr Rehabil* 2003;6:201-7.

3. Upadhyay SS, Nelson IW, Ho EK, et al. New prognostic factors to predict the final outcome of brace treatment in adolescent idiopathic scoliosis. *Spine* 1995;20:537-45.

4. Noonan KJ, Weinstein SL, Jacobson WC, et al. Use of the Milwaukee brace for progressive idiopathic scoliosis. *J Bone Joint Surg Am* 1996;78:557-67.

5. Spoonamore MJ, Dolan LA, Weinstein SL. Use of the Rosenberger brace in the treatment of progressive adolescent idiopathic scoliosis. *Spine* 2004;29:1458-64.

6. Emans JB, Kaelin A, Bancel P, et al. The Boston bracing system for idiopathic scoliosis. Follow-up results in 295 patients. *Spine* 1986;11:792-801.

7. Castro FP, Jr. Adolescent idiopathic scoliosis, bracing, and the Hueter-Volkmann principle. *Spine J* 2003;3:180-5.

8. Patwardhan AG, Bunch WH, Meade KP, et al. A biomechanical analog of curve progression and orthotic stabilization in idiopathic scoliosis. *J Biomech* 1986;19:103-17.

9. Stokes IA, Clark KC, Farnum CE, et al. Alterations in the growth plate associated with growth modulation by sustained compression or distraction. *Bone* 2007;41:197-205.

10. Villemure I, Aubin CE, Dansereau J, et al. Biomechanical simulations of the spine deformation process in adolescent idiopathic scoliosis from different pathogenesis hypotheses. *Eur Spine J* 2004;13:83-90.

11. Machida M. Cause of idiopathic scoliosis. *Spine* 1999;24:2576-83.

12. Clin J, Aubin CE, Labelle H. Virtual prototyping of a brace design for the correction of scoliotic deformities. *Med Biol Eng Comput* 2007;45:467-73.

13. Gignac D, Aubin CE, Dansereau J, et al. Optimization method for 3D bracing correction of scoliosis using a finite element model. *Eur Spine J* 2000;9:185-90.

14. Perie D, Aubin CE, Lacroix M, et al. Biomechanical modelling of orthotic treatment of the scoliotic spine including a detailed representation of the brace-torso interface. *Med Biol Eng Comput* 2004;42:339-44.

15. Perie D, Aubin CE, Petit Y, et al. Boston brace correction in idiopathic scoliosis: a biomechanical study. *Spine* 2003;28:1672-7.

16. Wynarsky GT, Schultz AB. Optimization of skeletal configuration: studies of scoliosis correction biomechanics. *J Biomech* 1991;24:721-32.

17. Aubin CE, Descrimes JL, Dansereau J, et al. [Geometrical modeling of the spine and the thorax for the biomechanical analysis of scoliotic deformities using the finite element method]. *Ann Chir* 1995;49:749-61.

18. Cheriet F, Remaki L, Bellefleur C, et al. A new X-ray calibration/reconstruction system for 3D clinical assessment of spinal deformities. *Stud Health Technol Inform* 2002;91:257-61.

19. Kadoury S, Cheriet F, Laporte C, et al. A versatile 3D reconstruction system of the spine and pelvis for clinical assessment of spinal deformities. *Med Biol Eng Comput* 2007;45:591-602.

20. Kadoury S, Cheriet F, Dansereau J, et al. Three-dimensional reconstruction of the scoliotic spine and pelvis from uncalibrated biplanar x-ray images. *J Spinal Disord Tech* 2007;20:160-7.

21. Delorme S, Petit Y, de Guise JA, et al. Assessment of the 3-d reconstruction and high-resolution geometrical modeling of the human skeletal trunk from 2-D radiographic images. *IEEE Trans Biomed Eng* 2003;50:989-98.

22. Pazos V, Cheriet F, Danserau J, et al. Reliability of trunk shape measurements based on 3-D surface reconstructions. *Eur Spine J* 2007;16:1882-91.

23. Pazos V, Cheriet F, Song L, et al. Accuracy assessment of human trunk surface 3D reconstructions from an optical digitising system. *Med Biol Eng Comput* 2005;43:11-5.

24. Fortin D, Cheriet F, Beausejour M, et al. A 3D visualization tool for the design and customization of spinal braces. *Comput Med Imaging Graph* 2007;31:614-24.

25. Aubin CE, Dansereau J, De Guise JA, et al. [A study of biomechanical coupling between spine and rib cage in the treatment by orthosis of scoliosis]. *Ann Chir* 1996;50:641-50.

26. Perie D, Aubin CE, Petit Y, et al. Personalized biomechanical simulations of orthotic treatment in idiopathic scoliosis. *Clin Biomech (Bristol, Avon)* 2004;19:190-5.

27. Petit Y, Aubin CE, Labelle H. Patient-specific mechanical properties of a flexible multi-body model of the scoliotic spine. *Med Biol Eng Comput* 2004;42:55-60.

28. Cheng CK, Chen HH, Chen CS, et al. Segment inertial properties of Chinese adults determined from magnetic resonance imaging. *Clin Biomech (Bristol, Avon)* 2000;15:559-66.

29. Liu YK, Laborde JM, Van Buskirk WC. Inertial properties of a segmented cadaver trunk: their implications in acceleration injuries. *Aerosp Med* 1971;42:650-7.

30. Pearsall DJ, Reid JG, Livingston LA. Segmental inertial parameters of the human trunk as determined from computed tomography. *Ann Biomed Eng* 1996;24:198-210.

31. Pearsall DJ, Reid JG, Ross R. Inertial properties of the human trunk of males determined from magnetic resonance imaging. *Ann Biomed Eng* 1994;22:692-706.

32. Sanders JE, Greve JM, Mitchell SB, et al. Material properties of commonly-used interface materials and their static coefficients of friction with skin and socks. *J Rehabil Res Dev* 1998;35:161-76.

33. Zhang M, Mak AF. In vivo friction properties of human skin. *Prosthet Orthot Int* 1999;23:135-41.

34. Box GEP, Hunter JS. 2k-p fractional factorial designs. Part I. *Technometrics* 2000;42:28-47.

35. Stokes IA. Analysis and simulation of progressive adolescent scoliosis by biomechanical growth modulation. *Eur Spine J* 2007;16:1621-8.

36. Rowe DE, Bernstein SM, Riddick MF, et al. A meta-analysis of the efficacy of non-operative treatments for idiopathic scoliosis. *J Bone Joint Surg Am* 1997;79:664-74.

37. Frost HM. Skeletal structural adaptations to mechanical usage (SATMU): 3. The hyaline cartilage modeling problem. *Anat Rec* 1990;226:423-32.

38. Frost HM. Skeletal structural adaptations to mechanical usage (SATMU): 1. Redefining Wolff's law: the bone modeling problem. *Anat Rec* 1990;226:403-13.

39. Stokes IA, Aronsson DD, Dimock AN, et al. Endochondral growth in growth plates of three species at two anatomical locations modulated by mechanical compression and tension. *J Orthop Res* 2006;24:1327-34.

40. Odermatt D, Mathieu PA, Beausejour M, et al. Electromyography of scoliotic patients treated with a brace. *J Orthop Res* 2003;21:931-6.

41. Wynarsky GT, Schultz AB. Trunk muscle activities in braced scoliosis patients. *Spine* 1989;14:1283-6.

42. Nachemson AL. Disc pressure measurements. *Spine* 1981;6:93-7.

7.3 Étude supplémentaire sur 30 patients

L'article 5, dont les résultats ont été obtenus en milieu de thèse, a présenté pour 3 patients une étude de corrélation entre la correction immédiate des courbures scoliotiques coronales et le moment d'inflexion latéral sur les vertèbres apicales. Comme souligné dans la discussion de l'article, le nombre limité de patients restreint la portée de certaines conclusions. Une étude élargie sur 30 patients a donc été menée pour compléter cette étude acceptée pour publication. Le tableau 7.5 résume les indices cliniques de ces 30 patients présentant une scoliose idiopathique adolescente. Ces patients sont issus de la banque de données de scoliose de l'hôpital Sainte-Justine.

Tableau 7.5 : Indices cliniques des 30 patients

Indices (°)	Moy.	Min.	Max.
Cobb Thoracique	31	4	46
Cobb Lombaire	30	15	45
Cyphose	23	1	46
Lordose	39	18	58
Gibbosité	11	4	25
Rotation axiale maximale	15	5	26

Pour chacun des trente patients, le modèle du tronc a été construit. Tout comme dans l'article 5, deux flexibilités du rachis ont été testées (rachis 'flexible' et rachis 'rigide'). Pour chaque patient et chaque modèle de flexibilité du rachis, 768 différents corsets ont été testés (total de 69120 corsets testés). Ces 768 différents corsets proviennent d'un plan d'expériences incluant 13 paramètres de conception et globalement semblable à celui décrit dans l'article 5. Parmi les changements à noter, la position de l'extension trochantérique possédait dans ce plan 3 modalités (droite, gauche, ou absente) et seuls des corsets

«thoraciques», selon la dénomination des corsets de Boston, ont été testés. Pour chaque corset testé, la correction immédiate des angles de Cobb coronaux et le moment d'inflexion latérale agissant sur les vertébrales apicales ont été calculés. Leur corrélation a été étudiée.

La corrélation trouvée dans l'article 5 a été confirmée par cette étude. En moyenne, le coefficient de corrélation R^2 valait 0.86 (tableau 7.6). Le niveau de correction immédiate de l'angle de Cobb nécessaire pour inverser le moment d'inflexion latéral était en moyenne de 49% pour les courbures flexibles et de 35% pour les courbures rigides (tableau 7.6, seuil de correction). Pour les courbures flexibles, cette étude confirme la règle empirique fréquemment utilisé par les orthésistes (Emans, 1986, 2003), à savoir qu'au moins 50% de correction immédiate est nécessaire pour inverser l'asymétrie des contraintes en compression à l'apex des courbures scoliotiques et donc stopper la progression des courbures scoliotiques (principe de Hueter-Volkmann). Toutefois, pour les courbures rigides, cette étude suggère qu'une correction immédiate inférieure à 50% peut être suffisante pour empêcher la progression de la scoliose.

Tableau 7.6 : Résultats de l'étude de corrélation

Modèle du rachis		**Moyenne (Min - Max)** *Courbure* *Thoracique*	*Lombaire*
Flexible	r^2	0.83 (0.53 - 0.98)	0.89 (0.56 - 0.99)
	Seuil de correction (%)	48 (14 - 99)	49 (30 - 89)
Rigide	r^2	0.86 (0.33 - 0.99)	0.89 (0.57 - 0.99)
	Seuil de correction (%)	35 (10 - 69)	33 (21 - 62)

CHAPITRE 8: DISCUSSION GÉNÉRALE

Le traitement de la scoliose idiopathique par corset, bien que très largement adopté pour les déformations modérées, nécessite encore un processus de rationalisation et d'optimisation. La revue de la littérature a montré que de nombreuses questions demeurent quant à l'efficacité du traitement par corset et aux facteurs influençant cette efficacité.

Pour tenter de répondre à ces questions et apporter une base théorique supplémentaire à l'amélioration du traitement de la scoliose par corset, un nouveau modèle de simulation par éléments finis a été développé. Les bases de ce modèle avaient été précédemment introduites par Lacroix (2003) et Périé (2004), puis ont continué à être développées par Clin (2005, 2007) au cours de son projet de maîtrise. De nombreuses améliorations ont été apportées à ce modèle au cours de ce projet de doctorat. Tel que souligné par le deuxième article, l'inclusion des forces de gravité dans le processus de simulation a permis d'évaluer l'effet du traitement par corset sur les efforts internes à la colonne vertébrale mais a aussi modifié de façon importante les corrections géométriques prédites par le modèle. L'intégration de la surface externe du patient dans la représentation du tronc scoliotique a permis de modéliser des corsets sur mesure, ouvrant le chemin à une future fabrication de ces corsets virtuels. Une part très importante du travail mené a été l'amélioration du taux de convergence de la simulation et la réduction du temps de calcul. Le taux de convergence du modèle est actuellement évalué à 95%. Les études décrites dans les chapitres 6 et 7 montrent que le simulateur permet de tester efficacement un très grand nombre de corsets sur un patient donné mais aussi qu'il s'adapte facilement à différents patients. De plus, le temps de simulation d'un corset se situe entre 3 et 5 minutes sur un ordinateur de bureau usuel (processeur Intel Core 2 Duo 2.6 GHz, 3 Go Ram).

Le modèle du tronc a également été amélioré durant ce projet. Outre l'inclusion de la surface et des tissus mous externes dans le modèle, les éléments poutres constitutifs du rachis, de la cage thoracique et du bassin ont été remplacés par des éléments poutres de

nouvelle génération, plus robustes et plus rapides (dénomination ansys: beam 188). Ces nouveaux éléments poutres ont notamment permis le calcul et la représentation graphique des contraintes internes au niveau des plateaux vertébraux.

Certaines limites existent encore toutefois qui pourraient faire l'objet d'améliorations futures. Une représentation volumique détaillée des corps vertébraux et des disques intervertébraux pourrait être introduite pour raffiner le calcul des contraintes internes à la colonne vertébrale. La distribution des contraintes au niveau des plateaux vertébraux, du fait des équations inhérentes à la formulation poutre, était linéaire dans le modèle utilisé (figure 3.7). L'utilisation d'éléments volumiques permettrait d'obtenir des distributions plus générales. Évidemment, une représentation volumique du rachis augmenterait en contrepartie le temps de calcul d'une simulation. De plus, il faut souligner que l'approximation du rachis par un modèle poutre respecte tout à fait les hypothèses de validité de ce modèle : le rachis, pris dans sa globalité, est en effet une structure élancée (sa longueur est beaucoup plus grande que son épaisseur). Les différences de contraintes moyennes en compression entre la concavité et la convexité des courbures scoliotiques qui ont été calculées grâce au modèle poutre utilisé dans ce projet sont semblables aux récents résultats publiés sur des modèles volumiques (Driscoll, 2009). Des études préliminaires ont également été menées durant ce projet pour remplacer les éléments poutres du rachis par des éléments volumiques. Les différences de contraintes moyennes en compression entre la concavité et la convexité des courbures scoliotiques au sein des deux modèles ont été comparées et les résultats se sont avérés équivalents.

Il a été souligné dans les différents articles que l'absence d'une modélisation explicite du système musculaire était une limite des études présentées. L'absence de muscles a notamment un impact sur le calcul des contraintes internes à la colonne vertébrale puisqu'environ 50 % du chargement du rachis en position debout provient de l'action musculaire (Nachemson, 1981). Toutefois, la modélisation du système musculaire représente un défi de recherche en soi. Les particularités de l'action musculaire chez les sujets scoliotiques ont notamment été peu étudiées. De plus certains éléments du modèle décrit dans ce projet représentent une modélisation implicite des muscles. Ainsi les forces

de réaction présentes au niveau de T1 du fait des conditions limites imposées (pas de déplacement dans le plan transverse) correspondent à la sommation des forces musculaires requises pour obtenir l'équilibre global du tronc. De même, les forces transverses appliquées lors du processus d'optimisation de la géométrie en apesanteur (article 1) pourraient être interprétées en termes d'efforts musculaires.

Dans l'ensemble des articles présentés, des études paramétriques de sensibilité ont été menées pour évaluer l'influence de la rigidité des disques intervertébraux sur les résultats obtenus. Ces études ont confirmé l'importance de ce paramètre. Il a notamment été montré dans l'article 5 (chapitre 7) que la correction immédiate nécessaire pour empêcher la progression des déformations scoliotiques dépendait de la rigidité du rachis. Dans le cadre d'une future application clinique, il serait important d'introduire dans le processus de modélisation une personnalisation de la flexibilité du modèle du tronc pour chaque patient. Des études ont déjà été menées dans ce sens par Petit (2004) en se basant sur les tests de flexibilité par inflexion latérale. Récemment, un nouveau test de flexibilité particulièrement prometteur a également été introduit (Lamarre, 2009). Ce test utilise un système de suspension du patient grâce à un harnais placé sous ses aisselles. La réduction des ses courbures scoliotiques s'effectue donc via la traction générée par le propre poids du patient. De ce fait ce test de flexibilité est calibré et permet de calculer la rigidité des courbures scoliotiques et pas seulement leur réductibilité, par opposition au test d'inflexion latérale (Lamarre, 2009). Une modélisation de ce test de suspension pourrait donc permettre de personnaliser la rigidité du modèle du tronc à chaque patient. Dans cette personnalisation il serait intéressant de ne pas se restreindre à ajuster la rigidité des disques intervertébraux. D'autres éléments, tels la rigidité des ligaments, des tissus mous externes ou encore des liaisons costo-vertébrales et costo-transverses devraient être inclus. De plus les rigidités de différents segments du rachis devraient être ajustées de façon indépendante.

L'effet à long-terme des corsets testés a été interprété dans ce projet à partir de l'analyse des différences de compression sur les plateaux vertébraux entre les côtés concaves et convexes des courbures scoliotiques. Cette interprétation se base notamment sur le principe de modulation de croissance de Hueter-Volkmann et sur les travaux de Villemure (2004) et

Stokes (2007). Il serait particulièrement intéressant dans de futurs travaux d'intégrer un modèle de croissance qui permettrait de simuler explicitement l'effet à long-terme du corset, comme a pu le faire Carrier (2004) pour les opérations chirurgicales de resection des côtes chez les sujets scoliotiques. Un tel modèle se base également sur l'analyse des contraintes mécaniques sur les plaques de croissance mais permet de simuler et visualiser la croissance asymétrique des corps vertébraux (cunéiformisation) et donc la progression des déformations scoliotiques du patient (Villemure, 2004 ; Stokes, 2007 ; Lin, 2009). Il serait ainsi possible de simuler l'évolution (progression, stabilisation ou diminution) des déformations scoliotiques d'un patient lors de la durée de son traitement par corset (2 ou 3 ans) afin de conclure sur l'efficacité du corset à long-terme.

L'évaluation des effets de différents paramètres de conception des corsets décrite aux chapitres 6 et 7 a permis de détecter certains des paramètres les plus influents sur l'efficacité du corset, notamment la position de l'extension trochantérique, la tension et le nombre de courroies, la forme de la coque rigide ou la position de l'ouverture. Ceci jette les bases d'un réel processus d'optimisation. Cela permet en effet de mieux cerner quelles sont les variables d'optimisation, les critères de design, qui devront être utilisées. Une fonction d'optimisation représentative des objectifs de correction d'un orthésiste doit encore être définie. Pour ce faire, une étude similaire à celle de Majdouline (2007, 2009), qui a défini une telle fonction dans le cadre du traitement chirurgical de la scoliose en soumettant un questionnaire auprès de 32 chirugiens, pourrait être réalisée. Une méthode d'optimisation appropriée devra également être définie. Divers éléments non considérés dans ce projet devront être pris en compte, tel que les notions de confort (via la pression et la chaleur) ou d'esthétisme du corset. Enfin, une fois que le corset «optimal», selon la définition établie, sera défini, une méthode de fabrication de ce corset devra être choisie et appliquée.

Un point crucial du développement de tout modèle est sa validation. Dans quelle mesure le modèle, qui est forcément basé sur un certain nombre d'hypothèses et d'approximations, représente-t-il la réalité ? Il faut toutefois faire la distinction entre les résultats qui sont validables et ceux qui ne le sont pas du fait du manque de données expérimentales disponibles. Par exemple, la distribution et l'amplitude des pressions asymétriques

s'exerçant sur les plateaux vertébraux d'un patient scoliotique n'ont pas encore été mesurées expérimentalement. Les difficultés techniques reliées à une telle mesure restent encore importantes, même si de récents travaux présentent des progrès intéressants. Ainsi Meir (2007) a mesuré le profil de contraintes dans les disques intervertébraux de patients scoliotiques lors de chirurgies antérieures. Les patients étaient donc anesthésiés et en position de decubitus latéral. Il a trouvé des différences de compression entre les côtés concaves et convexes des courbures scoliotiques allant jusqu'à 1 MPa.

Les résultats concernant la distribution et l'amplitude des pressions asymétriques dans le rachis présentés dans ce projet s'avèrent cependant réalistes et plausibles dans le cadre des données expérimentales disponibles. La compression moyenne trouvée dans les disques lombaires des patients en position debout (0.2 Mpa) correspond à la contribution de la gravité aux pressions intradiscales mesurées chez des sujets sains (Nachemson, 1981; Wilke, 1999). La différence moyenne de compression entre les côtés concaves et convexes des courbures scoliotiques (entre 0.1 et 0.4 MPa) correspond aux valeurs expérimentales utilisées par Stokes pour induire une modulation de croissance dans des modèles animaux (Stokes, 2006, 2007). Les différences maximales de compression entre les côtés concaves et convexes des courbures scoliotiques sont du même ordre de grandeur que les valeurs trouvées expérimentalement par Meir (2007).

Il est en théorie possible de valider la géométrie 3D d'un patient dans son corset prédite par la simulation à l'aide des radiographies du patient dans son corset réel. Les études présentées dans l'article 2 (Figures 4.4, 4.5), et dans le chapitre 4.3 représentent un premier niveau d'évaluation. Elles ont montré que le modèle a le potentiel de reproduire les corrections géométriques produites par les corsets réels et que les pressions calculées à l'interface tronc-corset correspondent aux données expérimentales. Par ailleurs, l'article 4 présenté au chapitre 6 a permis de montrer que nombre des effets des paramètres de conception correspondaient aux données disponibles dans la littérature et que le modèle avait un comportement réaliste. La validation devra être poursuivie en modélisant précisément les corsets réels d'une cohorte de patients et en mesurant la flexibilité de ces patients afin de l'intégrer au modèle. Il serait également approprié de chercher à mesurer la

variabilité de la géométrie corrigée d’un patient lorsqu’on installe plusieurs fois le même corset, avec la même tension de courroie. Cela permettra de disposer d’une plage de variabilité expérimentale par rapport à laquelle comparer les résultats de la simulation.

CONCLUSION

Durant ce projet doctoral, un modèle original et innovant de simulation du traitement par corset a été développé. Ce modèle a permis d'évaluer pour la première fois l'effet d'un corset sur les contraintes internes de la colonne vertébrale qui sont impliquées dans le processus d'évolution des déformations scoliotiques selon le principe de modulation de croissance de Hueter-Volkmann. Le travail effectué pour obtenir un modèle robuste, c'est-à-dire un taux de convergence élevé, a permis de tester un très grand nombre de corsets différents (70 000 approximativement, dans l'étude présentée au chapitre 7.3).

Ce modèle a ainsi permis de rationaliser, de mieux comprendre certains aspects de la biomécanique du traitement par corset. L'étude menée dans l'article 2 a montré que le corset pour le traitement de la scoliose ne doit pas être seulement perçu comme un medium applicateur de forces correctrices mais aussi comme un support contre l'action des forces de gravité. L'action biomécanique du corset de Charleston a été explicitée. Sa capacité à inverser l'asymétrie des contraintes de compression au niveau de la courbure principale a été démontrée et quantifiée. Toutefois son effet potentiellement négatif sur la courbure secondaire a été souligné. Une hiérarchie des paramètres de conception des corsets selon leur influence sur les corrections géométriques 3D a été établie dans l'article 4. Le rôle fondamental de l'extension trochantérique a notamment été détecté et son action mécanique de bras de levier pour le comportement global du corset a été analysée. Il a été montré que les coques rigides symétriques, tel le module de base du corset de Boston, limitaient le potentiel de correction. Un autre point particulièrement intéressant a été soulevé: la position de l'ouverture du corset, et donc des couroies de serrage, modifie le comportement global du corset et l'effet des autres paramètres de conception. Cette avenue devra être explorée plus avant afin d'exploiter cette caractéristique à fins d'optimisation. Enfin, nous avons réalisé une démonstration biomécanique d'un principe empirique largement utilisé en cadre clinique, à savoir que l'effet immédiat d'un corset permet de prédire son efficacité à long-terme, soit sa capacité à stopper la progression des déformations scoliotiques. Toutefois

cette étude a révélé que le niveau de correction immédiate des courbures nécessaire pour stopper la progression des déformations pourrait ne pas être forcément le «50%» utilisé généralement par les orthésistes. Si cette étude a confrmé ce chiffre pour les courbures flexibles, il semblerait qu'un niveau de correction immédiate inférieure pourrait être suffisant pour des courbures plus rigides.

Certains développements devront être prioritaires lors de la continuation de ce projet afin de renforcer son potentiel d'application clinique. La personnalisation des propriétés mécaniques du modèle à chaque patient et l'intégration d'un modèle de croissance explicite de croissance devront être effectuées. Le processus de validation des corrections géométriques et des pressions à l'interface corset-tronc devra être poursuivi. La capacité du modèle à prédire adéquatement si un corset donné peut stopper la progression des déformations scoliotiques devra être vérifié.

Ce projet, en permettant une compréhension et une connaissance approfondie de la biomécanique des processus impliqués, pourra alors éventuellement permettre la conception de corsets plus performants, et, ce qui reste l'objectif ultime, une amélioration du traitement des patients.

BIBLIOGRAPHIE

Andriacchi, T. P., Schultz, A. B., Belytschko, T. B., & Dewald, R. (1976). Milwaukee brace correction of idiopathic scoliosis. A biomechanical analysis and a restrospective study. *J Bone Joint Surg Am, 58*(6), 806-815.

Aubin, C. E., Dansereau, J., De Guise, J. A., & Labelle, H. (1996). A study of biomechanical coupling between spine and rib cage in the treatment by orthosis of scoliosis. *Ann Chir, 50*(8), 641-650.

Aubin, C. E., Dansereau, J., de Guise, J. A., & Labelle, H. (1997). Rib cage-spine coupling patterns involved in brace treatment of adolescent idiopathic scoliosis. *Spine, 22*(6), 629-635.

Carlson, M. (2003). Clinical biomechanics of orthotic treatment of idiopathic scoliosis. *Journal of Prosthetics and Orthotics, 15*, 17-30.

Carrier, J., Aubin, C. E., Villemure, I., & Labelle, H. (2004). Biomechanical modelling of growth modulation following rib shortening or lengthening in adolescent idiopathic scoliosis. *Med Biol Eng Comput, 42*(4), 541-548.

Carrier, J., Aubin, C.-E., Trochu, F., & Labelle, H. (2003). Optimization of rib surgery parameters for the correction of scoliotic deformities using dual kriging. *Journal of Biomechanical Engineering*.

Castro, F. P., Jr. (2003). Adolescent idiopathic scoliosis, bracing, and the Hueter-Volkmann

principle. *Spine J, 3*(3), 180-185.

Chase, A. P., Bader, D. L., & Houghton, G. R. (1989). The biomechanical effectiveness of the Boston brace in the management of adolescent idiopathic scoliosis. *Spine, 14*(6), 636-642.

Clin, J. (2005). *Simulation biomécanique du traitement de la scoliose idiopatique par orthèse: application à la conception rationelle de corsets.* Mémoire de maîtrise inédit, École Plytechnique de Montréal, Montréal.

Clin, J., Aubin, C. E., & Labelle, H. (2007). Virtual prototyping of a brace design for the correction of scoliotic deformities. *Med Biol Eng Comput, 45*(5), 467-473.

Coillard, C., Vachon, V., Circo, A. B., Beausejour, M., & Rivard, C. H. (2007). Effectiveness of the SpineCor brace based on the new standardized criteria proposed by the scoliosis research society for adolescent idiopathic scoliosis. *J Pediatr Orthop, 27*(4), 375-379.

D'Amato, C. R., Griggs, S., & McCoy, B. (2001). Nighttime bracing with the Providence brace in adolescent girls with idiopathic scoliosis. *Spine, 26*(18), 2006-2012.

Danielsson, A. J., Hasserius, R., Ohlin, A., & Nachemson, A. L. (2007). A prospective study of brace treatment versus observation alone in adolescent idiopathic scoliosis: a follow-up mean of 16 years after maturity. *Spine (Phila Pa 1976), 32*(20), 2198-2207.

Dickson, R. A., & Weinstein, S. L. (1999). Bracing (and screening)--yes or no? *J Bone Joint Surg Br, 81*(2), 193-198.

Driscoll, M., Aubin, C. E., Moreau, A., Villemure, I., & Parent, S. (2009). The role of spinal concave-convex biases in the progression of idiopathic scoliosis. *Eur Spine J, 18*(2), 180-187.

Emans, J. (2003). The Bracing Manual, The Boston Brace. *Scoliosis Research Society (www.srs.org).*

Emans, J. B., Kaelin, A., Bancel, P., Hall, J. E., & Miller, M. E. (1986). The Boston bracing system for idiopathic scoliosis. Follow-up results in 295 patients. *Spine, 11*(8), 792-801.

Gignac, D., Aubin, C. E., Dansereau, J., & Labelle, H. (2000). Optimization method for 3D bracing correction of scoliosis using a finite element model. *Eur Spine J, 9*(3), 185-190.

Goldberg, C. J., Moore, D. P., Fogarty, E. E., & Dowling, F. E. (2001). Adolescent idiopathic scoliosis: the effect of brace treatment on the incidence of surgery. *Spine, 26*(1), 42-47.

Hooper, R. (2003). The Bracing manual, The Charleston Brace. *Scoliosis Research Society (www.srs.org).*

Katz, D. E., Richards, B. S., Browne, R. H., & Herring, J. A. (1997). A comparison between the Boston brace and the Charleston bending brace in adolescent idiopathic scoliosis. *Spine, 22*(12), 1302-1312.

Korovessis, P., Kyrkos, C., Piperos, G., & Soucacos, P. N. (2000). Effects of

thoracolumbosacral orthosis on spinal deformities, trunk asymmetry, and frontal lower rib cage in adolescent idiopathic scoliosis. *Spine (Phila Pa 1976), 25*(16), 2064-2071.

Labelle, H., Dansereau, J., Bellefleur, C., & Poitras, B. (1992). [3-D study of the immediate effect of the Boston brace on the scoliotic lumbar spine]. *Ann Chir, 46*(9), 814-820.

Labelle, H., Dansereau, J., Bellefleur, C., & Poitras, B. (1996). Three-dimensional effect of the Boston brace on the thoracic spine and rib cage. *Spine, 21*(1), 59-64.

Lacroix, M. (2003). *Modélisation biomécanique de l'interaction entre le corset et le tronc dans le traitement de la scoliose.* Mémoire de maîtrise inédit, École Polytechnique de Montréal

Lamarre, M. E., Parent, S., Labelle, H., Aubin, C. E., Joncas, J., Cabral, A., et al. (2009). Assessment of spinal flexibility in adolescent idiopathic scoliosis: suspension versus side-bending radiography. *Spine, 34*(6), 591-597.

Liao, Y. C., Feng, C. K., Tsai, M. W., Chen, C. S., Cheng, C. K., & Ou, Y. C. (2007). Shape modification of the Boston brace using a finite-element method with topology optimization. *Spine, 32*(26), 3014-3019.

Lin, H., Aubin, C. E., Parent, S., & Villemure, I. (2009). Mechanobiological bone growth: comparative analysis of two biomechanical modeling approaches. *Med Biol Eng Comput, 47*(4), 357-366.

Lonstein, J. E. (2003). The Bracing Manual, The Milwaukee Brace. *Scoliosis Research Society (www.srs.org).*

Lonstein, J. E., & Winter, R. B. (1994). The Milwaukee brace for the treatment of adolescent idiopathic scoliosis. A review of one thousand and twenty patients. *J Bone Joint Surg Am, 76*(8), 1207-1221.

Mac-Thiong, J. M., Petit, Y., Aubin, C. E., Delorme, S., Dansereau, J., & Labelle, H. (2004). Biomechanical evaluation of the Boston brace system for the treatment of adolescent idiopathic scoliosis: relationship between strap tension and brace interface forces. *Spine, 29*(1), 26-32.

Majdouline, Y., Aubin, C. E., Robitaille, M., Sarwark, J. F., & Labelle, H. (2007). Scoliosis correction objectives in adolescent idiopathic scoliosis. *J Pediatr Orthop, 27*(7), 775-781.

Majdouline, Y., Aubin, C. E., Sangole, A., & Labelle, H. (2009). Computer simulation for the optimization of instrumentation strategies in adolescent idiopathic scoliosis. *Med Biol Eng Comput, 47*(11), 1143-1154.

Nachemson, A. L. (1981). Disc pressure measurements. *Spine, 6*(1), 93-97.

Nachemson, A. L., & Peterson, L. E. (1995). Effectiveness of treatment with a brace in girls who have adolescent idiopathic scoliosis. A prospective, controlled study based on data from the Brace Study of the Scoliosis Research Society. *J Bone Joint Surg Am, 77*(6), 815-822.

Noonan, K. J., Weinstein, S. L., Jacobson, W. C., & Dolan, L. A. (1996). Use of the Milwaukee brace for progressive idiopathic scoliosis. *J Bone Joint Surg Am, 78*(4), 557-567.

Odermatt, D., Mathieu, P. A., Beausejour, M., Labelle, H., & Aubin, C. E. (2003). Electromyography of scoliotic patients treated with a brace. *J Orthop Res, 21*(5), 931-936.

Olafsson, Y., Saroste, H., Sodeolund, V., & Hoffston, M. (1995). Boston brace in the treatment of idiopathic scoliosis. *Journal of Prosthetics and Orthotics, 15*(4), 524-527.

Parent, S., Labelle, H., Skalli, W., & de Guise, J. (2004). Thoracic pedicle morphometry in vertebrae from scoliotic spines. *Spine, 29*(3), 239-248.

Patwardhan, A. G., Bunch, W. H., Meade, K. P., Vanderby, R. J., & Knight, G. W. (1986). A biomechanical analog of curve progression and orthotic stabilization in idiopathic scoliosis. *J Biomech, 19*(2), 103-117.

Perie, D., Aubin, C. E., Lacroix, M., Lafon, Y., & Labelle, H. (2004). Biomechanical modelling of orthotic treatment of the scoliotic spine including a detailed representation of the brace-torso interface. *Med Biol Eng Comput, 42*(3), 339-344.

Perie, D., Aubin, C. E., Petit, Y., Beausejour, M., Dansereau, J., & Labelle, H. (2003). Boston brace correction in idiopathic scoliosis: a biomechanical study. *Spine, 28*(15), 1672-1677.

Perie, D., Aubin, C. E., Petit, Y., Labelle, H., & Dansereau, J. (2004). Personalized biomechanical simulations of orthotic treatment in idiopathic scoliosis. *Clin Biomech (Bristol, Avon), 19*(2), 190-195.

Perie, D., Sales De Gauzy, J., Sevely, A., & Hobatho, M. C. (2001). In vivo geometrical

evaluation of Cheneau-Toulouse-Munster brace effect on scoliotic spine using MRI method. *Clin Biomech (Bristol, Avon), 16*(2), 129-137.

Petit, Y., Aubin, C. E., & Labelle, H. (2004). Patient-specific mechanical properties of a flexible multi-body model of the scoliotic spine. *Med Biol Eng Comput, 42*(1), 55-60.

Price, C. T., Scott, D. S., Reed, F. R. J., Sproul, J. T., & Riddick, M. F. (1997). Nighttime bracing for adolescent idiopathic scoliosis with the Charleston Bending Brace: long-term follow-up. *J Pediatr Orthop, 17*(6), 703-707.

Rigo, M., Negrini, S., Weiss, H. R., Grivas, T. B., Maruyama, T., & Kotwicki, T. (2006). 'SOSORT consensus paper on brace action: TLSO biomechanics of correction (investigating the rationale for force vector selection)'. *Scoliosis, 1*, 11.

Roach, J. W. (1999). Adolescent idiopathic scoliosis. *Orthop Clin North Am, 30*(3), 353-365, vii-viii.

Roaf, R. (1960). Vertebral growth and its mechanical control. *J Bone Joint Surg Br, 42-B*, 40-59.

Rogala, E. J., Drummond, D. S., & Gurr, J. (1978). Scoliosis: incidence and natural history. A prospective epidemiological study. *J Bone Joint Surg Am, 60*(2), 173-176.

Rowe, D. E., Bernstein, S. M., Riddick, M. F., Adler, F., Emans, J. B., & Gardner-Bonneau, D. (1997). A meta-analysis of the efficacy of non-operative treatments for idiopathic scoliosis. *J Bone Joint Surg Am, 79*(5), 664-674.

Schiller, J. R., Thakur, N. A., & Eberson, C. P. (2010). Brace management in adolescent idiopathic scoliosis. *Clin Orthop Relat Res, 468*(3), 670-678.

Stokes, I. A. (2007). Analysis and simulation of progressive adolescent scoliosis by biomechanical growth modulation. *Eur Spine J, 16*(10), 1621-1628.

Stokes, I. A., Aronsson, D. D., Dimock, A. N., Cortright, V., & Beck, S. (2006). Endochondral growth in growth plates of three species at two anatomical locations modulated by mechanical compression and tension. *J Orthop Res, 24*(6), 1327-1334.

Stokes, I. A., Clark, K. C., Farnum, C. E., & Aronsson, D. D. (2007). Alterations in the growth plate associated with growth modulation by sustained compression or distraction. *Bone, 41*(2), 197-205.

Upadhyay, S. S., Nelson, I. W., Ho, E. K., Hsu, L. C., & Leong, J. C. (1995). New prognostic factors to predict the final outcome of brace treatment in adolescent idiopathic scoliosis. *Spine, 20*(5), 537-545.

Villemure, I., Aubin, C. E., Dansereau, J., & Labelle, H. (2004). Biomechanical simulations of the spine deformation process in adolescent idiopathic scoliosis from different pathogenesis hypotheses. *Eur Spine J, 13*(1), 83-90.

White, A., & Panjabi, M. (Eds.). (1990). *Clinical biomechanics of the spine* (2nd ed^{e} éd.). Philadelphia: Lippincott.

Wilke, H. J., Neef, P., Caimi, M., Hoogland, T., & Claes, L. E. (1999). New in vivo measurements of pressures in the intervertebral disc in daily life. *Spine, 24*(8), 755-

762.

Willers, U., Normelli, H., Aaro, S., Svensson, O., & Hedlund, R. (1993). Long-term results of Boston brace treatment on vertebral rotation in idiopathic scoliosis. *Spine, 18*(4), 432-435.

Wong, M. S., Mak, A. F., Luk, K. D., Evans, J. H., & Brown, B. (2000). Effectiveness and biomechanics of spinal orthoses in the treatment of adolescent idiopathic scoliosis (AIS). *Prosthet Orthot Int, 24*(2), 148-162.

Wynarsky, G. T., & Schultz, A. B. (1989). Trunk muscle activities in braced scoliosis patients. *Spine, 14*(12), 1283-1286.

Wynarsky, G. T., & Schultz, A. B. (1991). Optimization of skeletal configuration: studies of scoliosis correction biomechanics. *J Biomech, 24*(8), 721-732.